ABSTRACT

YUNCU, BILGEN. Removal of 2-Methylisoborneol and Geosmin by High-Silica Zeolites and Powdered Activated Carbon in the Absence and Presence of Ozone. (Under the direction of Dr. Detlef Knappe.)

Earthy and musty odors in drinking water are frequently attributed to the presence of 2-methylisoborneol (MIB) and geosmin. Treatment costs associated with taste and odor control can be high, and the desired water quality is not always met with existing treatment technologies such as chemical oxidation and activated carbon adsorption. Therefore, more selective and effective treatment processes to reliably remove taste and odor causing compounds like MIB and geosmin from drinking water sources are needed. The main objective of this research was to investigate two innovative treatment methods for the removal of MIB and geosmin from drinking water. The first treatment method is an adsorption/reaction process based on the use of high-silica zeolites, and the second treatment method is an adsorption/oxidation process based on the combined use of high-silica zeolites and ozone.

The potential for adsorptive and reactive removal of MIB and geosmin by high-silica zeolites was assessed in longer-term isotherm experiments and in short-term kinetic tests. Single-solute batch experiments were conducted in ultrapure water (UPW) to identify the characteristics of high-silica zeolites that are most suitable for the adsorptive removal of MIB and geosmin. In these experiments, effects of zeolite pore size and hydrophobicity/acidity on

MIB and geosmin removals were evaluated. In addition, the effectiveness of zeolites was compared to one coal-based and one coconut-shell-based activated carbon. Background water matrix effects [cations, natural organic matter (NOM)] on MIB and geosmin removal were determined by conducting experiments in salt-amended UPW and in Lake Michigan water (LMW).

Among the tested high-silica zeolites, the mordenite framework type exhibited the largest MIB adsorption capacity while both mordenite and Y framework types were effective for geosmin adsorption. Single solute MIB and geosmin adsorption capacities of the tested high-silica zeolites were smaller than those of the tested activated carbons. With respect to zeolite hydrophobicity, results for both MIB and geosmin showed that adsorption capacities increased as the SiO_2/Al_2O_3 ratio (hydrophobicity) increased. Also, differences in MIB removal between experiments conducted with ^{14}C-labelled MIB and non-labelled MIB suggest that MIB was removed by a reactive mechanism on some zeolites. MIB and geosmin removals by mordenite zeolites were markedly decreased by LMW constituents. While LMW constituents did not have a measurable effect on geosmin removal by Y zeolite, they were able to almost completely displace MIB in isotherm experiments. Apart from NOM, cations in the background water (e.g., Ca^{2+}, Na^{+}) strongly affected MIB and geosmin removal by mordenite zeolites.

To assess the adsorption capacity of zeolites for ozone, ozone uptake experiments were completed with mordenite and Y zeolites. Results of the uptake experiments indicated that

mordenite and Y zeolites are capable of adsorbing ozone such that the ozone concentration in zeolite pores can exceed the bulk water ozone concentration by approximately three orders of magnitude. To investigate the effectiveness of ozonation for MIB and geosmin removal in the presence of zeolites or activated carbon, three sets of batch experiments for MIB and geosmin removal were performed in both ozone-demand free UPW and LMW as follows: (1) MIB/geosmin removal by ozone only, (2) MIB/geosmin removal by zeolite or carbon only, and (3) MIB/geosmin removal by zeolite or carbon and ozone. Results obtained for both MIB and geosmin removal from UPW and LMW showed that the presence of zeolites or activated carbon during ozonation did not offer a measurable advantage over conventional ozonation for MIB removal. In contrast, the presence of Y zeolite during ozonation improved geosmin removal over ozonation or zeolite addition alone.

Removal of 2-Methylisoborneol and Geosmin by High-Silica Zeolites and Powdered Activated Carbon in the Absence and Presence of Ozone

by
Bilgen Yuncu

A dissertation submitted to the Graduate Faculty of
North Carolina State University
in partial fulfillment of the
requirements for the Degree of
Doctor of Philosophy

Civil Engineering

Raleigh, North Carolina

2010

APPROVED BY:

_____	_____
Joel J. Ducoste	Francis L. de los Reyes
_____	_____
Dean L. Hesterberg	Detlef R.U. Knappe Chair of Advisory Committee

DEDICATION

To my parents, Selma and Hafit YUNCU, and
my sister Eren YUNCU

For their unconditional love and support

BIOGRAPHY

Bilgen Yuncu graduated in June 2000 with a B.S. in Environmental Engineering from Middle East Technical University, Ankara, Turkey. After obtaining her M.S. degree in 2003 in the same department, Bilgen came to the United States in 2005 and continued her graduate studies towards a Ph.D. degree in the Department of Civil, Construction and Environmental Engineering at North Carolina State University under the direction of Dr. Detlef Knappe.

ACKNOWLEDGEMENTS

I would like to express my deepest gratitude to my advisor and mentor Dr. Detlef Knappe for his valuable guidance, encouragement, patience, and trust throughout this journey. I would like to thank the members of my advisory committee, Dr. Joel Ducoste, Dr. Francis de los Reyes, Dr. Dean Hesterberg, and Dr. George Roberts for their guidance and interest in this study. Also, I would like to acknowledge Water Research Foundation for funding this research.

I would like extend my thanks to all my friends and colleagues in Environmental Engineering Laboratory at North Carolina State University. Their company made the long hours in the lab enjoyable. Special thanks to David Black, Fang Xu and Qianru Deng for their help and effort in my experiments. Among all my great friends in and out of Raleigh who kept me sane for the last 5 years with all their support and motivation, I want to express my special appreciation to Ozge Kaplan Akman, Baha Akman and Onur Kurum for sharing good times along with the hard times.

And last but certainly not least, this dissertation is dedicated to my parents, Selma and Hafit Yuncu, and my sister, Eren Yuncu. This would not have been possible without them.

TABLE OF CONTENTS

LIST OF TABLES

LIST OF FIGURES

ABBREVIATIONS

1/n	Freundlich isotherm parameter
1MC	1-methylcamphene
2MB	2-methylenebornane
2M2B	2-methyl-2-bornene
Å	Ångstrom
AOP	advanced oxidation process
BET	Brunauer-Emmett-Teller
°C	degrees Celsius
C	aqueous phase concentration
C_0	initial aqueous phase concentration
CAL	calibration standard
CAS #	Chemical Abstracts Service registry number
C_e	equilibrium liquid-phase adsorbate concentration
CI	chemical ionization
CLCJAWA	Central Lake County Joint Action Water Agency
cm	centimeter
DOC	dissolved organic carbon
DVB	divinylbenzene
EI	electron ionization
g	gram
GAC	granular activated carbon
GC	gas chromatograph, gas chromatography
GC-CI/MS/MS	gas chromatography – chemical ionization tandem mass spectrometry
GC-EI/MS	gas chromatography – electron ionization mass spectrometry

h	hour
K	Freundlich isotherm parameter
K_p	partition coefficient
K_{ow}	octanol-water partition coefficient
k”	second order reaction rate constant
IS	internal standard
L	liter
LC-MS	liquid chromatography – mass spectrometry
LFB	laboratory fortified blank
LRB	laboratory reagent blank
LMW	Lake Michigan water
M	moles per liter
m	meter
mCi	milliCurie
MIB	2-methylisoborneol
mg	milligram
min	minute
mL	milliliter
mM	millimoles per liter
mm	millimeter
MS	mass spectrometer, mass spectrometry
MTBE	methyl *tertiary*-butyl ether
MWDSC	Metropolitan Water District of Southern California
µL	microliter
µg	microgram
µm	micrometer
N	equivalents per liter = normality
ng	nanogram
nm	nanometer
NOM	natural organic matter

oz	fluid ounce
PAC	powdered activated carbon
PDMS	polydimethylsiloxane
PTFE	polytetrafluoroethylene = “Teflon”
q_e	equilibrium solid phase adsorbate concentration = “adsorption capacity”
q_{10}	adsorption capacity at an aqueous phase concentration of 10 ng/L
R^2	coefficient of determination
s	second
SEM	scanning electron micrograph
S-PAC	sub-micrometer diameter powdered activated carbon
SPME	solid-phase microextraction
SiO_2/Al_2O_3	molar silica to alumina ratio of zeolites; an increasing SiO_2/Al_2O_3 ratio indicates increasing zeolite hydrophobicity
TCE	trichloroethene = trichloroethylene
T&O	taste and odor
TOC	total organic carbon
TRW	Tar River water
UPW	ultrapure water
UV	ultraviolet
V	volt

CHAPTER 1

INTRODUCTION AND OBJECTIVES

Algae and cyanobacteria (blue-green algae) are responsible for many episodes of unpleasant taste and odor in drinking water sources (e.g. Izaguirre et al. 1982, 2004, Jüttner 1983, Burlingame et al. 1986, 1992, AwwaRF and Lyonnaise des Eaux 1987, 1995). Taste and odor problems in drinking water continue to be widespread; e.g., utility responses to a survey conducted by Suffet et al. (1996) showed that 43% of North American utilities experienced taste and odor episodes that lasted more than one week. Among the most frequent and challenging taste and odor problems are those associated with earthy and musty odors attributed to the presence of 2-methylisoborneol (MIB) and (E)-1,10-dimethyl-9-decalol (geosmin). MIB and geosmin present treatment challenges to utilities because of (1) their low odor threshold concentrations, (2) their resistance to oxidation by common oxidants, and (3) the moderate effectiveness of activated carbon adsorption processes.

Odor threshold concentrations for MIB and geosmin are approximately 9 and 4 ng/L, respectively (AwwaRF and Lyonnaise des Eaux 1995), but odor thresholds can be lower for some drinking water consumers (e.g., Young et al. 1996). To avoid consumer complaints, utilities therefore need to remove MIB and geosmin to levels that are lower than the maximum contaminant levels (MCLs) of most regulated organic contaminants. Adding to

this challenge is that MIB and geosmin, two alicyclic alcohols, are difficult to remove by conventional oxidants. Poor removal in ultrapure water suggests that molecular ozone is not effective for MIB and geosmin oxidation (Lalezary et al. 1986, Peter and von Gunten 2007). On the other hand, ozone is moderately effective in natural water because hydroxyl radical formation rates are higher in the presence of NOM and other natural water constituents (Glaze et al. 1990, Ho et al. 2004). Limitations with ozone-based oxidation processes for taste and odor control include cost related to high ozone dose requirements and bromate formation.

Many utilities rely on the addition of powdered activated carbon (PAC) to control seasonal occurrences of earthy/musty odors. The effectiveness of PAC is typically compromised by the presence of natural organic matter (NOM), interfering water treatment chemicals (e.g., coagulant, chlorine), short contact times, and limitations associated with the PAC feed equipment. When chlorine comes into contact with PAC, the PAC surface is oxidized by chlorine and becomes less effective for MIB and geosmin adsorption (e.g., Gillogly et al. 1998a). Furthermore, only a fraction of the available adsorption capacity of PAC is used when contact times are short. Granular activated carbon (GAC) adsorption has been applied with reasonable success for taste and odor control; however, GAC bed life can vary greatly. NOM adsorption adversely affects the performance of GAC in adsorption mode while the presence of microorganisms capable of degrading MIB and geosmin can yield very long

GAC bed lives because the GAC functions primarily as a biological filter. The latter situation particularly applies to GAC filters that receive ozonated water. While biological MIB/geosmin removal in biological filters is possible (Tanaka et al. 1996, Saito et al. 1999, Ho et al. 2007), it is not reliably observed in all studies.

Overall, treatment costs associated with taste and odor control can be high, and the desired water quality is not always met with existing treatment technologies. There is considerable need, therefore, to develop and evaluate innovative water treatment processes for their potential to reliably remove taste and odor (T&O) causing compounds such as MIB and geosmin from drinking water sources in a cost-effective manner.

The principal objective of this research was to investigate two innovative treatment methods for the control of earthy/musty odors associated with the presence of MIB and geosmin in drinking water. The first treatment method is an adsorption/reaction process based on the use of high-silica zeolites, a class of catalytic adsorbents that has not been studied extensively for water treatment applications. The second treatment method is an adsorption/oxidation process based on the combined use of high-silica zeolites and ozone (zeolite-enhanced ozonation). Specific objectives of this study were:

(1) Determine zeolite pore sizes and SiO_2/Al_2O_3 ratios (zeolite hydrophobicity increases with increasing SiO_2/Al_2O_3 ratio) that are most suitable for the adsorptive/reactive removal of MIB and geosmin from water,

(2) Assess the effects of co-adsorbing background water matrix constituents (NOM, cations) on MIB/geosmin removal by high-silica zeolites,

(3) Measure ozone adsorption capacities of high-silica zeolites,

(4) Compare MIB/geosmin removal rates achievable with zeolite-enhanced ozonation to those achievable with conventional ozonation,

(5) Determine whether the presence of PAC during ozonation affects the removal of MIB/geosmin

Experiments were conducted with high-silica zeolites exhibiting different pore sizes (silicalite, mordenite, beta, and Y) and a wide range of SiO_2/Al_2O_3 ratios (12-810). For reference, MIB and geosmin uptake data were also obtained for two activated carbons (one coal-based and one coconut-shell-based). Experiments were conducted in ultrapure water (UPW), salt-amended UPW (NaCl, $CaCl_2$, and salt mixture), and Lake Michigan water (LMW) to assess background water matrix effects on MIB/geosmin removal. Furthermore, batch adsorption experiments were conducted to measure ozone uptake by high-silica zeolites and to evaluate how the presence of zeolites or PAC affects the removal of MIB and geosmin during ozonation. Results for the adsorptive/ reactive removal of MIB and geosmin

by high-silica zeolites and PACs are summarized in Chapter 4 while results obtained with zeolites and PAC in the presence of ozone are presented in Chapter 5.

CHAPTER 2

LITERATURE REVIEW

2.1 MIB AND GEOSMIN

Several species of cyanobacteria and actinomycetes are capable of producing the off-flavor compounds 2-methylisoborneol and geosmin (AwwaRF and Lyonnaise des Eaux 1995, Izaguirre and Taylor 2004, Zaitlin and Watson 2006). Odor threshold concentrations for MIB and geosmin are approximately 9 and 4 ng/L, respectively (AwwaRF and Lyonnaise des Eaux 1995), and odor thresholds can be lower for some drinking water consumers (e.g., Young et al. 1996). Molecular structures of MIB and geosmin are shown in Figure 2.1, and selected parameters describing the physicochemical characteristics of the two alicyclic alcohols are summarized in Table 2.1. Comparing MIB and geosmin, the parameters in Table 2.1 illustrate that geosmin molecules are larger and more hydrophobic than MIB molecules.

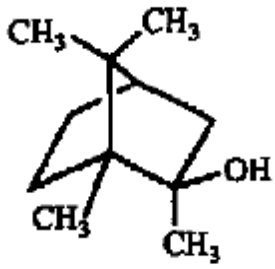

MIB

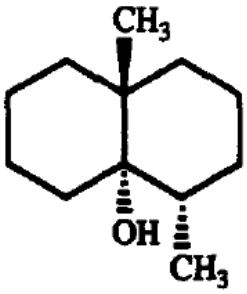

Geosmin

Figure 2.1 Molecular structures of MIB and geosmin

Table 2.1 Properties of MIB and geosmin

Compound name	**2-MIB**	**Geosmin**
CAS #	2371-42-8	23333-91-7
Formula	$C_{11}H_{20}O$	$C_{12}H_{22}O$
Molecular Weight	168.28 g/mol	182.31 g/mol
Log K_{ow} [*]	3.31	3.57
Aqueous Solubility (25°C) [*]	305–345 mg/L	157–295 mg/L
Molar Volume (20°C) [†]	173.7 cm^3/mol	184.9 cm^3/mol

[*] EPI Suite v4.0 prediction (http://www.epa.gov/oppt/exposure/pubs/episuitedl.htm)
[†] Estimates from ACD/ChemSketch 11.0 Freeware (http://www.acdlabs.com)

2.2 ZEOLITES

The zeolite group of minerals was discovered in 1756 by the Swedish mineralogist Baron Cronstedt. It was only in the 1950s, however, when these sediments were studied in more detail by means of X-ray diffraction, that scientists and engineers began to envision industrial uses for zeolites (Pfenninger 1998). Today, zeolites are a high-value family of commercial materials. Currently, some 40 different natural zeolite forms are known and well characterized (Pfenninger 1998), and the number of structure types confirmed by 2001, considering both natural and synthetic materials, was 133 (McCusker and Baerlocher 2001). Zeolites are microporous materials with uniform pore dimensions, and they are attractive materials for many applications because they are (1) selective adsorbents, (2) ion exchangers, (3) solid acid catalysts, and (4) thermally stable (Pfenninger 1998, Szostak 1998). In 1997, the total world usage of zeolites was approaching 1.6 million tons per year, the detergent industry being the biggest consumer. In the field of adsorption and desiccation, zeolites are being used for the removal of moisture and undesired substances from gas or liquid mixtures. For catalysis, zeolites are mostly used for fluid catalytic cracking applications and in the hydrocracking market (Pfenninger 1998). Natural zeolites have been used as a soft, high-brightness additive to paper and as a selective ion exchange agent for the removal or concentration and isolation of radioactive species from waste waters generated by nuclear installations. Another application for natural zeolites is NH_4^+ removal in municipal

wastewater treatment plants (Pfenninger 1998). Recent studies have also shown that high-silica zeolites are effective for the removal of the fuel additive methyl tertiary-butyl ether (MTBE) from water (Anderson 2000, Li et al. 2003, Knappe et al. 2007, Rossner and Knappe 2008).

The primary zeolite building blocks are TO_4 tetrahedra, where T is either a $Si^{(IV)}$ or $Al^{(III)}$ atom located at the center of the tetrahedron (Figure 2.2).

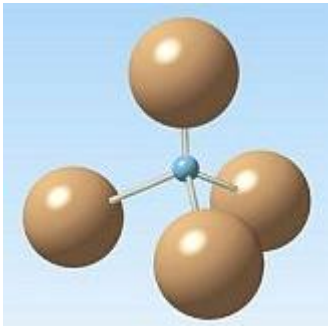

Source: Tarbuck et al. (2002)

Figure 2.2 Primary tetrahedral building unit of zeolites. Small atom at center is silicone, larger atoms defining the edges of tetrahedron are oxygen.

Tetrahedra are linked via their oxygen atoms to other tetrahedra to form structural subunits, such as the sodalite unit (Figure 2.3a), that define the framework of zeolites. Figure 2.3a depicts two alternative visualizations of the sodalite unit — one shows only T atoms (represented by the junctions of the schematic) while the other shows both T and O atoms. Figure 2.3b summarizes eight common structural subunits of zeolites. The linking of

recurring structural subunits produces the crystalline framework structure of a zeolite, within which exist voids and channels of discrete and regular size. This pore size regularity makes zeolites different from other molecular sieves such as microporous charcoal and amorphous carbon. Zeolite pore openings range from 3 to > 7 Å depending on the framework structure (Szostak 1998).

(a)

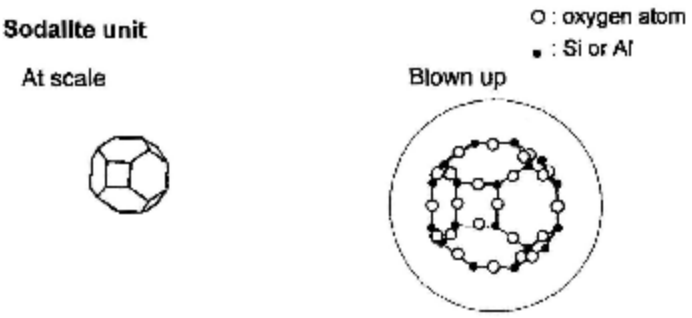

(b)

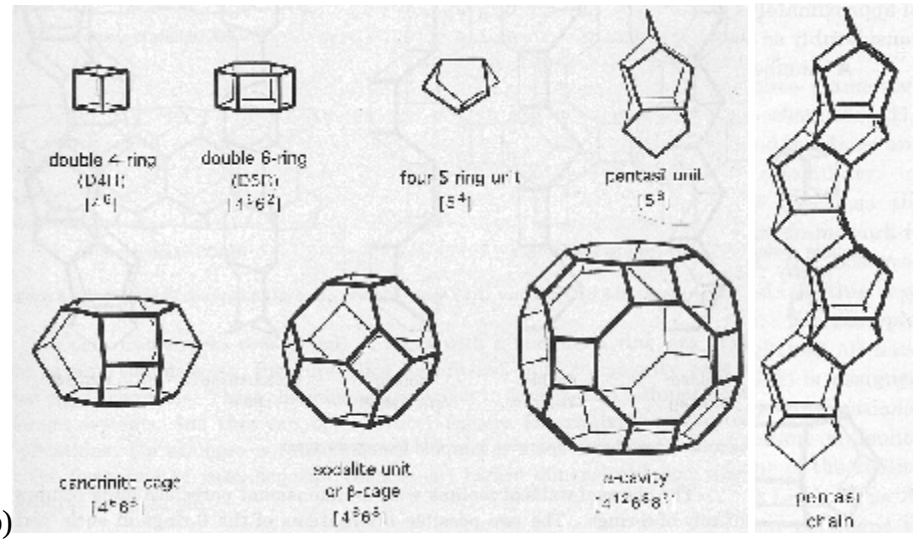

Sources: (a) Rouquerol et al. (1999), (b) McCusker and Baerlocher (2001)

Figure 2.3 Structural subunits of zeolites: (a) the sodalite cage, (b) common structural subunits

The crystalline zeolite framework carries a negative charge, and its magnitude depends on the amount of isomorphically substituted $Al^{(III)}$. This charge is balanced by cations localized in non-framework positions (cavities or channels) to obtain a neutral net charge of the structure. Typical cations include the alkaline (Li^+, Na^+, K^+, Rb^+, Cs^+) and the alkaline earth (Mg^{2+}, Ca^{2+}, Ba^{2+}) elements, as well as NH_4^+, H_3O^+ (H^+), TMA^+ (tetramethylammonium) and other nitrogen-containing organic cations (Szostak 1998). The framework charge and exchangeable cations are important as they determine the ion exchange and catalytic properties of zeolites. Zeolites with low $Al^{(III)}$ content or constituted exclusively of $Si^{(IV)}$ in the tetrahedral centers have either a small negative or no framework charge and therefore exhibit a high degree of hydrophobicity and poor ion exchange capacity (Szostak 1998). The degree of hydrophobicity, which increases with increasing SiO_2/Al_2O_3 ratio of the structure, determines a zeolite's suitability for the removal of organic contaminants from aqueous solutions (e.g., Kawai et al. 1994, Li et al. 2003, Knappe et al. 2007). In contrast, the catalytic activity of zeolites increases with increasing zeolite acidity (or decreasing SiO_2/Al_2O_3 ratio).

Among the many zeolites structures presently known, this work focused on four: ZSM-5/Silicalite (MFI), Mordenite (MOR), Beta (*BEA), and Y (FAU) zeolites.

2.2.1 ZSM-5/Silicalite (MFI) zeolites

The most important member of the MFI family is the ZSM-5 zeolite and its pure silica form, which is known as silicalite. The 'hollow tube' representation of ZSM-5 (MFI) zeolite pores and the MFI framework are presented in Figure 2.4. Zeolite ZSM-5 is constructed from pentasil units that are linked together in pentasil chains (see Figure 2.3b). Mirror images of these chains are connected by oxygen bridges to form corrugated sheets with ten-ring channel openings (i.e. the perimeter of the elliptical channel opening is formed by ten T atoms). Figure 2.4a highlights such a corrugated sheet in the y-z plane. Oxygen bridges link each sheet to the next to form a three-dimensional structure with straight ten-ring channels parallel to the corrugations in the y-dimension. These channels are intersected by sinusoidal ten-ring channels in the x-y plane (Figure 2.4b). The minor and major axis dimensions are, respectively, 5.1×5.5 Å for the sinusoidal channels and 5.3×5.6 Å for the straight channels. The SiO_2/Al_2O_3 ratio of this zeolite type ranges from about 20 to infinity (Szostak 1992).

(a) 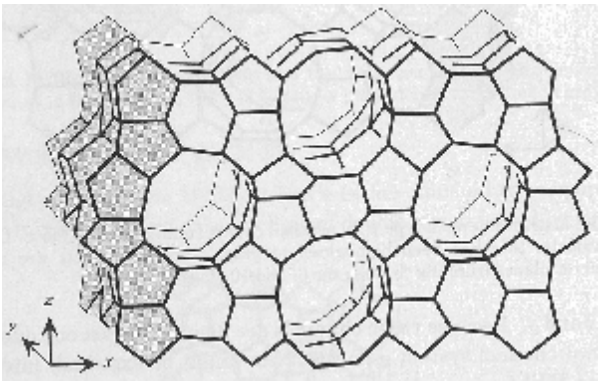 **(b)** 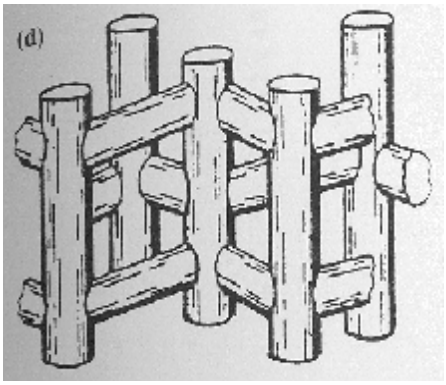

Sources: (a) McCusker and Baerlocher (2001), (b) Szostak (1998) .
Figure 2.4 Schematics of ZSM-5 zeolite pores: (a) the MFI framework and (b) the 'hollow-tube' representation

Water adsorption studies showed that (1) the quantity of adsorbed water in ZSM-5 zeolites is dependent on the zeolite hydrophobicity and (2) the three-dimensional array of hydrogen-bonded water molecules cannot easily penetrate the pores of ZSM-5 zeolites without considerable distortion of the hydrogen bonds (Carrott et al. 1991). Because of its negligible $Al^{(III)}$ content, silicalite is a hydrophobic zeolite and thus exhibits a low affinity for water (Kenny and Sing 1990).

2.2.2 Mordenite (MOR) zeolite

The Mordenite framework type is formed with the "four 5-ring" subunits shown in Figure 2.3b. These units are linked to one another by common edges to form chains as illustrated in Figure 2.5, and mirror images of these chains are connected by oxygen bridges to form corrugated sheets (highlighted in gray in Figure 2.5a). The corrugated sheets are connected

together to form oval twelve- and eight-ring channels along the z direction (Figure 2.5). These channels are connected by eight-ring channels that are displaced with respect to one another (Figure 2.5b). The twelve- and eight-ring channels have dimensions of 6.5 × 7.0 Å and 2.6 × 5.7 Å, respectively. Given the small size of the eight-ring channels, the MOR channel system is effectively one-dimensional (McCusker and Baerlocher 2001). Mordenite with a low SiO_2/Al_2O_3 ratio is highly selective for cesium and strontium, making it suitable for the treatment of radioactive waste (Szostak 1992).

(a) 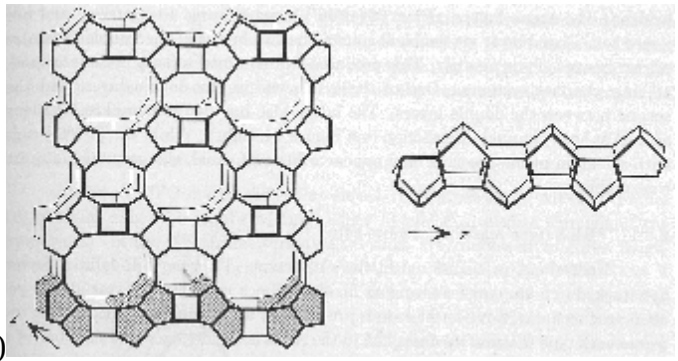 (b) 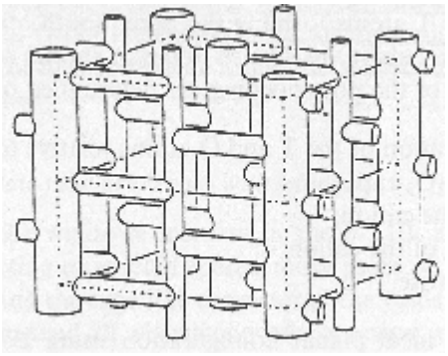

Sources: (a) McCusker and Baerlocher (2001), (b) Szostak (1998).

Figure 2.5 Schematics of mordenite (MOR) zeolite pores: (a) the MOR framework and (b) the 'hollow-tube' representation

2.2.3 Beta (*BEA) zeolite

Beta zeolites have well-defined layers (composed of "four 5-ring" subunits (see Figure 2.3b) joined by 4-ring subunits) that are stacked in a disordered way along the z direction. No ordered material has been produced to date. The asterisk preceding the three-letter code for

this zeolite type denotes that the framework type in Figure 2.6 is an idealized end member of a series. Adjacent layers, shown separately in Figure 2.6, are connected by a rotation of 90°. The rotation can be in a clockwise or counterclockwise direction, generating the disorder of the framework. Despite this disorder, a three-dimensional twelve-ring channel system is formed (McCusker and Baerlocher 2001). The pore dimensions of the channel system are 6.5 × 5.6 Å and 7.5 × 5.7 Å (Szostak 1992).

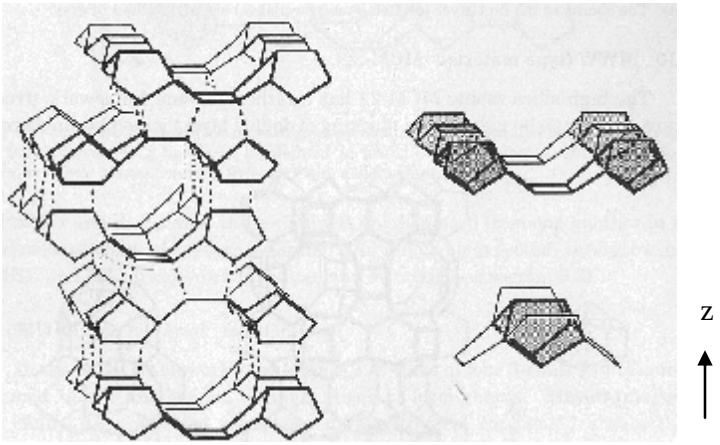

Source: McCusker and Baerlocher (2001)
Figure 2.6 The idealized *BEA framework type with all layers related to one another via 90° counterclockwise rotation. The well-defined layer and its building unit are shown separately.

2.2.4 Y (FAU) zeolite

The framework of the faujasite structure can be described as a linkage of TO_4 tetrahedra in a truncated octahedron. The truncated octahedron is referred to as the sodalite unit or sodalite

cage (Figure 2.3a) (Szostak 1992). In the faujasite structure, the sodalite units are linked together at the six-ring ends (i.e., the hexagonal faces of the sodalite unit) in a manner that is analogous to the arrangement of C-atoms in diamonds (Figure 2.7). The Y-zeolite (faujasite structure) has circular, 12-ring windows with a diameter of 7.4 Å (or 7.4 × 7.4 Å) and supercages with a diameter of about 13 Å (Rouquerol et al. 1999).

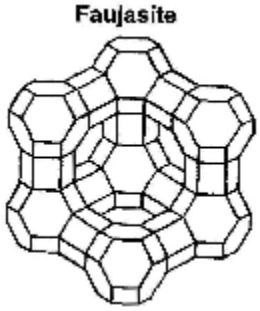

Source: Rouquerol et al. (1999).
Figure 2.7 The faujasite framework type

2.3 REMOVAL OF ORGANIC MICROPOLLUTANTS BY HIGH-SILICA ZEOLITES

Ellis and Korth (1993) were among the first researchers to evaluate the effectiveness of high-silica zeolites for the removal of trace organic compounds in a drinking water treatment context. Studying the adsorption of MIB and geosmin from aqueous solution, Ellis and Korth (1993) made two important observations: (1) the addition of humic acid to ultrapure water did not change the effectiveness of the tested Y-zeolite for MIB and geosmin removal, and (2) MIB and geosmin removal did not only occur by adsorption but also via a dehydration

reaction on Brønsted acid sites of the tested Y-zeolite (SiO_2/Al_2O_3 = 80) that led to formation of non-odorous dehydration products. For the latter observation, the data of Ellis and Korth (1993) were qualitative at best, however, because dehydration products were measured after dissolving the zeolite in hydrofluoric acid to recover adsorbed compounds. As a result, it was not clear to what extent the dehydration reaction was attributable to Brønsted acid sites of the zeolite and to what extent to the hydrofluoric acid addition.

Kawai et al. (1994) studied chloroform adsorption from water using ZSM-5 and Y zeolites (SiO_2/Al_2O_3 ratios ranged from 25 to 1000 for ZSM-5 zeolites and from 5.5 to 770 for Y zeolites). For ZSM-5 zeolites, Kawai et al. (1994) obtained a large increase in chloroform adsorption capacity between SiO_2/Al_2O_3 ratios of 25 and 70, but only a smaller increase between SiO_2/Al_2O_3 ratios of 70 and 1000. For Y zeolites substantial increases in chloroform adsorption capacity were observed between SiO_2/Al_2O_3 ratios of 5.5 and 224, but above this value, only small differences were obtained. These results suggest that SiO_2/Al_2O_3 ratios in excess of about 100 may only have a small effect on organic contaminant adsorption from the aqueous phase. In agreement with these data, results of Knappe et. al (2007) showed that MTBE adsorption from water onto ZSM-5 zeolite was relatively constant when SiO_2/Al_2O_3 ratios ranged from 90-400.

Centi et al. (2002) found that the exchangeable cation of ZSM-5 zeolites plays a critical role in the adsorption and hydrolysis of MTBE. When exposed to a hydrogen-form ZSM-5 zeolite (SiO_2/Al_2O_3=25), MTBE hydrolyzed to form tertiary butyl alcohol (TBA) and methanol. In contrast, the sodium-form of ZSM-5 with the same SiO_2/Al_2O_3 ratio did not react with MTBE. Centi et al. (2002) also found that a hydrogen-form ZSM-5 zeolite with a SiO_2/Al_2O_3 ratio of 80 had an increased catalytic activity and adsorption capacity compared to a hydrogen-form ZSM-5 zeolite with a SiO_2/Al_2O_3 ratio of 25. Using hydrogen-form ZSM-5 zeolites with SiO_2/Al_2O_3 ratios ranging from 90-400, Knappe et al. (2007) did not find evidence for MTBE hydrolysis, however, when experiments were conducted in buffered ultrapure water that contained Na^+ concentrations that are typical for many natural waters (~1.5 mM).

Because of their well-defined pore sizes it may be possible to select high-silica zeolites that target the removal of specific micropollutants while minimizing access of interfering NOM constituents that decrease the adsorption capacity of traditional adsorbents such as powdered and granular activated carbon. For example, silicalite appears to be especially suitable for the adsorptive removal of MTBE from drinking water sources and exhibits a larger MTBE adsorption capacity than activated carbons with a considerably larger BET surface area (Knappe et al. 2007). Furthermore, in a packed bed adsorber application, silicalite was immune to NOM preloading effects that markedly decreased the MTBE removal

effectiveness of a granular activated carbon (GAC) adsorber that was operated in parallel to the silicalite adsorber (Rossner and Knappe 2008).

In terms of material cost, high-silica zeolites (~$7/lb and up) are more expensive than activated carbons (~1-2/lb). However, the results of Knappe et al. (2007) showed that the higher MTBE adsorption capacity of zeolites compared to activated carbon was sufficient to make up a large part of the cost difference. Also, it may be possible to regenerate spent high-silica zeolite with steam or microwave methods rather than with more energy-intensive thermal methods because NOM removal is not a requirement during the regeneration step. This opportunity could further lower the life-cycle cost of zeolite-based adsorption systems. High-silica zeolites are marketed in the form of powders or extrudates. As a result, zeolites can be applied in water treatment plants in a manner that is analogous to activated carbon; i.e., addition of the powdered form at the intake or near the head of the plant or use of the extrudate form in a packed bed adsorber configuration.

2.4 OXIDATION OF MIB AND GEOSMIN WITH OZONE

Numerous studies have shown that ozone successfully oxidizes MIB and geosmin at sufficiently large doses (Hattori 1988, Lundgren et al. 1988, Terashima 1988, Glaze et al. 1990). For example, Terashima (1988) observed a 75-100% decrease in geosmin and MIB

concentrations with ozone doses of 2-5 mg/L. Likewise, an ozone dose of 3 mg/L oxidized geosmin and MIB below the threshold odor concentration (Hattori 1988). MIB and geosmin oxidation by ozone occurs more readily in natural waters than in pure water because hydroxyl radical formation is favored in natural waters (Terashima 1988, McGuire and Gaston 1988, Glaze et al. 1990, Liang 2006). The hydroxyl radical, which forms as ozone decomposes in water, is a more effective oxidant for geosmin and MIB than ozone itself (Glaze et al. 1990, Westerhoff et al. 2006, Peter and von Gunten 2007). As a result, the effectiveness of ozone for MIB and geosmin removal was lower in the work of Lalezary et al. (1986), in which highly purified water was employed. Second order rate constants describing the oxidation of MIB and geosmin by ozone and the hydroxyl radical were recently determined by Peter and von Gunten (2007) and are summarized in Table 2.2.

Table 2.2 Second order rate constants for the oxidation of MIB and geosmin by ozone and the hydroxyl radical

	k''_{O3} (M^{-1} s^{-1})	$k''_{.OH}$ (10^9 M^{-1} s^{-1})
MIB	0.35	5.09
Geosmin	0.10	7.80

The effectiveness of ozone for MIB and geosmin oxidation depends on the ozone dose to total organic carbon ratio (O_3/TOC) as well as the alkalinity and pH of the water. Based on the results of Glaze et al. (1990), Ferguson et al. (1990), and Nerenberg et al. (2000), O_3/TOC ratios of about 0.7 to 0.8 yield MIB removals in the range of about 40 to 80%. In

contrast, MIB removals of 73 to 92% were observed at O_3/TOC ratios of about 1.4 to 1.6. At a given pH and O_3/TOC ratio, the effectiveness of ozone for MIB and geosmin oxidation is greater in low alkalinity waters, in which hydroxyl radical scavenging by (bi)carbonate ions is less important (Glaze et al. 1990). In addition, hydroxyl radical formation is facilitated as pH increases, which suggests that the effectiveness of ozone for MIB and geosmin oxidation is greater at higher pH values for a given alkalinity and O_3/TOC ratio.

2.5 ZEOLITE-ENHANCED OZONATION

The zeolite-enhanced ozonation process concept was introduced by Fujita et al. (2004a,b). Recognizing that high-silica zeolites are capable of adsorbing organic compounds, Fujita et al. (2004a) further showed that hydrophobic ZSM-5 (or silicalite) and mordenite zeolites are capable of adsorbing ozone from the aqueous phase. Thus, in the zeolite-enhanced ozonation process, both the targeted micropollutant and the oxidant are concentrated inside of zeolite pores. As a result, micropollutant oxidation rates, which are first order with respect to the ozone concentration and first order with respect to the micropollutant concentration, can be greatly enhanced compared to those obtained with conventional ozonation processes. For example, Fujita et al. (2004b) showed that the oxidation of trichloroethylene (TCE) reached nearly 75% after a contact time of 7.5 seconds in the zeolite-enhanced ozonation process (ozone dose = 1.5 mg/L) while it was <10% at the same contact time for conventional

ozonation (ozone dose = 6.5 mg/L). Experiments with TCE were conducted by dosing ozone into the feed water that was passed through a column, which, in the zeolite-enhanced ozonation case was packed with a silicalite zeolite. Using MIB as a target compound, Sagehashi et al. (2005a) developed rate data in ultrapure water suggesting that 90% MIB conversion can be achieved in the zeolite-enhanced ozonation process with an ozone dose of 0.07 mg/L and a contact time of 1 minute. However, a follow-up study conducted with natural water showed that ~95% MIB conversion required an ozone dose of 4.18 mg/L and a contact time of 18 seconds. In the latter study, treatment conditions that would have been required to achieve the same level of MIB conversion by conventional ozonation were not shown. For MIB removal experiments, Sagehashi et al. (2005a,b) employed a Y zeolite for zeolite-enhanced ozonation experiments.

Although the results of Sagehashi et al. (2005a,b) suggest that zeolite-enhanced ozonation may be an effective process for the removal of MIB, several issues require further investigation. For example, Sagehashi et al. (2005b) worked with very high MIB concentrations (0.2 - 1.5 mg/L), and even higher initial MIB concentrations (up to 7.4 mg/L) were used in experiments conducted with ultrapure water (Sagehashi et al. 2005a). To assess whether the zeolite-enhanced ozonation process is effective for drinking water treatment, the effectiveness of the zeolite-enhanced ozonation process needs to be studied at environmentally relevant MIB concentrations. Also, Sagehashi et al. (2005a,b) conducted

their studies with a Y zeolite that does not effectively adsorb ozone (Fujita et al. 2004a) and on which adsorbed MIB can be displaced be natural organic matter (Sagehashi et al. 2005b). Therefore, zeolites with different pores sizes should be investigated to identify whether zeolite framework types exist that can effectively adsorb both MIB in the presence of NOM and that are also effective adsorbents for ozone. Finally, no information on geosmin removal by the zeolite-enhanced ozonation process is available to date.

2.6 ACTIVATED CARBON

2.6.1 Ozonation in the Presence of Activated Carbon

Promoters that enhance the formation of hydroxyl radicals have been used to increase the efficiency of ozonation process for the oxidation of micropollutants. Such processes are known as advanced oxidation processes (AOPs). Because of their high reactivity and low selectivity, hydroxyl radicals that are generated in AOPs are mostly consumed by competitive reactions with the water matrix. (e.g. by reactions with NOM constituents and with (bi)carbonate).

In order to overcome the shortcomings of AOPs, heterogenous catalytic ozonation has been introduced to increase ozonation performance. Activated carbon can also exhibit catalytic properties due to its very high surface area and surface-active functional groups. Numerous studies have shown that activated carbon can accelerate ozone decomposition resulting in the formation of stronger oxidative species such as hydroxyl radicals (Faria et. al. 2006, Sanchez-Polo et. al. 2005, Ma et. al. 2004, Oh et. al. 2004, Beltran et. al., 2002a, Jans et. al., 1998).

Jans and Hoigne (1998) showed that activated carbon enhanced the degradation of ozone without affecting the stoichiometric yield factor of hydroxyl radical formation from ozone. On the other hand, Sanchez-Polo et al. (2005) reported that the ratio of the concentrations of hydroxyl radicals and ozone was increased by a factor of 3-5 in the presence of activated carbon and the activity of activated carbon decreased for extended ozone exposures. They concluded that this decrease may indicate that activated carbon could be an initiator or promoter for the ozone transformation into hydroxyl radicals rather than acting as a catalyst.

Sanchez-Polo et al. (2005) also showed that the chemical and textural properties of the activated carbon are the governing factor for ozone transformation into hydroxyl radicals and that activated carbons with highest basicity and surface areas were the most efficient. Faria

et. al. (2006) also reported similar results for the effect of surface chemistry and textural properties of activated carbon on ozone decomposition.

The combined use of activated carbon and ozone can significantly increase the removal rate of organic pollutants compared to conventional ozonation (Beltran et. al., 2002b, Sanchez-Polo and Rivera-Utrilla 2003, Ma et. al. 2004, Oh et. al. 2004). Presence of activated carbon during ozonation can catalyze the oxidation of organic pollutants by enhancing the formation of hydroxyl radicals that are produced as a result of the interaction of ozone with the surface of activated carbon. To the knowledge of the author, ozonation of MIB or geosmin in the presence of activated carbon has not been studied to date.

2.6.2 Sub-micrometer Sized Powdered Activated Carbon

In water treatment plants, the adsorption capacity of PAC is not fully utilized if the PAC-water contact times are too short to reach adsorption equilibrium. Two options to more fully utilize the adsorption capacity of PAC are (1) to provide a sufficient PAC residence time or (2) to enhance the uptake rate of PAC. It is known that smaller PAC particles yield faster adsorption kinetics than larger PAC particles (Weber et. al. 1983, Najm et. al. 1990) so reducing the PAC particle size could provide faster adsorption kinetics. For this purpose,

Matsui et. al. (2005, 2007, 2008) recently investigated the application of submicron sized activated carbon (S-PAC) which is an activated carbon of much finer particle size than traditional PAC, which has a mean particle diameter in the range of 0.6 to 0.8 μm.

Matsui et al. (2007, 2008, 2009) compared geosmin removal from ultrapure water with a wood-based PAC and its corresponding S-PAC. S-PAC showed a very fast adsorptive removal rate for geosmin. E.g., geosmin removal after a PAC contact time of 30 minutes was ~30% for traditional PAC and ~90% for the same dose of the corresponding S-PAC (Matsui et al., 2009). To date, no data describing MIB removal by S-PAC have been published, and no performance data of S-PAC for taste and odor compound removal from natural water are available.

CHAPTER 3

MATERIALS AND METHODS

3.1 MATERIALS

3.1.1 Water

Single-solute experiments for the evaluation of MIB or geosmin removal by high-silica zeolites, activated carbon, and ozone were conducted in UPW. UPW consisted of Raleigh, NC tap water that was treated by reverse osmosis, ion exchange, and granular activated carbon adsorption. The resistance of UPW was $\geq$ 14.85 MΩ/cm.

The effect of the background water matrix (NOM, inorganic constituents) on MIB and geosmin removal was evaluated in salt-amended UPW (NaCl or $CaCl_2$) and with LMW. LMW was collected by the Central Lake County Joint Action Water Agency (CLCJAWA) in Lake Bluff, IL. Prior to use in experiments, LMW was vacuum-filtered through 1-μm glass fiber (Osmonics, MSI, Westboro, MA) and 0.45-μm nylon membrane (Magna-R, MSI, Westboro, MA) filters that were placed in a 47-mm glass microanalysis filter holder (Fisher Scientific, Pittsburgh, PA). The TOC and dissolved organic carbon (DOC) of filtered LMW were 2.0 and 1.8 mg/L, respectively, the UV_{254} absorbance was 0.017 cm^{-1}, and the pH was

approximately 7.9. The total alkalinity and total hardness were approximately 140 and 104 mg/L as $CaCO_3$, respectively.

Ozone-demand-free UPW used in ozone uptake and zeolite-enhanced ozonation experiments was prepared by adding 3 mg/L O_3 to UPW and letting the O_3 dissipate completely prior to the initiation of an experiment. In addition, any buffers used in experiments involving ozone were prepared from ozone-demand-free water.

3.1.2 Adsorbents

Commercially available high-silica zeolites with four different framework types were studied to test the effects of zeolite pore size on MIB and geosmin removal. To quantify effects of zeolite hydrophobicity (i.e. SiO_2/Al_2O_3 ratio) on MIB and geosmin removal, mordenite zeolites with SiO_2/Al_2O_3 ratios in the range of 20 to 230 and Y zeolites with SiO_2/Al_2O_3 ratios of 12 and 810 were compared. The sources and characteristics of the tested zeolites are summarized in Table 3.1. For reference, MIB and geosmin uptake experiments were conducted with three activated carbons: one coal-based powdered activated carbon in its as-received form (WPH, Calgon Carbon Corporation, Pittsburgh, PA) and in its sub-micrometer diameter form (S-WPH); and one coconut-shell-based granular activated carbon (CC-602 – redesignated as AquaCarb 1230C, Westates Carbon, Siemens, Roseville, MN) that was

pulverized as described below. The S-WPH was produced by wet-milling WPH PAC in a bead mill. The average diameter (d_{50}) of S-WPH was ~ 0.3 µm whereas the average diameter of as-received WPH is around 17µm.

To enhance adsorption rates, all pelletized zeolites and the GAC were pulverized with a mortar and pestle until 95% by mass passed a 74-µm sieve (200 U.S. mesh). Upon sieving, the portion remaining on the sieve was recombined with the portion that passed through the sieve to prevent bias as a result of any physical and/or chemical differences between the two fractions. The pulverized adsorbent was dried at 105°C for one day and stored in a desiccator.

Prior to ozone uptake and zeolite-enhanced ozonation experiments, zeolites were conditioned in a 2N ammonium chloride solution (USP/FCC, Fisher Scientific, Pittsburgh, PA) to minimize reactions between ozone and hydroxide ions (Sagehashi et al. 2005a).

Table 3.1 Zeolite characteristics

Manufacturer's ID code	Manufacturer	Cation (*)	Pore dimensions (*)	SiO_2/Al_2O_3 (*)	BET surface area (m^2/g)	Code used in this study
HiSiv 3000	UOP, Mount Laurel, NJ	-	0.53 nm*0.55 nm (10-ring)	700	282	Silicalite-700
HSZ-690HOA	Tosoh Corporation, Tokyo, Japan	H^+	0.65 nm*0.70 nm (12-ring)	230	505	H-mordenite-230
CBV-90A	Zeolyst International, Valley Forge, PA	H^+	0.65 nm*0.70 nm (12-ring)	90	341	H-mordenite-90-1
H-MOR-90	Süd-Chemie, Munich, Germany	H^+	0.65 nm*0.70 nm (12-ring)	90	421	H-mordenite-90-2
H-MOR-40	Süd-Chemie, Munich, Germany	H^+	0.65 nm*0.70 nm (12-ring)	40	443	H-mordenite-40
H-MOR-20	Süd-Chemie, Munich, Germany	H^+	0.65 nm*0.70 nm (12-ring)	20	355	H-mordenite-20
CP811C-300	Zeolyst International, Valley Forge, PA	H^+	0.76 nm*0.64 nm (12-ring)	300	544	H-beta-300
HiSiv 1000	UOP, Mount Laurel, NJ	-	0.74 nm*0.74 nm (12-ring)	12	550	Y-12
HSZ-390HUA	Tosoh Corporation, Tokyo, Japan	H^+	0.74 nm*0.74 nm (12-ring)	810	806	H-Y-810

3.1.3 Adsorbates

The targeted taste and odor compounds in this study were 2-methylisoborneol (MIB) and geosmin. Stock solutions for each compound were prepared from pure MIB and geosmin (Wako Chemicals USA, Inc., Richmond, VA). To prepare stock solutions, 5 mg of MIB or geosmin were dissolved in 100 mL of UPW in the absence of an organic solvent carrier (Ho et al. 2004). Aqueous MIB and geosmin stock solutions were stored at 4°C, at which temperature they are stable for several years (Newcombe 2005). Over the 2.5-year period of this study, no change in MIB or geosmin concentrations was observed in the aqueous stock solutions. Additional experiments were conducted with ^{14}C-labeled MIB (American Radiolabeled Chemicals, Inc., St. Louis, MO). The ^{14}C-labeled MIB had a specific activity of 55 mCi/mmol and was dissolved in pure methanol. The methanol stock solution was stored in a refrigerator at 1.8°C.

3.1.4 Ozone stock solution

Ozone was produced with a bench-scale ozone generator (G11, Pacific Ozone Technology, Benicia, CA) using oxygen as the feed gas. Upon exiting the ozone generator, the gas was routed through two gas washing bottles (one empty, one containing pH 6 phosphate buffer) and subsequently bubbled through 1.5 L of ultrapure water in a round bottom flask that was

placed in an ice bath. The steady state concentration of the ozone stock solution was approximately 30 mg/L.

3.2 METHODS

3.2.1 Isotherm experiments

Adsorption isotherm experiments were conducted using high-silica zeolite doses between 4 and 1,000 mg/L and activated carbon doses between 0.15 and 30 mg/L. For single-solute experiments, adsorbents were transferred into 8-oz, 16-oz. or 32-oz. amber glass bottles depending on the targeted adsorbent dose (larger bottles for smaller doses). Adsorbents were added either in dry form (for doses $\geq$ 5 mg/L) or as a slurry (for doses <5 mg/L). The bottles were subsequently filled to the neck with UPW. After filling the bottles with UPW, a pre-determined volume of stock solution (^{14}C-labeled MIB, non-labeled MIB or geosmin) was added with a constant rate syringe (CR-700-200, Hamilton Co., Reno, NV) to yield an initial concentration of ~100 ng/L.

For experiments conducted with LMW, adsorbents were added after filling the bottles with LMW and spiking the target compound. Adsorbents were added last to simulate the

concurrent adsorption of MIB/geosmin and background water constituents (NOM, cations) that would take place when a powdered adsorbent is added in a treatment plant.

Bottles were capped with PTFE-faced silicon septa and open-top closures. The headspace in the bottles was ~5 mL or less, and results obtained in this study and at least one prior study (Chen et al. 1997) showed that a small headspace does not lead to MIB or geosmin losses. For isotherm experiments, a mixing time of 10 days in a rotary tumbler was used to obtain adsorption equilibrium. MIB or geosmin losses were not observed in triplicate blanks containing no adsorbent over that time period. Upon equilibration, samples were filtered through 0.22-µm MAGNA nylon membrane filters (Osmonics/MSI, Westboro, MA) that were placed in a 25-mm stainless steel syringe filter holder (Fisher, Pittsburgh, PA). The filters were soaked overnight in organic-free water prior to use. No buffer was added in single-solute isotherm experiments to eliminate possible effects of cations associated with the buffer salts on possible reactions of MIB and geosmin with Brønsted acid sites of zeolites.

3.2.2 MIB/geosmin uptake kinetics

To assess the effects of background matrix constituents (NOM, salts) on MIB/geosmin removal, batch kinetic tests were performed with powdered mordenite zeolites and with WPH PAC at adsorbent doses of 15.5 and 2 mg/L. Additional batch kinetic tests were

conducted with H-Y-810 zeolite, WPH PAC and S-WPH S-PAC at an adsorbent dose of 5 mg/L. Kinetic tests were conducted in UPW, UPW amended with 1 mM sodium chloride (NaCl, ACS grade, Fisher Scientific, Pittsburgh, PA) or 1 mM calcium chloride ($CaCl_2$, 99%, Sigma-Aldrich, St. Louis, MO) or a salt mixture containing 1 mM $CaCl_2$, 0.4 mM $MgCl_2$, 0.28 mM NaCl, 0.03 mM KCl (to match the approximate cation composition and ionic strength of LMW), and LMW. Non-labeled MIB and geosmin was spiked at an initial concentration of ~100 ng/L into a 32-oz. amber glass bottles containing the desired background water and mixed by using a PTFE-coated magnetic stir bar. After taking duplicate samples for determining the initial MIB/geosmin concentration, the desired amount of adsorbent was added under continued mixing. Samples for MIB/geosmin analysis were taken in duplicate at contact times of 15, 30, 60 and 120 minutes. Solution pH was measured at the beginning and end of each kinetic test (Orion pH meter 420 A, Fisher Scientific, Pittsburgh, PA).

3.2.3 Batch experiments for measuring ozone uptake by high silica zeolites

To measure ozone uptake by high-silica zeolites, batch experiments were performed in a borosilicate spinner flask (Fisher Scientific, Pittsburgh, PA) with a PTFE-coated magnetic spinner and PTFE-coated caps (Figure 3.1).

Figure 3.1 Spinner flask

Prior to ozone uptake experiments, the spinner flask and its components were cleaned with sodium persulfate (98+%, Fisher Scientific, Pittsburgh, PA) to oxidize ozone-demanding substances on materials coming into contact with ozone-spiked solutions. The spinner flask was placed on a magnetic stir plate, and the powdered zeolite was kept in suspension with the rotating spinner and an additional PTFE-coated magnetic stir bar. All ozone uptake experiments were conducted in UPW amended with 50 mM phosphoric acid (ACS grade, Sigma-Aldrich, St. Louis, MO) at pH 2 to minimize ozone decomposition in the aqueous phase. Also, the headspace was kept at minimum to prevent the volatilization of ozone. Samples were taken with a gas-tight syringe that was connected via a luer lock fitting to a stainless steel needle that was installed in the center lid of the spinner flask.

Ozone uptake experiments were conducted with H-Mordenite-230, H-Mordenite-90-1, H-Mordenite-40 and H-Y-810 zeolites using zeolite doses between 0.5 and 4 g/L. Experiments were initiated by adding ozone stock solution into ozone demand-free water to yield initial ozone concentrations of ~1.5 mg/L or ~0.75 mg/L. The aqueous ozone concentration was then measured over a period of 30 minutes. After 30 minutes, zeolite was added to the spinner flask, and the aqueous ozone concentration was monitored for an additional 90 minutes. Prior to spectrophotometric ozone analysis, all samples were filtered through a 0.22-μm PTFE membrane syringe filter with a polyethylene housing (Fisher Scientific, Pittsburgh, PA). This filter did not measurably alter the aqueous-phase ozone concentration, as established in screening tests. Ozone concentration profiles in the presence of zeolite were compared to those obtained in the absence of zeolite. Ozone uptake by the zeolite was calculated using Equation 3.1:

$$q_{O_3} = \frac{[O_3]_{zeolite-free\ blank} - [O_3]_{zeolite-containing\ sample}}{m_{zeolite}/V} \qquad (3.1)$$

where q_{O3} is the solid-phase ozone concentration, $[O_3]_{zeolite\text{-}free\ blank}$ is the average aqueous ozone concentration measured for the last three data points collected during the experiment in which no zeolite was added, $[O_3]_{zeolite\text{-}containing\ sample}$ is the average aqueous ozone concentration measured for the last three data points collected during the experiment in which zeolite was added, $m_{zeolite}$ is the mass of zeolite added, and V is the solution volume.

At the completion of each ozone uptake test, the solution pH was measured to ascertain that the desired pH of 2 was maintained throughout the experiment.

3.2.4 Batch experiments to evaluate the effectiveness of ozonation in the presence of zeolites or powdered activated carbon

The effects of adding zeolites or PAC on MIB and geosmin removal by ozone was evaluated in batch tests. For batch experiments, MIB and geosmin were spiked into UPW or LMW to yield an initial concentration of ~100 ng/L. Subsequently, powdered zeolite or activated carbon and ozone were added simultaneously into the flask. The aqueous ozone and T&O compound concentrations were measured for 60 minutes by periodically removing 5 mL aliquots with a gas tight syringe. When taking samples designated for MIB and geosmin analysis, 125 μL of 10 mM cinnamic acid (99+%, Alfa Aesar, Ward Hill, MA) was added to the syringe to quench the residual ozone (Dodd et al. 2006) and subsequently filtered through a 0.22-μm PTFE membrane syringe filter with a polyethylene housing (Fisher Scientific, Pittsburgh, PA). Samples designated for ozone analysis were directly filtered into 20-mL glass scintillation vials containing indigo reagent. H-Mordenite-90-1 and H-Y-810 zeolites were used at doses of 2 and 5 mg/L to evaluate the zeolite-enhanced ozonation process. To evaluate the effectiveness of ozonation in the presence of PAC, WPH and S-WPH activated

carbons were used at a dose of 5 mg/L. No pH adjustment was used for UPW or LMW. Solution pH was measured at the completion of each test.

3.2.5 Preparation of MIB dehydration products

A mixture of MIB dehydration products was prepared according to a procedure described by Schumann and Pendleton (1997). Briefly, 1 mg of MIB (neat form) was dissolved in 2 mL of ethyl acetate. To this solution, two drops of a solution prepared from 2 mL of ethyl acetate and 2 drops of concentrated H_2SO_4 were added. The mixture was heated for 30 minutes at 75°C. According to Schumann and Pendleton (1997), the reaction between MIB and H_2SO_4 at these conditions yields 3% 2-methyl-2-bornene (2M2B), 51% 1-methylcamphene (1MC), and 46% 2-methylenebornane (2MB).

3.2.6 MIB and geosmin analysis

Aqueous-phase concentrations of MIB and geosmin were analyzed with a gas chromatograph (GC) (Varian 3800, Palo Alto, CA) equipped with a split/splitless injector, a 30-m column (Factor Four VF-5ms low bleed, I.D. 0.25 mm, film thickness 0.25 μm, Palo Alto, CA), and a mass spectrometer (MS) (Varian Saturn 2200, Palo Alto, CA) that was used in the chemical ionization (CI) tandem mass spectrometry (MS/MS) mode. The GC oven temperature was

maintained at 50ºC for 1 minute, increased to 200ºC at 10ºC/min and held at 200ºC for 2 minutes, and finally increased to 240ºC at 10ºC/min and finally held at 240ºC for 5 minutes. Upon sample collection, 10-mL aliquots were transferred to 20-mL autosampler vials (Varian, Palo Alto, CA) that contained 2.5 g of NaCl. Isoborneol was used as the internal standard and was spiked at a concentration of 20 ng/L. Prior to analysis, analytes in samples were concentrated using headspace solid-phase microextraction (SPME) using a 1-cm 50/30 μm DVB/Carboxen/PDMS fiber (Supelco, St. Louis, MO). The SPME fiber was exposed to the headspace of the sample vial at a temperature of 65ºC for 30 minutes. The SPME fiber was then inserted into the injector of the GC oven (T= 250^{o}C, time = 4 minutes). The method detection limit for MIB and geosmin was 1 ng/L, and representative standard curves are shown in Figures 3.2 and 3.3 for MIB and geosmin, respectively. The GC-CI/MS/MS method used for analysis of MIB and geosmin was adapted from the standard operating procedure developed by the Metropolitan Water District of Southern California (MWDSC) and is described in detail in the Appendix.

Solutions containing ^{14}C-labeled MIB were analyzed by liquid scintillation counting. To obtain MIB concentrations, 5 mL of aqueous sample was mixed with 18 mL of scintillation cocktail (Ultima Gold, PerkinElmer Life And Analytical Sciences, Inc., Wellesley, MA) and analyzed in a liquid scintillation counter (TRI-CARB 2100TR, Packard Instrument

Company, Downers Grove, IL). For a 5-mL sample, the detection limit for the method was approximately 2 ng/L.

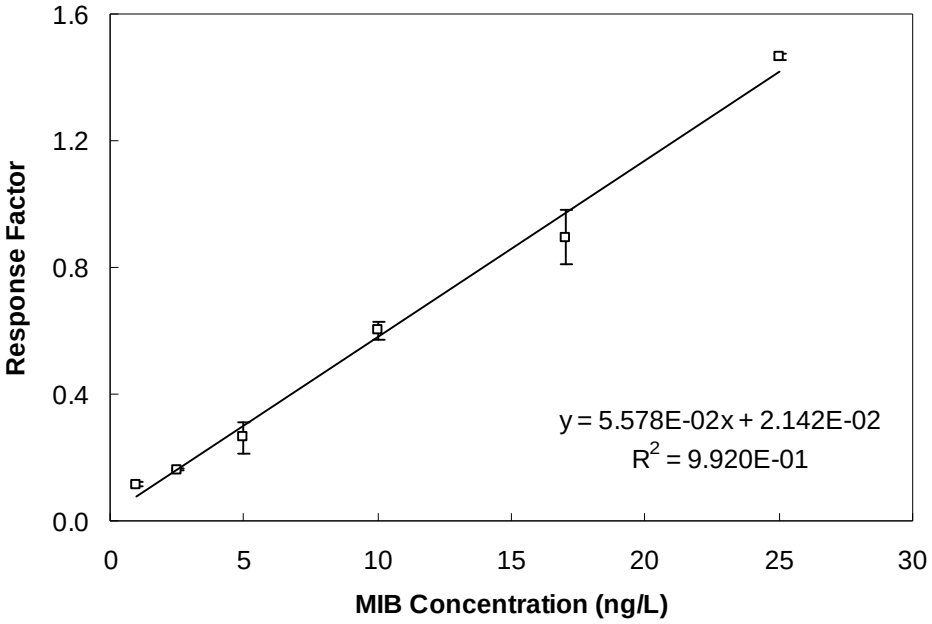

Figure 3.2 MIB standard curve for GC-CI/MS/MS method following headspace SPME preconcentration

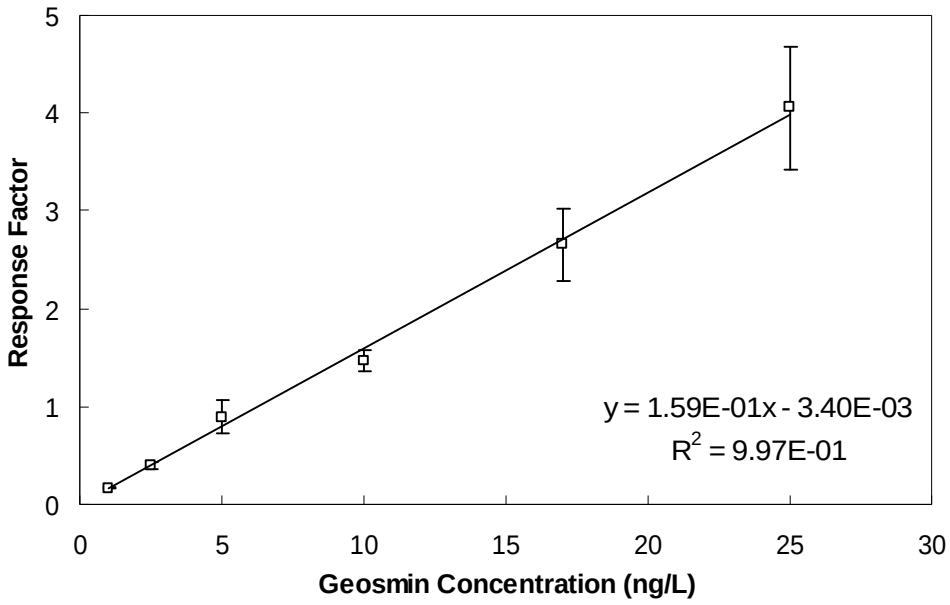

Figure 3.3 Geosmin standard curve for GC-CI/MS/MS method following headspace SPME preconcentration

3.2.7 Analysis of MIB dehydration products

To identify MIB dehydration products, GC/electron ionization (EI)–MS analyses were initially conducted by liquid injection of (1) the reaction mixture obtained from the preparation of MIB dehydration products (see p. 17/18) and (2) a non-reacted blank (1 mg of ^{12}C-MIB in 2.1 mL of ethyl acetate). As shown in the top panel of Figure 3.4, analysis of the non-reacted blank showed principally MIB (retention time = 15.242 minutes). In addition, two MIB-related peaks (based on mass spectra) were observed at retention times of 8.47 and 9.50 minutes. These retention times are similar to those for two MIB dehydration products,

but the mass spectra of the compounds observed in the non-reacted blank did not match those obtained for the MIB dehydration products.

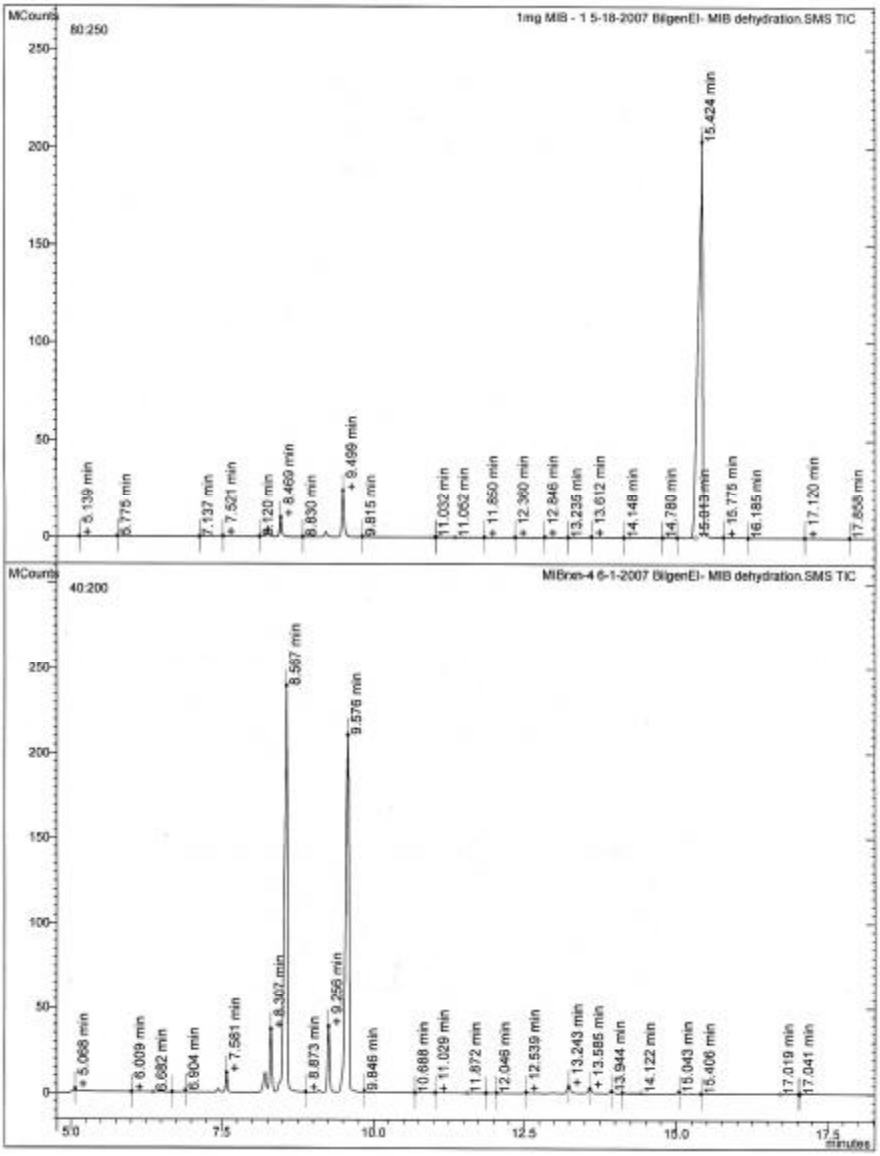

Figure 3.4 Chromatograms for MIB (top) and MIB dehydration products (bottom)

The bottom panel of Figure 3.4 shows the total ion chromatogram that was obtained for the reaction products. Upon reaction with H_2SO_4, the MIB peak disappeared completely, while four new peaks appeared. Based on published mass spectra (Schumann and Pendleton 1999) and relative retention times (Fravel et al. 2002), three of the new peaks were assigned to the MIB dehydration products 2M2B (8.30 min), 1MC (8.57 min), and 2MB (9.58 min). In addition, one additional unknown reaction product was detected (9.25 min). Based on peak areas, the reaction mixture contained 7% 2M2B, 50% 1MC, 38% 2MB, and 5 % of an unknown product. Overall, the composition of the reaction mixture obtained here was similar to that obtained by Schumann and Pendleton (1997). Mass spectra of the reaction products are shown in Figures 3.5 to 3.8.

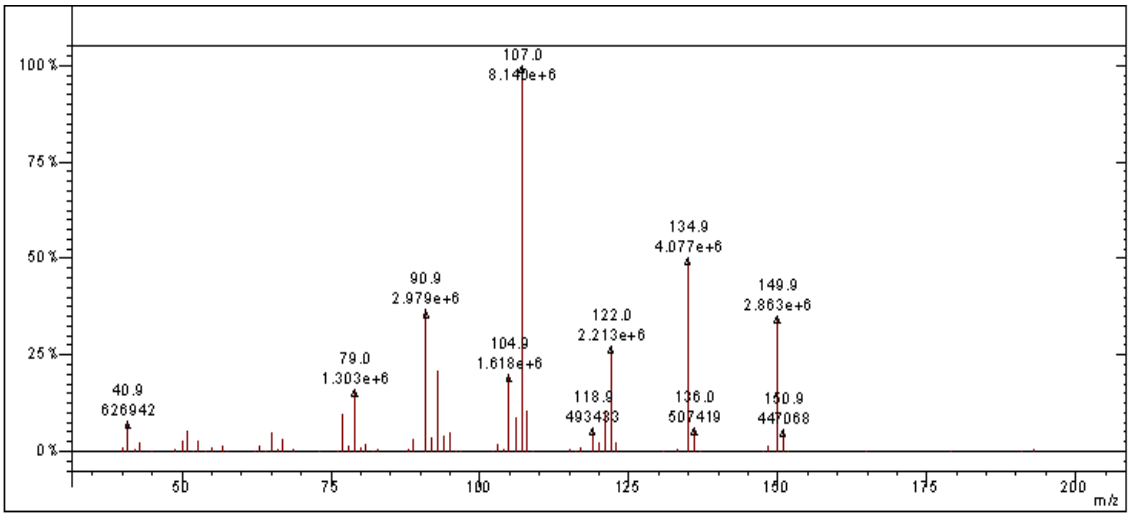

Figure 3.5 EI mass spectrum of 2-methyl-2-bornene (Retention time: 8.302 min). Note: principal difference to other MIB dehydration products is presence of ion at m/z=122.

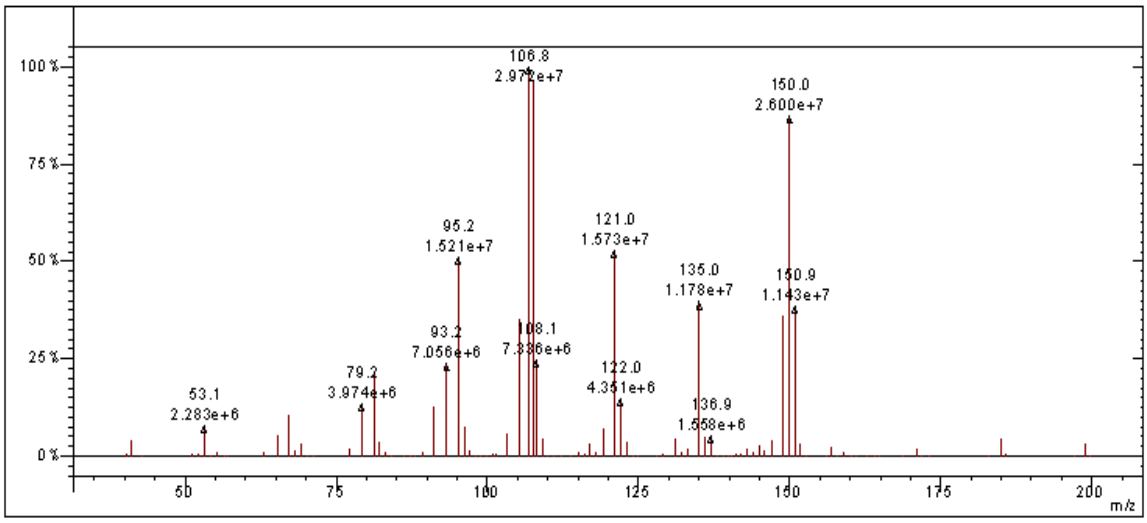

Figure 3.6 EI mass spectrum of 1-methylcamphene (Retention time: 8.567 min)

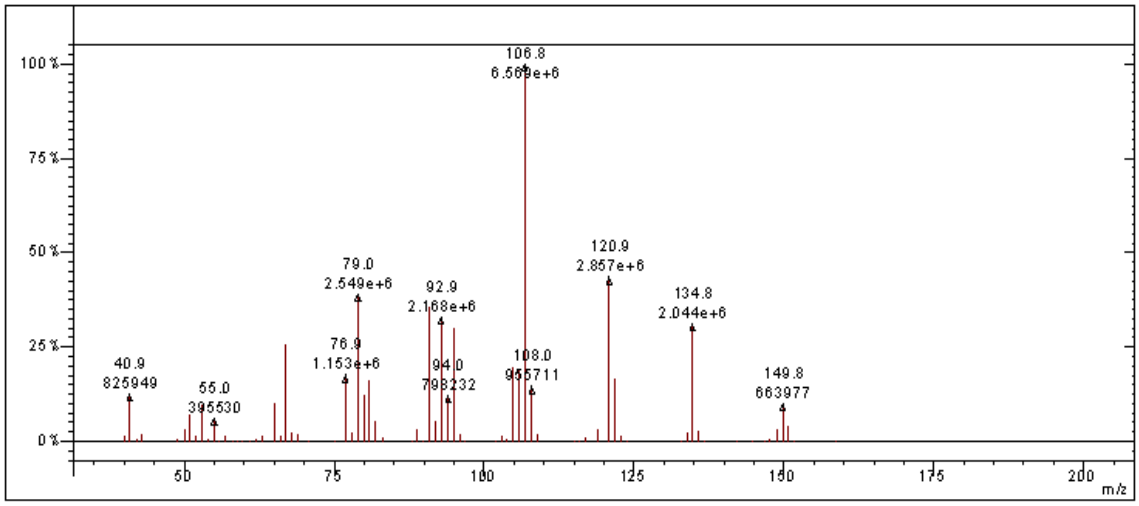

Figure 3.7 EI mass spectrum of unknown product (Retention time: 9.252 min)

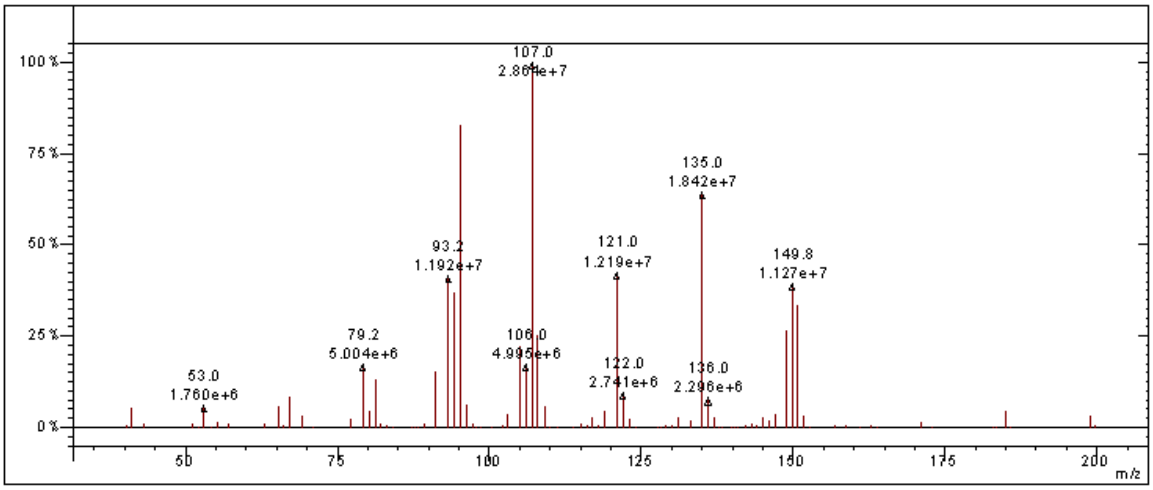

Figure 3.8 EI mass spectrum of 2-methylenebornane (Retention time: 9.576 min)

Subsequently, the GC–CI/MS/MS method for MIB and geosmin analyses (see section 3.2.6 and Appendix) was expanded to include the MIB dehydration products. This task was successfully completed by directly injecting the ethyl acetate reaction mixture. However, the method was not sufficiently sensitive when samples containing MIB dehydration products in the ng/L range (diluted ethyl acetate reaction mixture) were analyzed by headspace SPME. As a result, it was not possible to quantitatively assess the conversion of MIB to MIB dehydration products in this study.

3.2.8 Ozone analysis

Ozone concentrations in the ozone stock solution and in samples collected during the ozone uptake experiments were analyzed directly by measuring the UV absorbance at 258 nm with a spectrophotometer (DR 5000 UV-Vis Spectrophotometer, Hach, Loveland, CO). At a wavelength of 258 nm, the molar absorbance of ozone is 3,000 M^{-1} cm^{-1} (Peter and von Gunten 2007).

Aqueous ozone concentrations in the zeolite-enhanced ozonation experiments were measured with the indigo colorimetric method (Standard Method 4500-O_3 B, Indigo Colorimetric Method, AWWA 2005). Because the volume of the samples (5 mL) was much smaller than that required by the standard method, the volume of the indigo reagent was modified from the standard method and chosen such that the ratio of the molar indigo concentration to the molar ozone concentration was between 2 and 8. The change in absorbance of a sample relative to an ozone-free blank was measured at a wavelength of 600 nm. The standard curve obtained for the indigo method is presented in Figure 3.9.

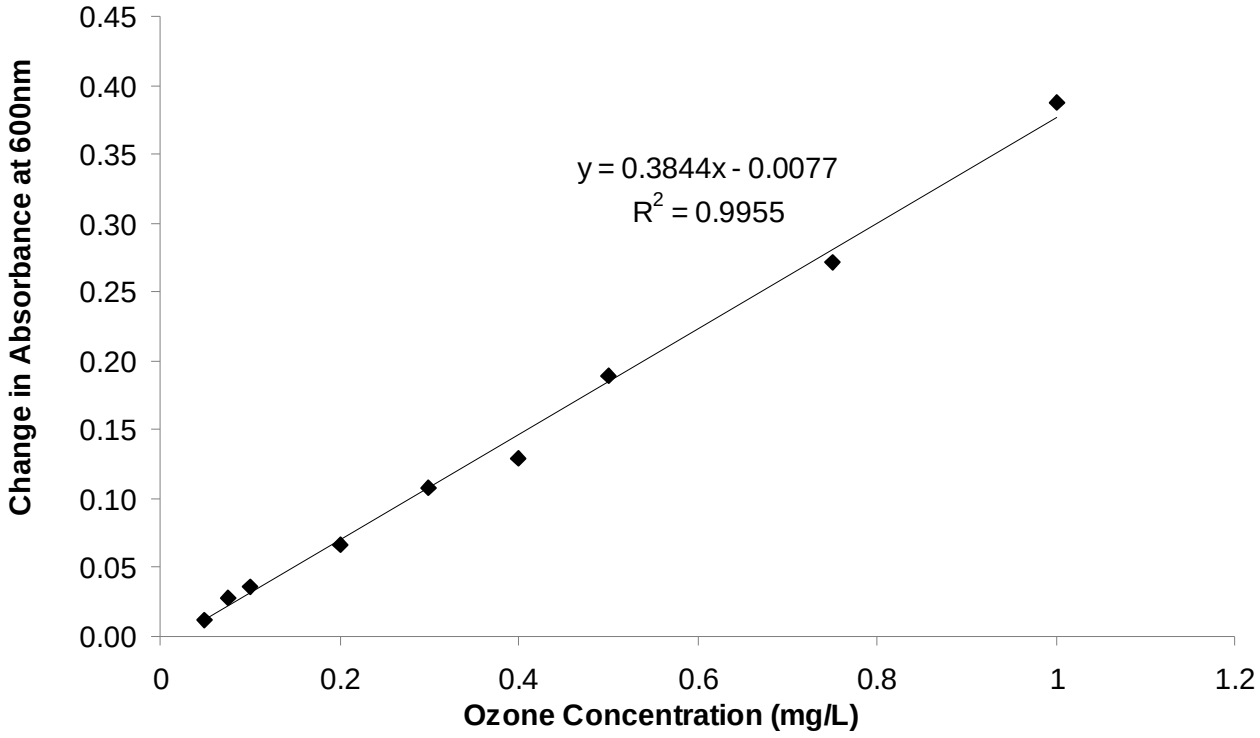

Figure 3.9 Ozone standard curve obtained with the indigo colorimetric method

CHAPTER 4

REMOVAL OF MIB AND GEOSMIN BY HIGH-SILICA ZEOLITES AND POWDERED ACTIVATED CARBON IN THE ABSENCE OF OZONE

In this chapter, the potential for adsorptive and reactive removal of MIB and geosmin by high-silica zeolites was assessed in longer-term isotherm experiments and in short-term kinetic tests. Four zeolite framework types (silicalite, mordenite, beta, and Y) were selected to evaluate pore size effects on MIB and geosmin removal from UPW. In addition, effects of zeolite hydrophobicity and reactivity on MIB and geosmin removal were probed with mordenite and Y zeolite exhibiting molar SiO_2/Al_2O_3 ratios ranging from 12 to 810. For reference, the MIB and geosmin removal effectiveness of high-silica zeolites was compared to that of a coal-based and a coconut-shell-based activated carbon. For MIB, experiments were conducted with both ^{12}C-MIB and ^{14}C-MIB to determine whether MIB removal by zeolites was aided by a chemical dehydration reaction. Finally, background matrix effects (cations, NOM) on MIB and geosmin removal were determined by conducting experiments in salt-amended UPW and in LMW.

4.1 EFFECT OF ZEOLITE FRAMEWORK TYPE ON MIB/GEOSMIN REMOVAL

To evaluate the effect of zeolite pore size on MIB and geosmin removal, adsorption isotherm data were collected with the following zeolite framework types:

- Silicalite (pore dimensions: 5.3 Å × 5.5 Å)
- Mordenite (pore dimensions: 6.5 Å × 7.0 Å)
- Beta (pore dimensions: 6.4 Å × 7.6 Å)
- Y (pore dimensions: 7.4 Å × 7.4 Å)

To minimize any confounding effects related to differences in zeolite hydrophobicity (SiO_2/Al_2O_3 ratio), the most hydrophobic form that was available for each zeolite was used (Silicalite-700, H-Mordenite-230, H-Beta-300, and H-Y-810) to isolate pore size effects. Previous studies (Kawai et al. 1994, Knappe et al. 2007) showed that the adsorption uptake of aqueous organic contaminants by a zeolite of a particular framework type became independent of the SiO_2/Al_2O_3 ratio when the SiO_2/Al_2O_3 ratio exceeded about 100. For the purposes of this evaluation, the smallest SiO_2/Al_2O_3 ratio was 230 (H-Mordenite-230). Characteristics and sources of the studied zeolites are summarized in Table 3.1.

Figure 4.1 summarizes MIB uptake data by H-Mordenite-230, H-Y-810, and two activated carbons (coal-based WPH PAC and coconut-shell-based CC-602). When solid-phase concentrations were normalized with respect to adsorbent mass (Figure 4.1a), the results illustrate that the highest MIB uptake was obtained with the two activated carbons. Among the studied zeolite framework types, MIB removal by H-Mordenite-230 was greater than by H-Y-810, and no or negligible MIB removal was obtained with the Silicalite-700 and H-Beta-300 zeolites (data not shown). Referring to the molecular dimensions of MIB (5.4 × 5.5 × 6.9 Å, Figure 4.2), it is reasonable to expect that MIB is adsorbed by mordenite and Y zeolites because the mordenite and Y channel openings are slightly larger than the dimensions of MIB. Given the closer match between the dimensions of the mordenite pore and MIB relative to those of the Y pore and MIB, it is further reasonable to expect that MIB would be preferably adsorbed by the mordenite. Similarly, the absence of MIB adsorption by the silicalite was expected because the MIB dimensions exceed those of the silicalite pores.

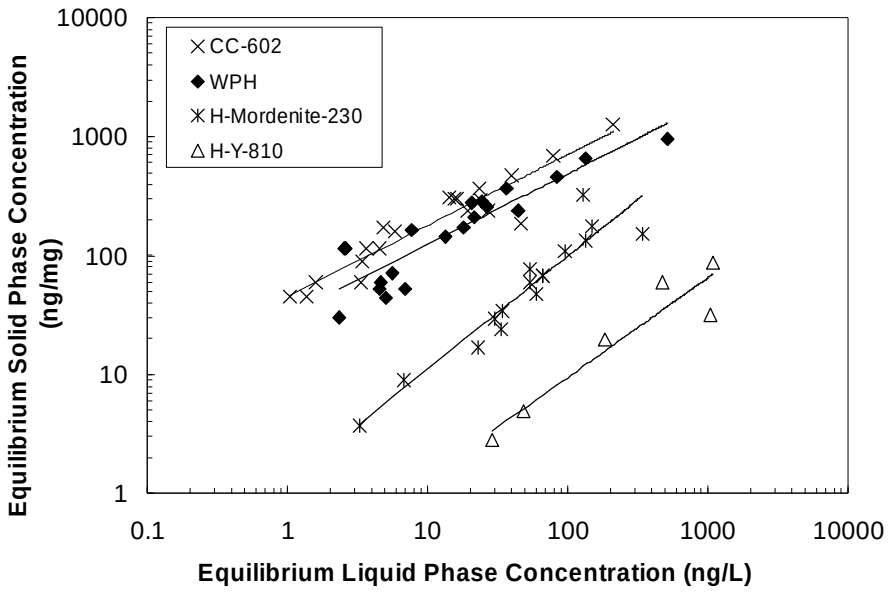

(a)

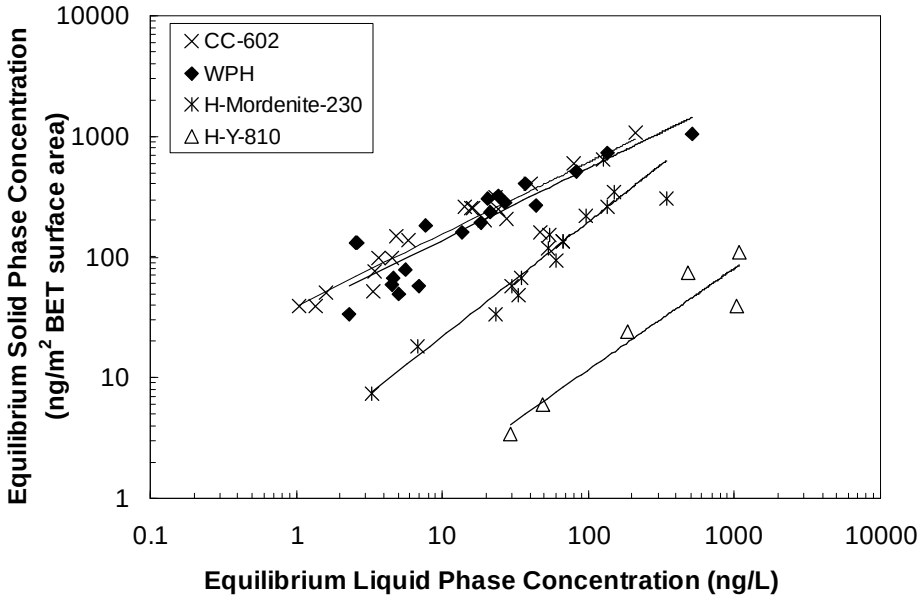

(b)

Figure 4.1 Single-solute MIB uptake by two activated carbons and two high-silica zeolites. Equilibrium solid phase concentrations were normalized by adsorbent mass in panel (a) and by BET surface area in panel (b). Data for the activated carbons represent pooled ^{12}C-MIB and ^{14}C-MIB data while data for the zeolites represent ^{14}C-MIB data only. Lines represent Freundlich isotherm model fits.

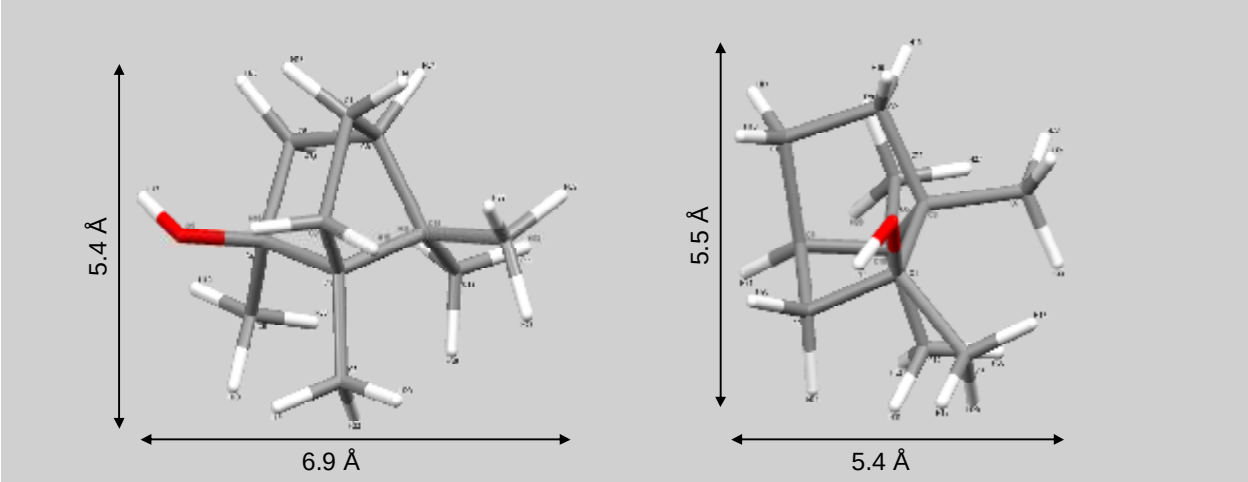

Figure 4.2 MIB dimensions. Calculated using Mercury v1.4.2 freeware (http://www.ccdc.cam.ac.uk/free_services/mercury/downloads/)

It is unclear why MIB uptake by the H-Beta-300 zeolite was negligible given that the pore dimensions of the beta framework slightly exceed the dimensions of MIB. It is possible that the H-Beta-300 pore dimensions did not match those of the idealized end member presented in section 2.2.3.

When solid-phase concentrations were normalized with respect to BET surface area (Figure 4.1b), it can be observed that the isotherm data collected with H-Mordenite-230 moved away from the H-Y-810 data and closer to the activated carbon data. This result suggests that the H-Mordenite-230 pore size was more suitable for MIB uptake than that of the H-Y-810 zeolite.

For the removal of geosmin, Figure 4.3 illustrates that the H-Y-810 zeolite was somewhat more effective than H-mordenite-230. However, geosmin uptake by the tested activated carbons was higher than that obtained with either zeolite. Compared to MIB, activated carbons exhibited a larger adsorption capacity for geosmin, a result that is consistent with those of other research groups (e.g., Newcombe and Cook 2002). The difference between geosmin uptake by the activated carbons and the high-silica zeolites (Figure 4.3) was larger than that observed with MIB (Figure 4.1). As was the case for MIB, no measurable geosmin removal was obtained with the Silicalite-700 and H-Beta-300 zeolites (data not shown).

When solid-phase geosmin concentrations were normalized with respect to adsorbent mass, Figure 4.3a suggests that the Y framework type was more suitable for geosmin removal than the mordenite framework type. However, upon normalization of the solid-phase concentrations by the adsorbent BET surface area, geosmin uptake by H-Y-810 and H-Mordenite-230 was almost identical (Figure 4.3b). Therefore, the pore dimensions of the Y and Mordenite framework types appear to be equally suitable for geosmin removal from water, and the main reason for the better performance of the H-Y-810 zeolite was due to its larger BET surface area. As shown in Figure 4.4, the longest geosmin dimension (7.5 Å) exceeds the largest dimension of the mordenite and Y zeolite channel openings; the second largest (6.2 Å) and smallest (5.7 Å) geosmin dimensions are sufficiently small, however, to give geosmin access to the internal pore structure of the mordenite and Y zeolites.

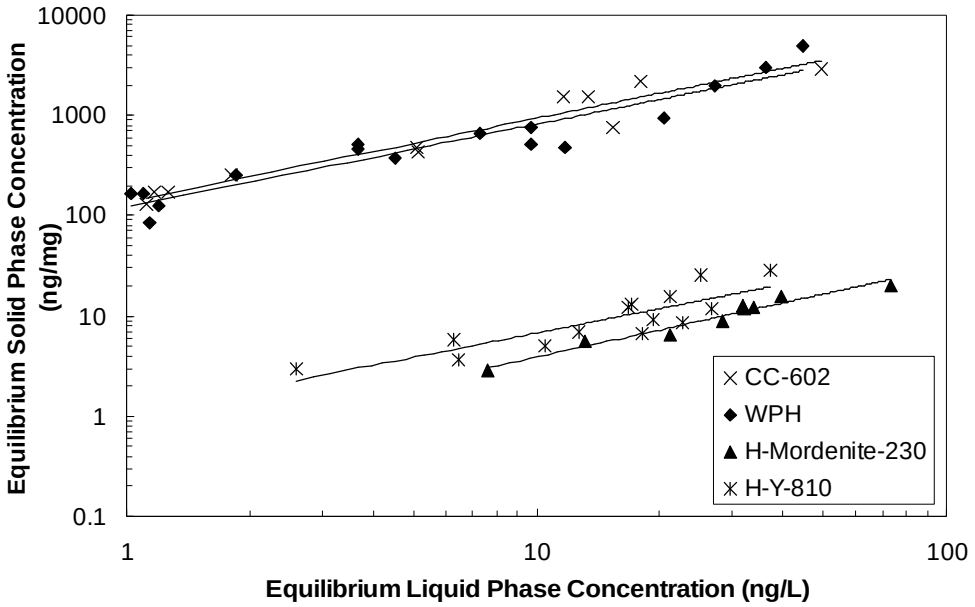

(a)

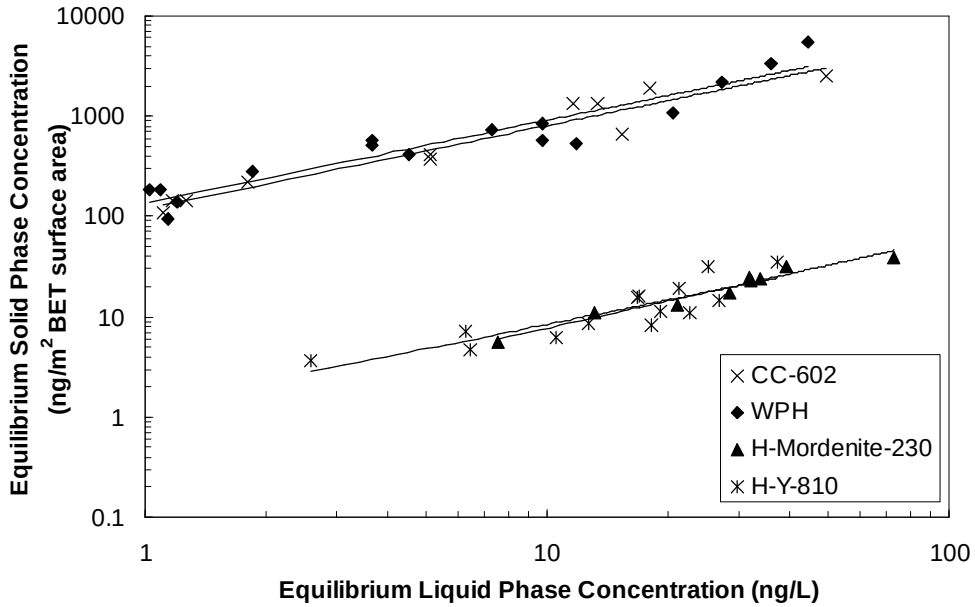

(b)

Figure 4.3 Single-solute geosmin uptake by two activated carbons and two high-silica zeolites. Equilibrium solid phase concentrations are normalized by adsorbent mass in panel (a) and by BET surface area in panel (b). Lines represent Freundlich isotherm model fits

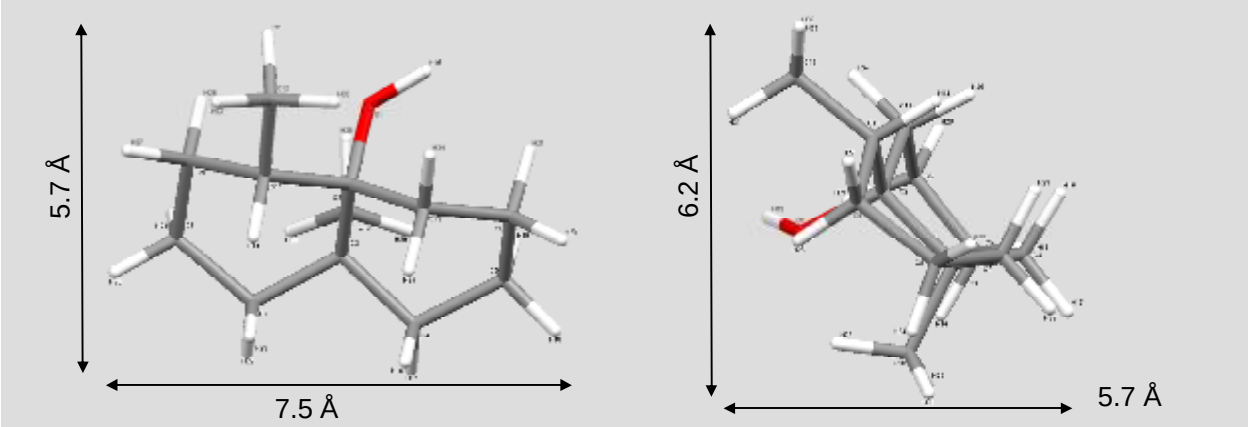

Figure 4.4 Geosmin dimensions. Calculated using Mercury v1.4.2 freeware (http://www.ccdc.cam.ac.uk/free_services/mercury/downloads/)

4.2 EFFECT OF ZEOLITE HYDROPHOBICITY ON MIB/GEOSMIN REMOVAL

Figures 4.5 and 4.6 depict the effect of zeolite hydrophobicity on ^{14}C-labeled MIB removal by mordenite and Y zeolites with different SiO_2/Al_2O_3 ratios, respectively. Results in Figure 4.5 show that MIB removal increased dramatically as the SiO_2/Al_2O_3 ratio of the mordenite zeolites increased from 20 to 90. In contrast, an increase in SiO_2/Al_2O_3 ratio from 90 to 230 yielded only a small increase in MIB removal. Among the studied Y zeolites, the more hydrophobic H-Y-810 was more effective for MIB removal than the Y-12 zeolite (Figure 4.6).

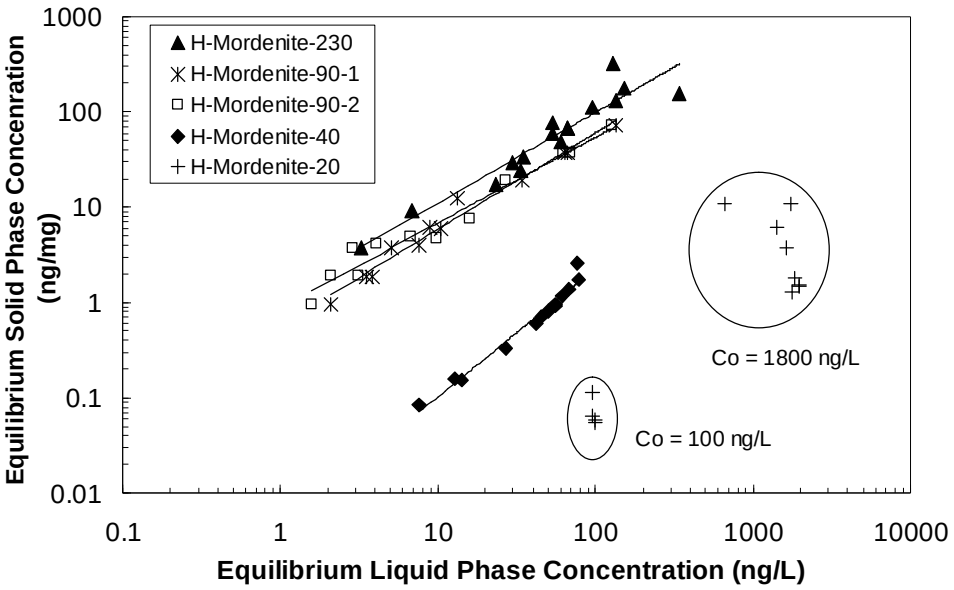

Figure 4.5 Effect of SiO_2/Al_2O_3 ratio on ^{14}C-labeled MIB removal by mordenite zeolites. Lines represent Freundlich isotherm model fits.

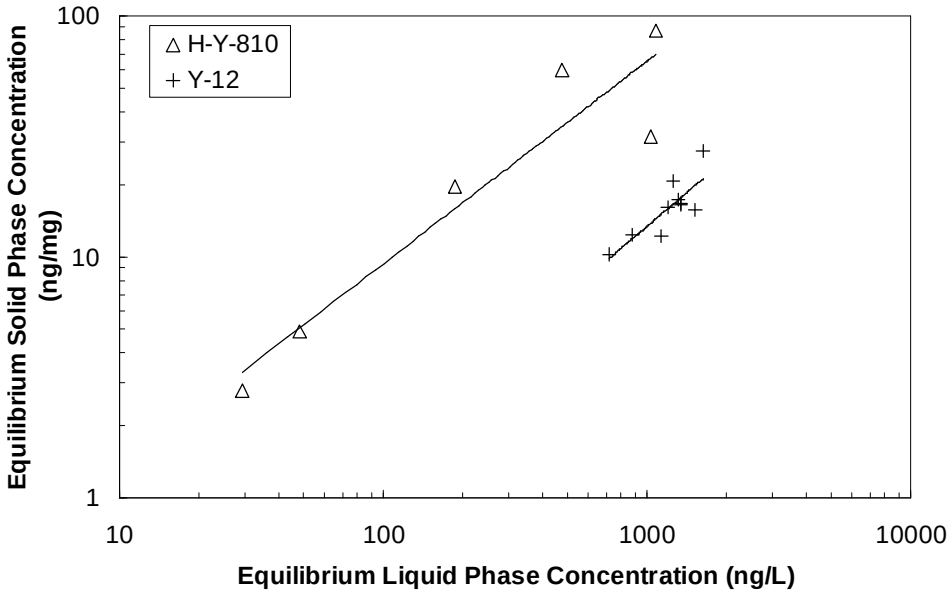

Figure 4.6 Effect of SiO_2/Al_2O_3 ratio on ^{14}C-labeled MIB removal by Y zeolites. Lines represent Freundlich isotherm model fits.

Figure 4.7 illustrates that geosmin removal also improved as the SiO_2/Al_2O_3 ratio of mordenites increased from 20 to 90 and that no additional increase in geosmin removal was observed as the SiO_2/Al_2O_3 ratio of mordenite increased from 90 to 230. Also, geosmin removal improved as the SiO_2/Al_2O_3 ratio of Y zeolites increased from 12 to 810 (Figure 4.8). The results in Figures 4.5 through 4.8 illustrate that more hydrophobic zeolites are more effective for MIB and geosmin removal than more hydrophilic zeolites, which is consistent with the general expectation of better adsorption of aqueous contaminants on more hydrophobic adsorbents (e.g Kawai et al. 1994, Li et al. 2003, Knappe et al. 2007). E.g., Kawai et al. (1994) studied chloroform adsorption from water using ZSM-5 and Y zeolites (SiO_2/Al_2O_3 ratios ranged from 25 to 1000 for ZSM-5 zeolites and from 5.5 to 770 for Y zeolites). For ZSM-5 zeolites Kawai et al. (1994) obtained a large increase in chloroform adsorption capacity between SiO_2/Al_2O_3 ratios of 25 and 70, but only a smaller increase between SiO_2/Al_2O_3 ratios of 70 and 1000. For Y zeolites substantial increases in chloroform adsorption capacity were observed between SiO_2/Al_2O_3 ratios of 5.5 and 224, but above this value, only small differences were obtained. These results along with the data obtained in this study suggest that SiO_2/Al_2O_3 ratios in excess of about 100 have only a small effect on organic contaminant adsorption from the aqueous phase.

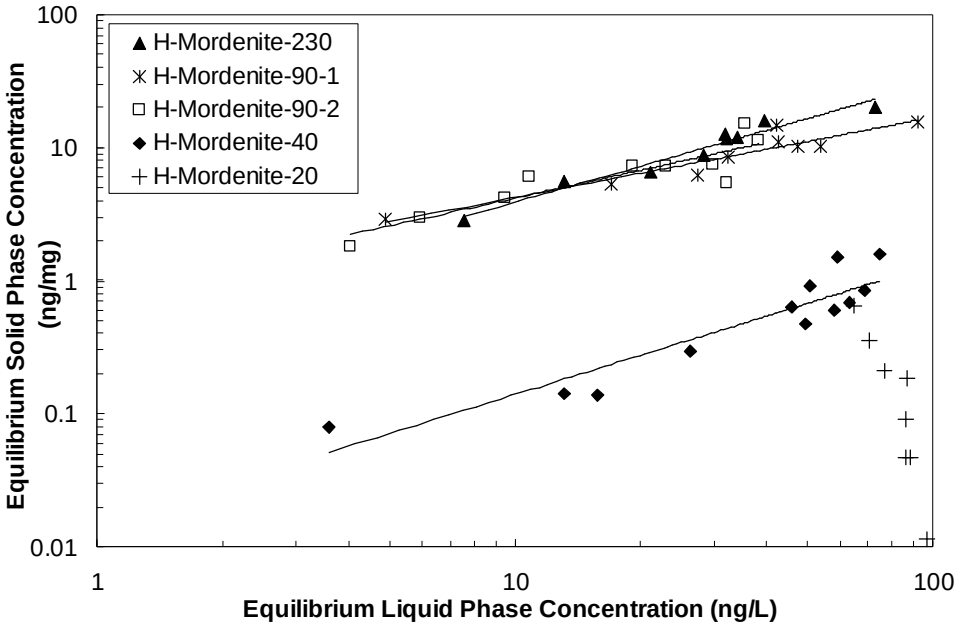

Figure 4.7 Effect of SiO_2/Al_2O_3 ratio on geosmin removal by mordenite zeolites. Lines represent Freundlich isotherm model fits.

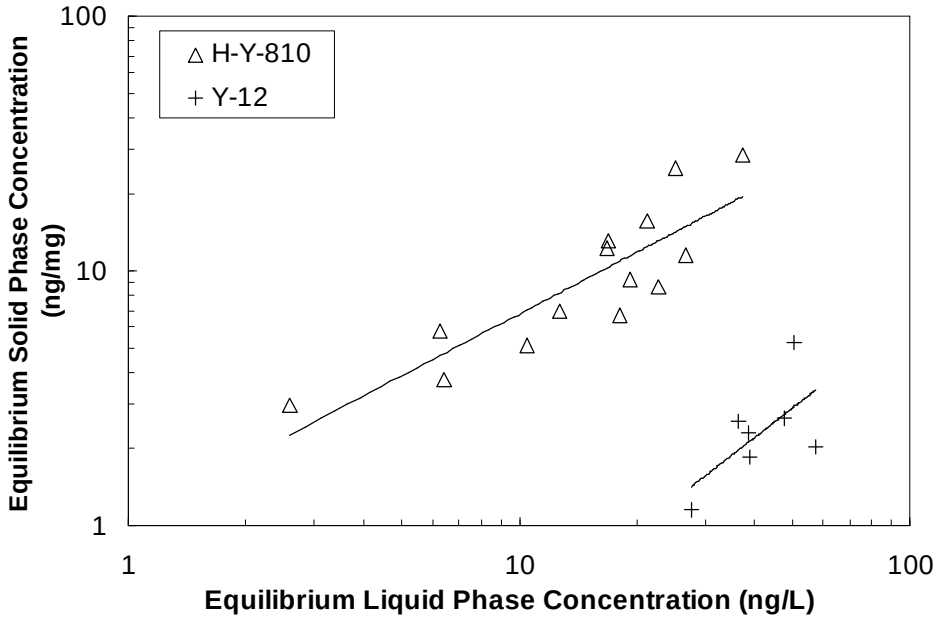

Figure 4.8 Effect of SiO_2/Al_2O_3 ratio on geosmin removal by Y zeolites. Lines represent Freundlich isotherm model fits.

4.3 FREUNDLICH ISOTHERM PARAMETERS DESCRIBING MIB/GEOSMIN UPTAKE

Adsorption isotherm data for both ^{14}C-labeled MIB and geosmin were effectively described by the Freundlich isotherm model ($q = K \cdot C^{1/n}$), where q and C are the equilibrium solid-phase and liquid-phase MIB/geosmin concentrations, respectively, and K and 1/n are fitting parameters that characterize the adsorption capacity of the adsorbent (at an equilibrium liquid phase concentration of 1 ng/L for the units chosen here) and the adsorbent heterogeneity, respectively. For both MIB and geosmin, Table 4.1 illustrates that the Freundlich K values for the mordenite and Y zeolites were lower than those for the activated carbons. Freundlich isotherm constants and MIB adsorption capacities obtained for the two activated carbons evaluated in this study were within ranges observed in previous studies, in which MIB adsorption isotherm data were collected in UPW and in which Freundlich isotherm constants were reported (Table 4.2). For example, the MIB adsorption capacity at an equilibrium liquid phase concentration of 10 ng/L (q_{10}) ranged from about 47 to 316 ng/mg in prior studies, and q_{10} values obtained in this study were 124 and 180 ng/mg. The large range of MIB adsorption capacities obtained in prior studies was primarily related to differences in activated carbon characteristics. Table 4.1 also illustrates that the geosmin uptake by activated carbon was larger than MIB uptake, a result that is attributable to the greater hydrophobicity of geosmin.

Table 4.1 also compares 1/n values that were derived from the MIB and geosmin isotherm data. With the exception of two geosmin isotherms, 1/n values for the zeolite data exceeded 0.8. Given that high-silica zeolites are relatively homogeneous adsorbents (i.e., they exhibit a uniform pore size), it is reasonable to expect 1/n values that are close to 1.

To date, only two studies have evaluated MIB uptake by high-silica zeolites (Ellis and Korth 1993, Sagehashi et al. 2005a), and only one measured geosmin uptake by high-silica zeolites (Ellis and Korth 1993). Only Y zeolites were evaluated in the two previous studies. Sagehashi et al. (2005a) reported partition coefficients for MIB that were derived from the assumption that MIB removal conformed to a linear isotherm model ($q = K_p \cdot C$), where K_p is the partition coefficient (units of L/mg). Ellis and Korth (1993) provided MIB and geosmin removal data at two zeolite doses and sufficient information for the calculation of K_p values. Table 4.3 summarizes K_p values presented by Sagehashi et al. (2005a), K_p values that were calculated from the data of Ellis and Korth (1993), and K_p values obtained in this study (values were calculated from $K_p = q_{10}$ (ng/mg) / 10 ng/L). Table 4.3 suggests that the K_p values obtained in this study agree more closely with those obtained by Ellis and Korth (1993), who evaluated MIB and geosmin uptake from UPW spiked with 180 ng/L of MIB and 96 ng/L of geosmin (i.e., conditions similar to the ones used in this study). In contrast, the K_p values of Sagehashi et al. (2005a) were one to two orders of magnitude larger than the values obtained in this study and by Ellis and Korth (1993). One possible reason for the discrepancy among the values is that Sagehashi et al. (2005a) spiked UPW with 6.4–7.7

mg/L of MIB. It is possible that MIB uptake is not completely linear in experiments that differ in their initial MIB concentration by about 4 orders of magnitude.

Table 4.1 Freundlich constants describing MIB and geosmin removal data

Compound	Adsorbent Type	Adsorbent	K (ng/mg) (L/ng)$^{1/n}$	1/n	R^2	q_{10} (ng/mg)
MIB	Activated Carbon	CC602	45.65	0.595	0.893	179.7
		WPH	31.41	0.595	0.812	123.6
	Mordenite	H-Mordenite-230	1.240	0.951	0.902	11.08
		H-Mordenite-90-1	0.571	1.011	0.979	5.856
		H-Mordenite-90-2	0.873	0.895	0.961	6.855
		H-Mordenite-40	0.0046	1.345	0.970	0.102
		H-Mordenite-20*	-	-	-	-
	Y	H-Y-810	0.196	0.840	0.896	1.356
		Y-12	0.022	0.929	0.673	0.187
Geosmin	Activated Carbon	CC602	138.2	0.829	0 .937	932.2
		WPH	122.0	0.825	0.902	815.4
	Mordenite	H-Mordenite-230	0.493	0.898	0.956	3.898
		H-Mordenite-90-1	1.054	0.602	0.899	4.215
		H-Mordenite-90-2	0.836	0.689	0.808	4.085
		H-Mordenite-40	0.015	0.979	0.854	0.143
		H-Mordenite-20*	-	-	-	-
	Y	H-Y-810	1.054	0.808	0.747	6.774
		Y-12	0.027	1.194	0.405	0.422

* negligible removal, data did not conform to Freundlich model

Table 4.2 Freundlich constants and MIB adsorption capacities obtained in prior studies

Carbon	Water	Contact Time	K $(ng/mg)(L/ng)^{1/n}$	1/n	q_{10} (ng/mg)	Ref.
Carbon C (coal)	Ultrapure	5 d	85	0.56	309	Newcombe et al., 1997
Hydrodarco-B PAC (lignite)	Ultrapure	3 d	36.3	0.118	47.6	Graham et al., 2000
Bituminous GAC (coal)	Ultrapure	5 d	72.3	0.64	316	Chen et al., 1997
Peat GAC			27.5	0.89	213	
Lignite GAC			24.9	0.72	131	
Wood GAC			8.8	0.73	47.3	
Watercarb PAC (wood)	Ultrapure	4 d	9.56	0.492	145	Gillogly et al., 1998b
Bituminous GAC (coal)	Natural (TOC = 3.5 mg/L)*	5 d	15.8	0.33	33.8	Chen et al., 1997
Peat GAC			12.5	0.21	20.3	
Cecarbon PAC (coal)	Natural (DOC = 1.8 mg/L)†	4 h	4.13	0.396	36.8	Gillogly et al., 1998b
WPH PAC (coal)			3.52	0.359	25.6	
Hydrodarco-B PAC (lignite)			2.49	0.341	16.4	
Watercarb PAC (wood)			2.50	0.216	8.24	
Nuchar PAC (wood)			2.20	0.418	22.1	

* Initial MIB concentration ($C_{0,MIB}$) = 1200 ng/L
† $C_{0,MIB}$ = 170–175 ng/L

Table 4.3 Partition coefficients describing MIB/geosmin uptake by Y zeolites

Adsorbent	K_p (L/mg)		Reference
	MIB	geosmin	
Y-80	0.030, 0.035[*]	0.525, 1.57[†]	Ellis and Korth (1993)
Y-70	3.8[‡]	-	Sagehashi et al. (2005a)
Y-12	2.6[‡]	-	Sagehashi et al. (2005a)
Y-5.4	0.4[‡]	-	Sagehashi et al. (2005a)
H-Y-810	0.14[§]	0.68[§]	This study
Y-12	0.019[§]	0.042[§]	This study

[*] C_0 = 180 ng/L
[†] C_0 = 96 ng/L
[‡] C_0 = 6.4–7.7 mg/L
[§] C_0 ~ 100 ng/L

4.4 EVIDENCE OF REACTIVE MIB REMOVAL BY ZEOLITES

To identify whether zeolites removed MIB by adsorption only or by a combination of adsorption and dehydration reaction, batch reactor data obtained with ^{14}C-labeled MIB (^{14}C-MIB) and non-labeled MIB (^{12}C-MIB) were compared for H-Mordenite-230, H-Mordenite-90-1, H-Mordenite-90-2, and H-Mordenite-40. Experiments completed with ^{14}C-MIB assess overall removal of ^{14}C by adsorption but do not specifically track MIB removal. If MIB reacted on the zeolite surface and formed dehydration products that subsequently desorbed from the zeolite pores into the bulk water, the equilibrium liquid phase ^{14}C concentration may be composed of a mixture of ^{14}C-MIB and ^{14}C-labeled MIB dehydration products. In

contrast, experiments completed with ^{12}C-MIB specifically assess the removal of MIB from the aqueous phase.

To verify the compatibility of ^{12}C- and ^{14}C-MIB data, results obtained from adsorption isotherm experiments for the two activated carbons were initially compared. Figure 4.9 depicts ^{12}C-MIB and ^{14}C-MIB adsorption data for WPH PAC, and Figure 4.10 depicts similar data for CC-602. For the two activated carbons, ^{14}C- and ^{12}C-MIB data are in good agreement, suggesting, as expected, that MIB removal takes place by adsorption only.

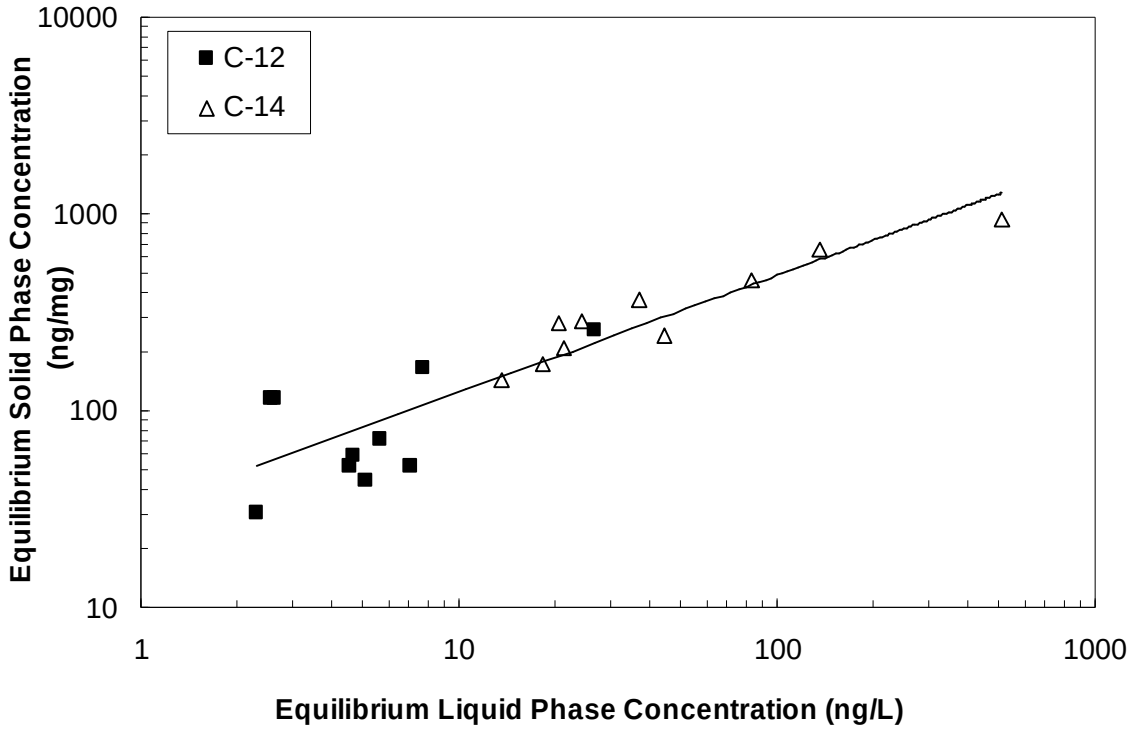

Figure 4.9 Comparison of ^{14}C- and ^{12}C-MIB removal data for activated carbon WPH. Line represents Freundlich isotherm model fit for pooled data set

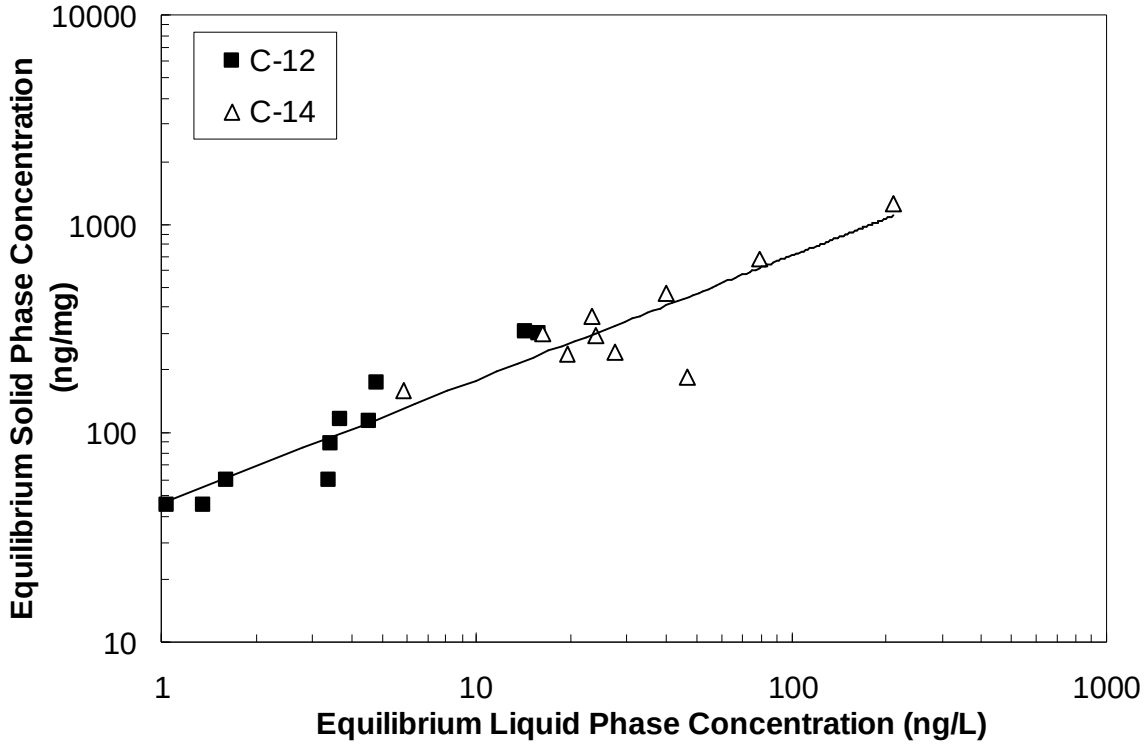

Figure 4.10 Comparison of ^{14}C- and ^{12}C-MIB removal data for activated carbon CC-602. Line represents Freundlich isotherm model fit for pooled data set.

For H-Mordenite-230, Figure 4.11 shows quite a bit of scatter in the ^{12}C-MIB data, but all ^{12}C-MIB data points fall above the Freundlich isotherm line established by the ^{14}C-MIB data. Therefore, it is possible that MIB removal was aided by a reactive mechanism (i.e., the measured ^{14}C liquid-phase concentrations are composed partly of MIB and partly of MIB dehydration products, whereas the ^{12}C data represents liquid-phase MIB concentrations only).

For H-Mordenite-90-1 and H-Mordenite-90-2, Figures 4.12 and 4.13 illustrate that the ^{12}C-MIB data differ more clearly from the ^{14}C-MIB data. These results substantiate that a reactive mechanism aided MIB removal by these zeolites, which are more acidic (SiO_2/Al_2O_3 ratio of 90) than the H-Mordenite-230 (SiO_2/Al_2O_3 ratio of 230). Reactive MIB removal is hypothesized to take place on Brønsted acid sites of zeolites (Ellis and Korth 1993); thus, more acidic zeolites, such as the H-Mordenite-90 zeolites, would be expected to be more reactive. The data in Figure 4.14, which compares ^{12}C-MIB and ^{14}C-MIB removal results obtained with H-Mordenite-40 further support to this hypothesis. Overall, the results in Figures 4.11 through 4.14 illustrate that the ^{12}C-MIB data differed from the ^{14}C-MIB data, and this difference increased as the SiO_2/Al_2O_3 ratio of the zeolites decreased (i.e., the acidity of the zeolite increased). Discrepancies between ^{14}C-MIB and ^{12}C-MIB data therefore indicate that both adsorption and reaction contributed to the removal of MIB by mordenite zeolites.

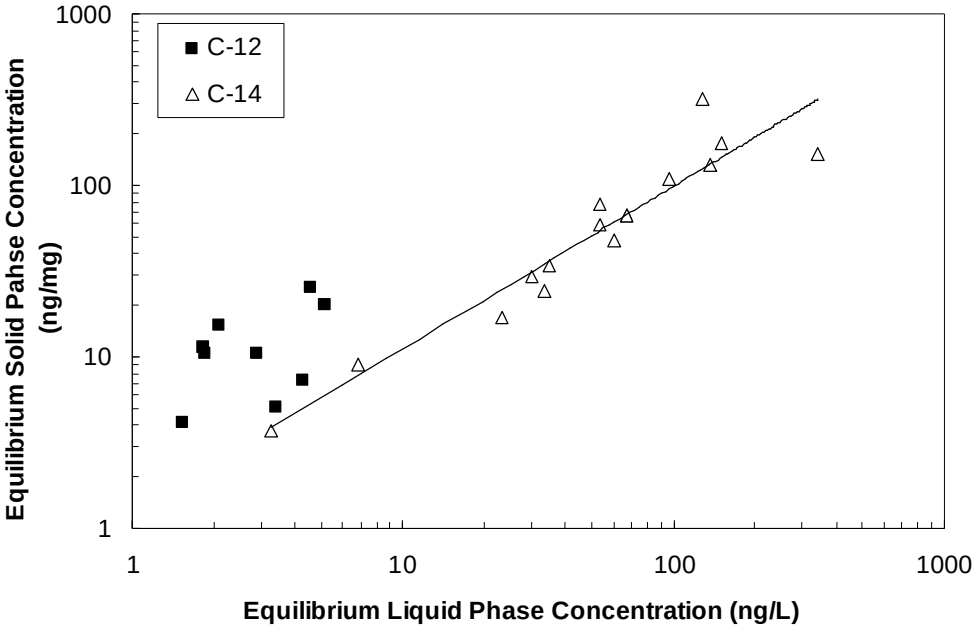

Figure 4.11 Comparison of ^{14}C- and ^{12}C-MIB removal data for H-Mordenite-230. Line represents Freundlich isotherm model fit for ^{14}C-MIB data only.

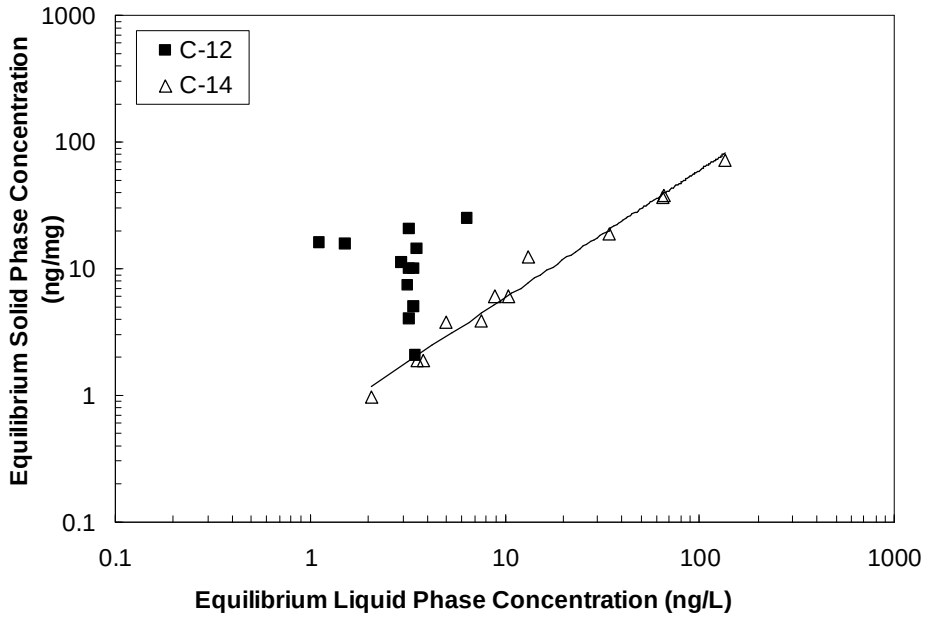

Figure 4.12 Comparison of ^{14}C- and ^{12}C-MIB removal data for H-Mordenite-90-1. Line represents Freundlich isotherm model fit for ^{14}C-MIB data only.

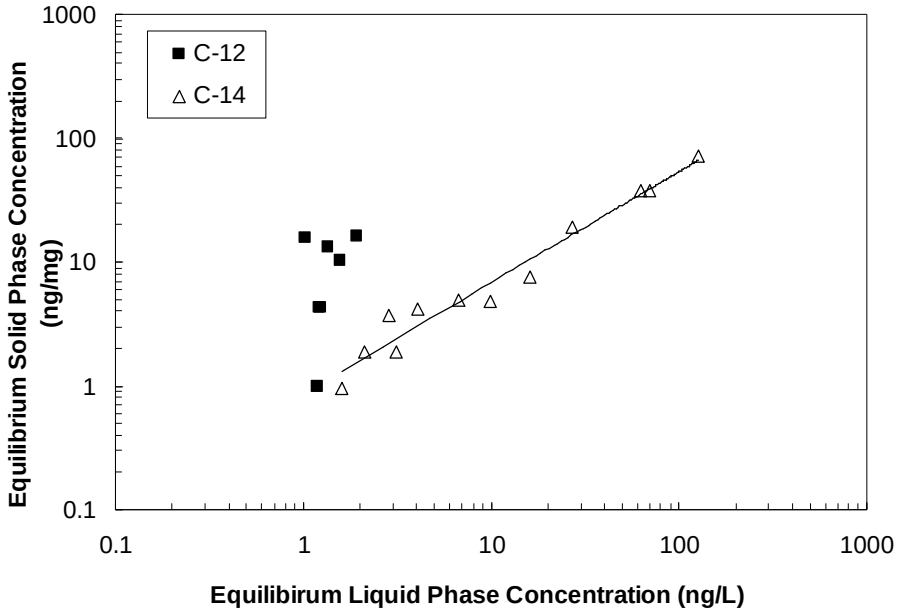

Figure 4.13 Comparison of ^{14}C- and ^{12}C-MIB removal data for H-Mordenite-90-2. Line represents Freundlich isotherm model fit for ^{14}C-MIB data only.

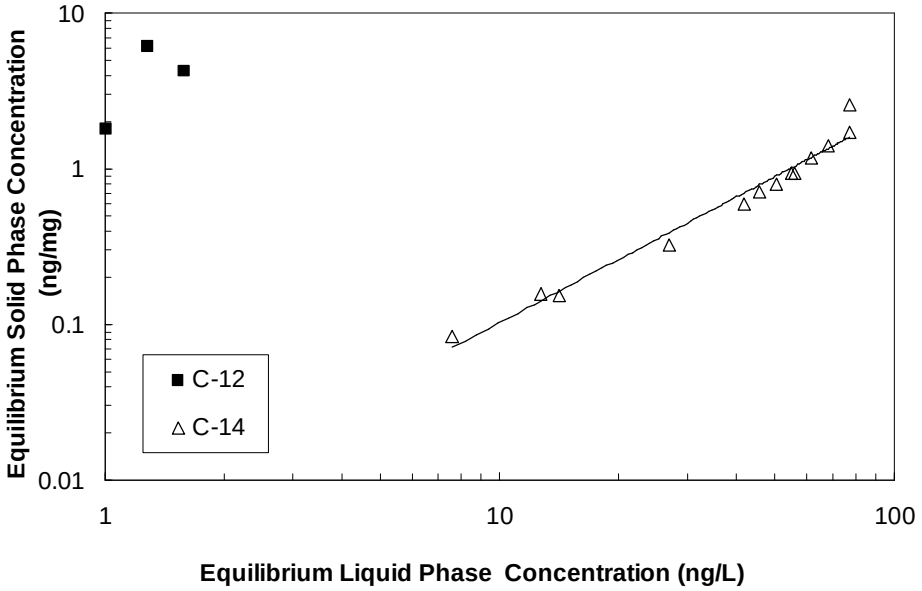

Figure 4.14 Comparison of ^{14}C- and ^{12}C-MIB removal data for H-Mordenite-40. Line represents Freundlich isotherm model fit for ^{14}C-MIB data only.

Figure 4.15 illustrates the hypothesized reaction mechanism of MIB on acidic zeolite surfaces and depicts the molecular structures of the non-odorous reaction products proposed by Ellis and Korth (1993) and Schumann and Pendleton (1997). Significant effort was expended during this study to identify and quantify MIB dehydration products in the aqueous phase that had been in contact with zeolites. While a GC-CI/MS/MS method for the dehydration products was developed (see section 3.2.7), the method was not sufficiently sensitive to detect MIB dehydration products at the ng/L level, however.

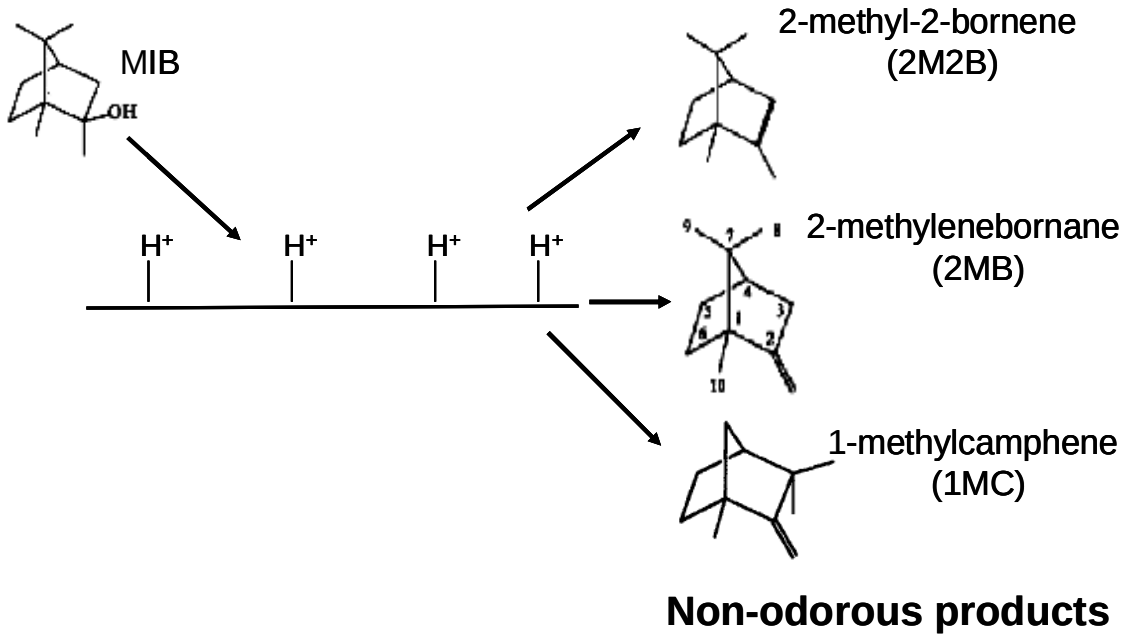

Figure 4.15 Proposed reaction between MIB and acidic zeolite surfaces

To further illustrate that MIB is acid-labile, MIB concentrations were measured over time in UPW acidified with phosphoric acid to pH 2. Figure 4.16 shows that the MIB concentration decreased at a rate of ~7.7 ng/h, and more than 90% of the initially added MIB had reacted away over a 12-hour period. This result has important practical implications for the storage of MIB samples between sample collection and analysis. The results obtained here show that acidification is an inappropriate means for preserving samples containing MIB. (Note: Standard Methods suggests that samples for the analysis of taste and odor compounds can be stored at 4°C for up to 3 days without the addition of a preservative, and $HgCl_2$ is recommended for sample preservation if storage exceeds 3 days).

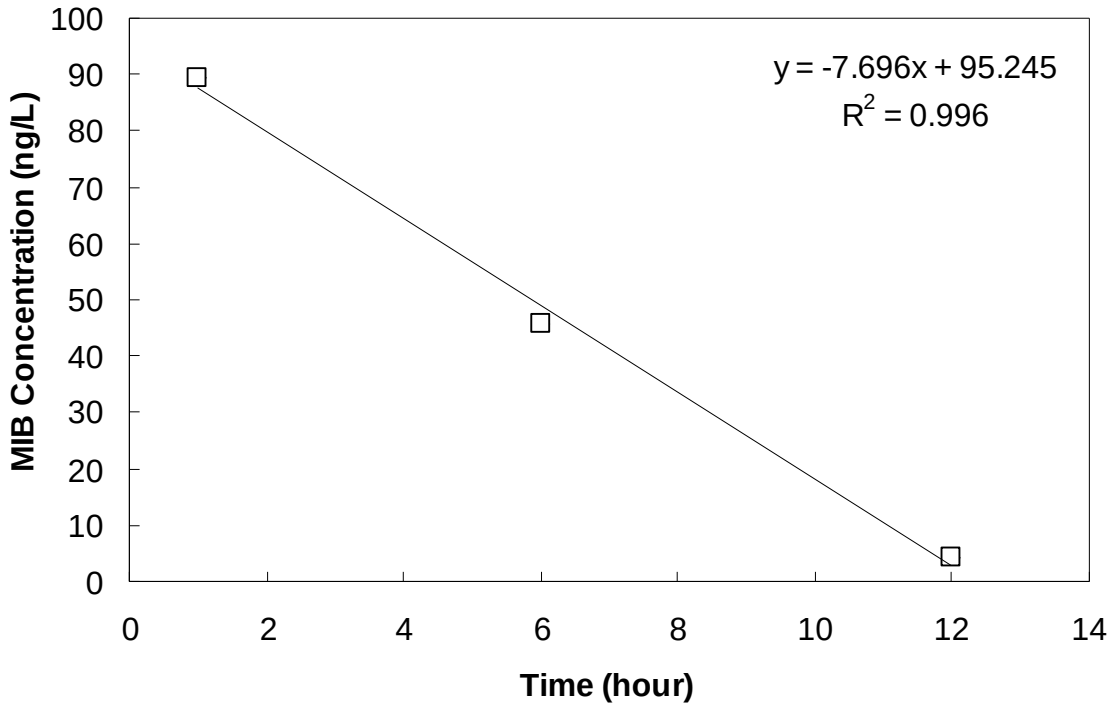

Figure 4.16 Rate of MIB removal in acidified UPW (pH 2). The initial MIB concentration was ~100 ng/L, and the temperature was 22°C.

4.5 BACKGROUND WATER MATRIX EFFECTS ON MIB AND GEOSMIN REMOVAL

Background water matrix effects (cations, NOM) on MIB and geosmin removal were assessed in longer-term isotherm experiments (in the case of MIB with both ^{14}C-MIB and ^{12}C-MIB) and in shorter-term kinetic experiments. LMW served as a natural water source, for which the combined effect of cations and NOM on MIB and geosmin removal was determined. Additional experiments were conducted with salt-amended UPW to determine the effects of cations (Na^+, Ca^{2+}, salt mixture) on MIB and geosmin removal.

4.5.1 MIB adsorption isotherms

Batch experiments were conducted with 0.45-µm membrane-filtered LMW to evaluate the combined effects of NOM and cations on MIB and geosmin removal. Figures 4.17 and 4.18 summarize results of MIB adsorption isotherm experiments that were conducted with the two activated carbons WPH and CC-602, respectively. The results show that the presence of NOM markedly decreased the adsorption capacity of both activated carbons (salts typically do not affect the adsorptive uptake of neutral organic contaminants on activated carbons). Table 4.4 compares MIB adsorption capacities at an equilibrium liquid-phase MIB concentration of 10 ng/L (q_{10}). When MIB was spiked into LMW at an initial concentration

of ~100 ng/L, MIB adsorption capacities were 7 and 6% of the single-solute q_{10} values for the activated carbons WPH and CC-602, respectively (Table 4.4).

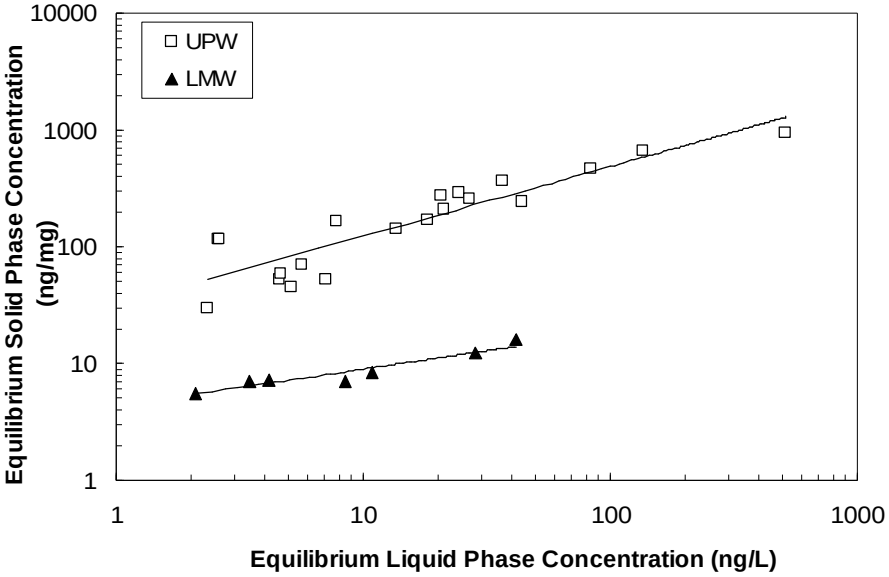

Figure 4.17 Comparison of MIB adsorption isotherms in UPW and LMW for activated carbon WPH. Lines represent Freundlich isotherm model fits.

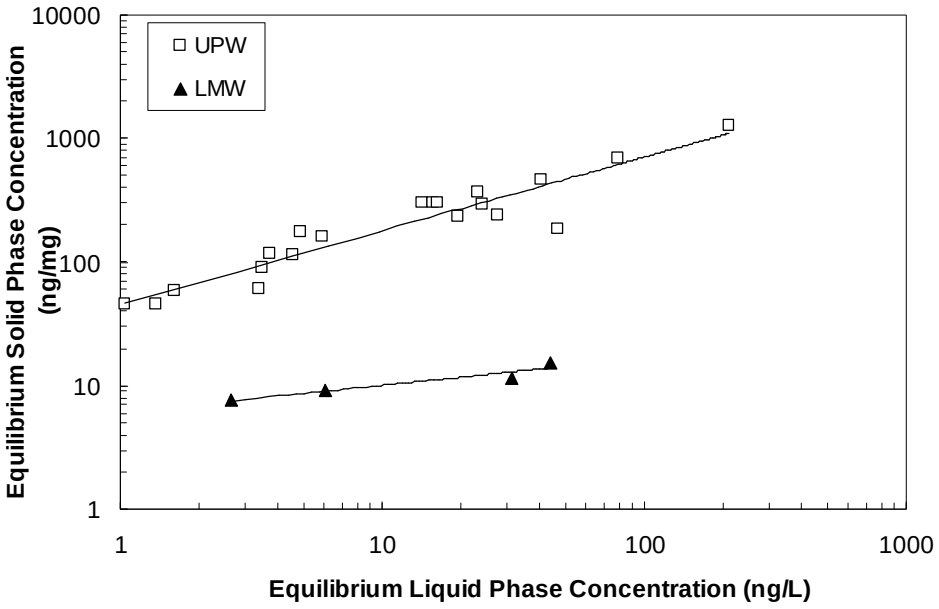

Figure 4.18 Comparison of MIB adsorption isotherms in UPW and LMW for activated carbon CC-602. Lines represent Freundlich isotherm model fits.

Table 4.4 Effect of background water constituents in LMW on MIB uptake.

Adsorbent	q_{10} (ng/mg)*		
	UPW	LMW	TRW
WPH	124	8.77	-
CC-602	180	10.2	-
H-Mordenite-230	11.1	1.12	3.67

* solid phase concentration at an equilibrium liquid phase concentration of 10 ng/L

It was hypothesized that MIB removal by H-Mordenite-230 would at most be minimally affected by the presence of NOM because size exclusion effects should prevent the adsorption of NOM. This hypothesis was based on earlier MTBE adsorption isotherm data (Knappe et al. 2007) collected with H-Mordenite-230 in Tar River Water (TRW, Greenville, NC). However, the ^{14}C-MIB results in Figure 4.19 illustrate that the presence of NOM and/or

cations in LMW dramatically reduced the ^{14}C-MIB/MIB dehydration product uptake by H-Mordenite-230. To determine whether the difference in results obtained with MIB and MTBE was attributable to differences in background water characteristics, an additional ^{14}C-MIB experiment was completed with H-Mordenite-230 in TRW. TRW has a higher DOC concentration (~6 mg/L) but a lower ionic strength than LMW. Figure 4.19 shows that ^{14}C-MIB/MIB dehydration product uptake was somewhat better in TRW than in LMW. Compared to the single-solute ^{14}C-MIB/MIB dehydration product uptake, however, the uptake measured in TRW was still dramatically lower. For H-Mordenite-230, q_{10} values were 10 and 33% of the single-solute values in LMW and TRW, respectively (Table 4.4).

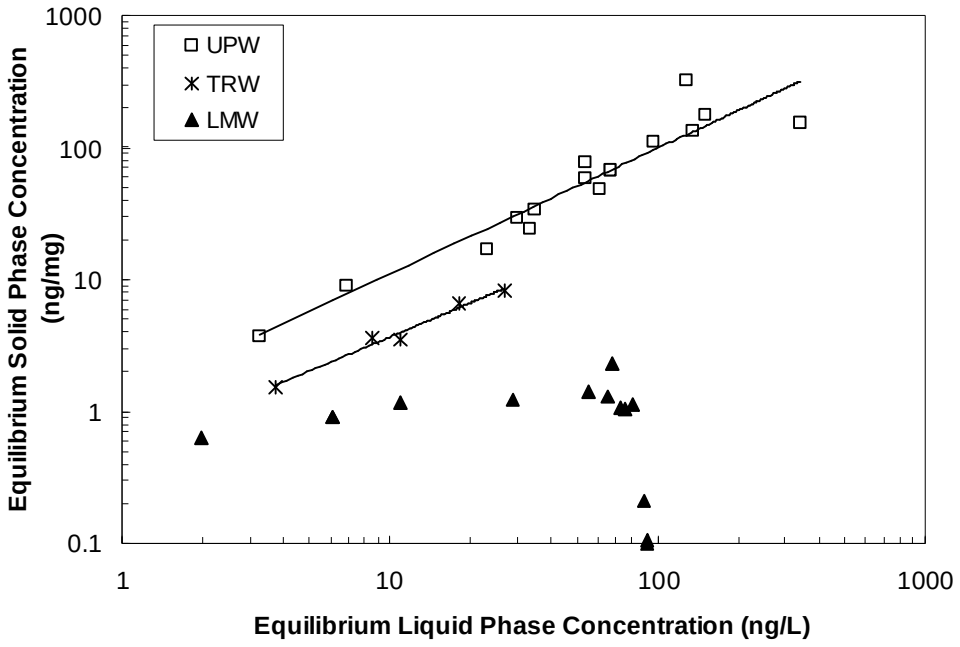

Figure 4.19 Comparison of ^{14}C-MIB/MIB dehydration product adsorption isotherms in UPW, LMW, and TRW for H-Mordenite-230. Lines represent Freundlich isotherm model fits.

One possibility for the adverse effect of the background water matrix on MIB removal by H-Mordenite-230 is that NOM molecules may have adsorbed near the entrances of zeolite pores and narrowed the pore entrance sufficiently to prevent MIB access to zeolite pores. In addition, cations such as Na^{+} and/or Ca^{2+} could have entered the pores of H-Mordenite-230 and replaced the smaller framework H^{+} ions such that the intraparticle diffusion resistance was increased. NOM and/or cation effects on MTBE adsorption by H-Mordenite-230 in a previous study may not have been as strong because (1) MTBE is a smaller molecule than MIB and (2) equilibrium MTBE concentrations were in the 1 to 100 μg/L range whereas equilibrium MIB concentrations were in the 2 to 100 ng/L range.

To check whether the background water matrix affected the external surface of H-Mordenite-230, zeolite crystals were analyzed by scanning electron microscopy before and after exposure to LMW. Figure 4.20 compares scanning electron micrographs (SEMs) of fresh H-Mordenite-230 (panels a and b) and of H-Mordenite-230 after exposure to LMW for 3 days (panels c and d). A comparison of panels b and d suggests that LMW constituents did leave a coating on the external zeolite surface that may have either blocked MIB access to zeolite pores and/or led to slower adsorption kinetics.

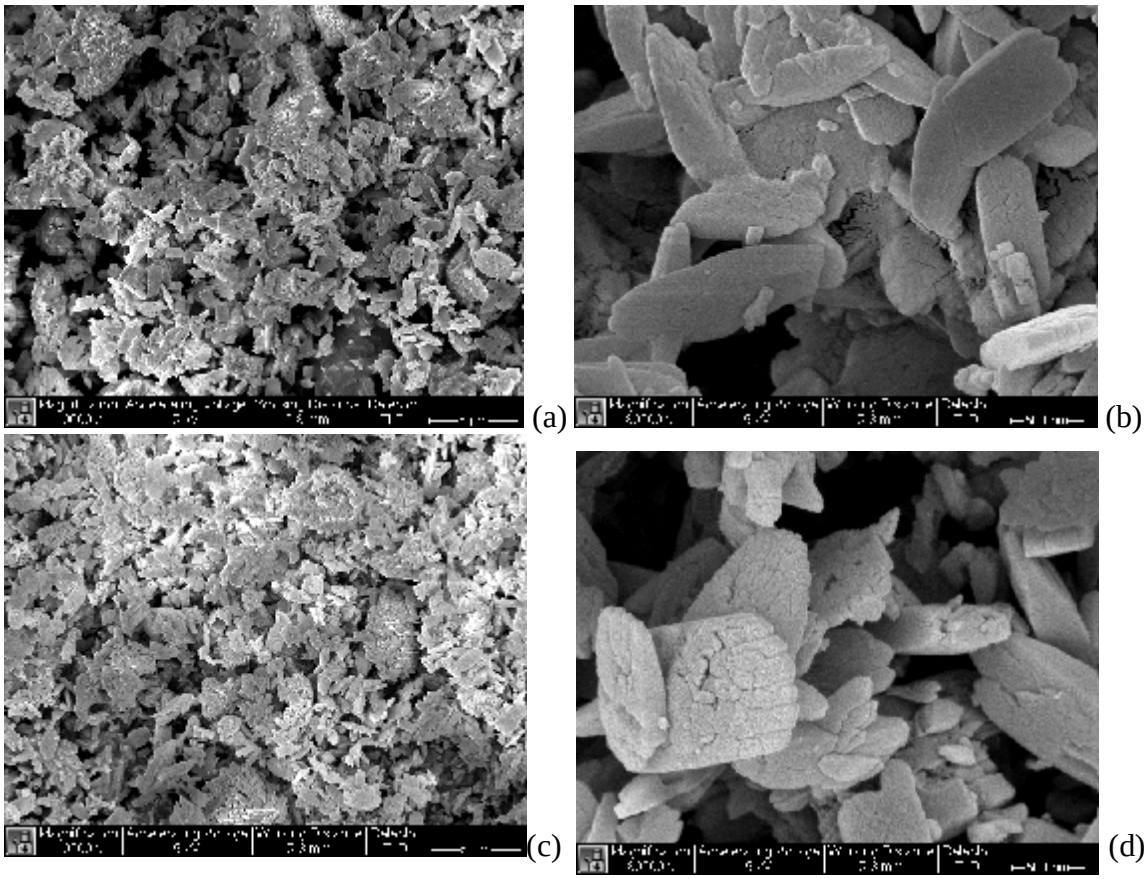

Figure 4.20 Scanning electron micrographs of fresh H-Mordenite-230 (panels a and b) and H-Mordenite-230 exposed to LMW for a period of 3 days (panels c and d). Magnification was 10,000× in panels a and c and 80,000× in panels b and d.

For the Y zeolite (H-Y-810), no measurable MIB removal was obtained in LMW at any of the tested zeolite doses (Figure 4.21). This result was not completely unexpected given that Sagehashi et al. (2005b) showed that river water NOM was able to completely displace MIB that was adsorbed on a Y zeolite.

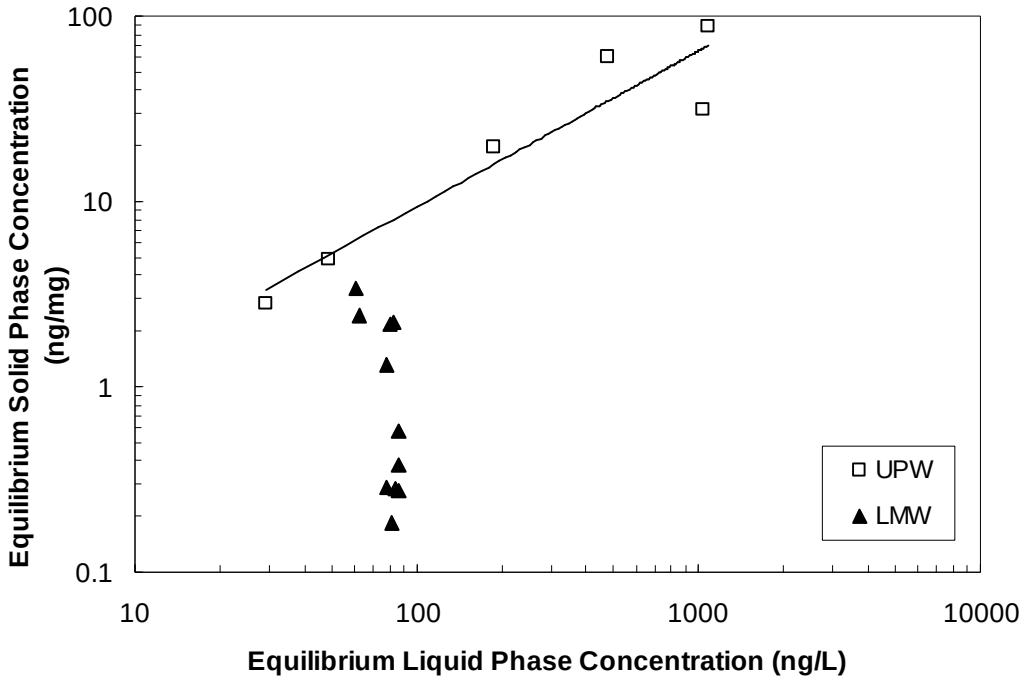

Figure 4.21 Comparison of ^{14}C-MIB/MIB dehydration product adsorption isotherms in UPW and LMW for H-Y-810. Line represents Freundlich isotherm model fit.

Apart from the ^{14}C-MIB data, 10-day batch data were also collected with ^{12}C-MIB to determine the effects of LMW constituents on the MIB removal effectiveness of H-Mordenite-90-1 and H-Mordenite-90-2. Figures 4.22 and 4.23 compare ^{12}C-MIB removal percentages obtained in UPW and LMW as a function of zeolite dose for H-Mordenite-90-1 and H-Mordenite-90-2, respectively. In both UPW and LMW, MIB removal was practically independent of zeolite dose over the tested range of zeolite dosages (~4-50 mg/L). However, LMW constituents adversely affected the MIB removal effectiveness of both zeolites and decreased MIB removal efficiency from >95% in UPW to about 80% in LMW (Figures 4.22 and 4.23). ^{12}C-MIB removal data obtained with the two mordenite zeolites did not conform

to the Freundlich isotherm model; therefore, it is likely that ^{12}C-MIB removal was aided by the proposed dehydration reaction (Figure 4.15) in addition to adsorption.

Figure 4.24 compares the ^{12}C-MIB removal effectiveness of H-Mordenite-90-1 and H-Mordenite-90-2 to that of the activated carbons WPH and CC-602. Adsorbents were added to LMW at doses ranging from about 3 to 16 mg/L, and the contact time was 10 days. The results in Figure 4.24 illustrate that ^{12}C-MIB removal at the low zeolite doses (<6 mg/L) was similar to or exceeded the levels obtained with the two activated carbons. At higher adsorbent doses, however, the activated carbons outperformed the mordenite zeolites.

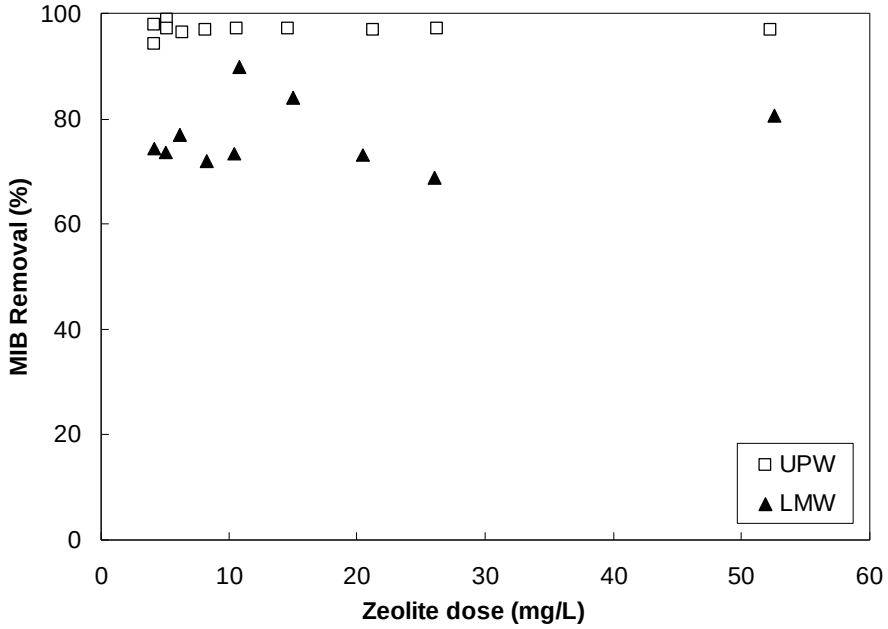

Figure 4.22 MIB removal from UPW and LMW as a function of H-Mordenite-90-1 dose. Contact time: 10 days.

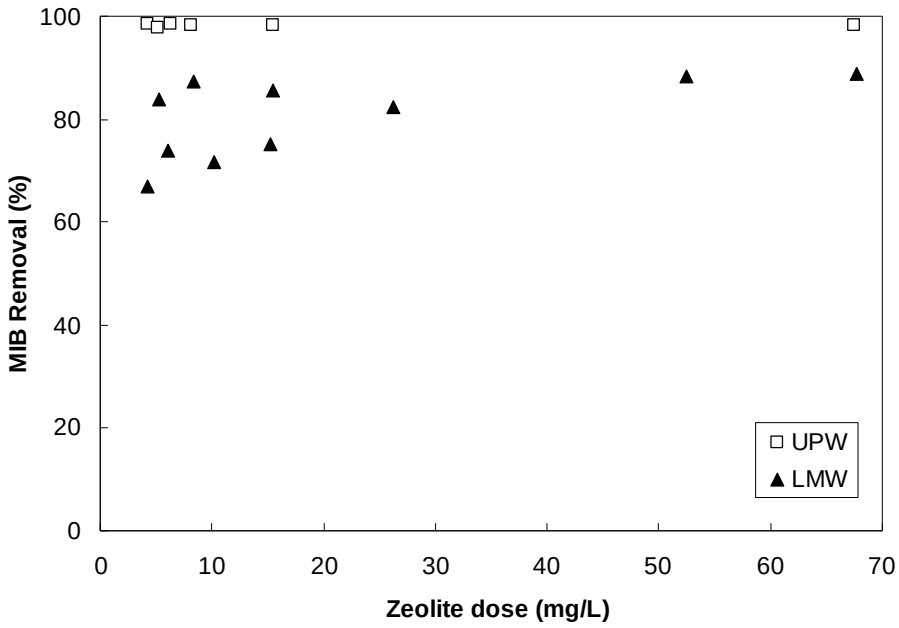

Figure 4.23 MIB removal from UPW and LMW as a function of H-Mordenite-90-2 dose. Contact time: 10 days.

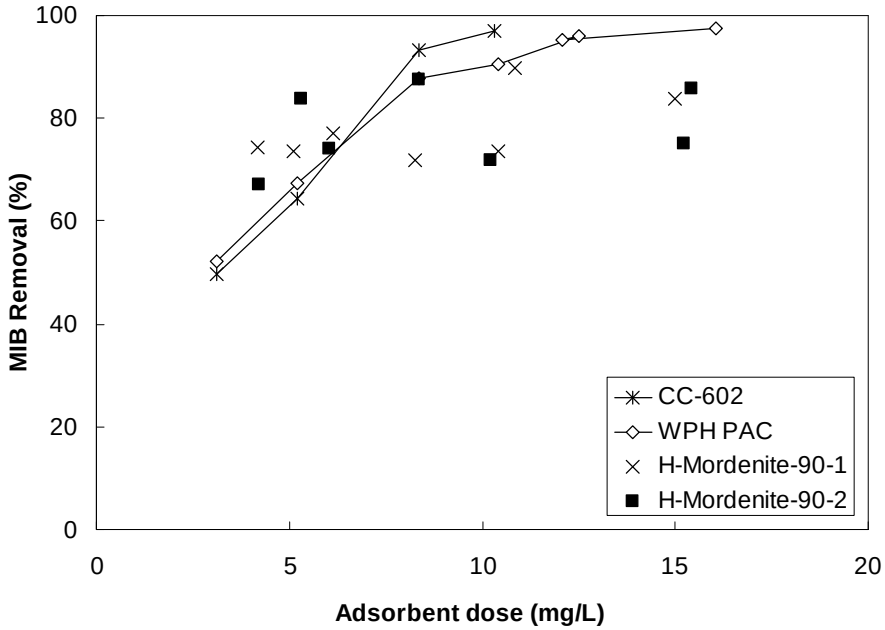

Figure 4.24 MIB removal from Lake Michigan water as a function of adsorbent dose for two activated carbons and two mordenite zeolites.

4.5.2 Geosmin adsorption isotherms

Geosmin adsorption isotherm data were collected in LMW for WPH and CC-602 PACs, H-Mordenite-230, and H-Y-810 and compared to the respective single-solute geosmin adsorption isotherms. NOM in LMW strongly affected geosmin uptake by WPH and CC-602 activated carbons as illustrated in Figures 4.25 and 4.26, respectively. As shown in Table 4.5, the q_{10} value for geosmin uptake from LMW was 2.3% and 2.4% of that obtained in UPW for WPH and CC-602, respectively.

For H-Mordenite-230, LMW constituents also adversely affected geosmin uptake (Figure 4.27), and the q_{10} value in LMW was approximately 25% of that obtained in UPW (Table 4.5). Interestingly, the effect of LMW constituents on geosmin adsorption was less than that measured for the adsorption of MIB and MIB dehydration products – for MIB, the q_{10} value in LMW was approximately 10% of that obtained in UPW. For both MIB and geosmin, q_{10} values for H-Mordenite-230 were similar (Tables 4.4 and 4.5). Compared to WPH and CC-602 PACs, the geosmin q_{10} value of H-Mordenite-230 was lower by a factor of almost 20.

Geosmin adsorption data obtained with H-Y-810 in UPW and LMW are compared in Figure 4.28. A substantial number of the data points obtained in LMW were scattered about the single-solute isotherm, suggesting that LMW constituents had little effect on geosmin

adsorption. However, the data points associated with the three largest zeolite doses (20, 25, and 30 mg/L) exhibited substantially lower geosmin adsorption capacities. Overall, it appeared that it was not possible to decrease the aqueous phase geosmin concentration below ~15 ng/L (the initial geosmin concentration for this test was 98.7 ± 6.0 ng/L — mean and standard deviation of triplicate analyses of three adsorbent-free blanks) with H-Y-810. One could argue that the geosmin data obtained with H-Y-810 in LMW are more reminiscent of the ^{12}C-MIB data obtained with mordenite zeolites in UPW (Figures 4.11 through 4.14), for which a reactive removal mechanism was proposed. However, it is unclear why a reactive removal mechanism would be observed for geosmin in LMW when it did not appear to play a role in the single-solute experiment. Another interesting observation can be made by comparing MIB and geosmin removal data that were obtained with H-Y-810 in LMW. For MIB, which is a slightly smaller molecule than geosmin, background matrix constituents in LMW were able to completely displace MIB from the zeolite pores, but the same did not occur with geosmin. Thus, small differences in adsorbate molecular shape and size can lead to very different adsorption behavior with molecular sieve adsorbents such as high-silica zeolites.

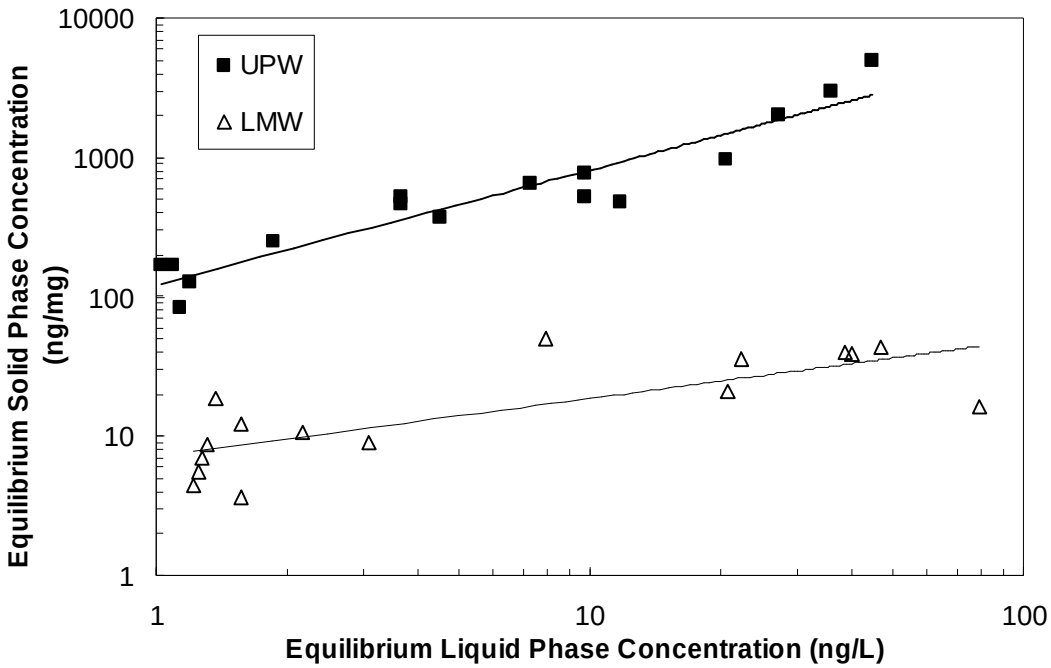

Figure 4.25 Comparison of geosmin adsorption isotherms in UPW and LMW for activated carbon WPH. Lines represent Freundlich isotherm model fits.

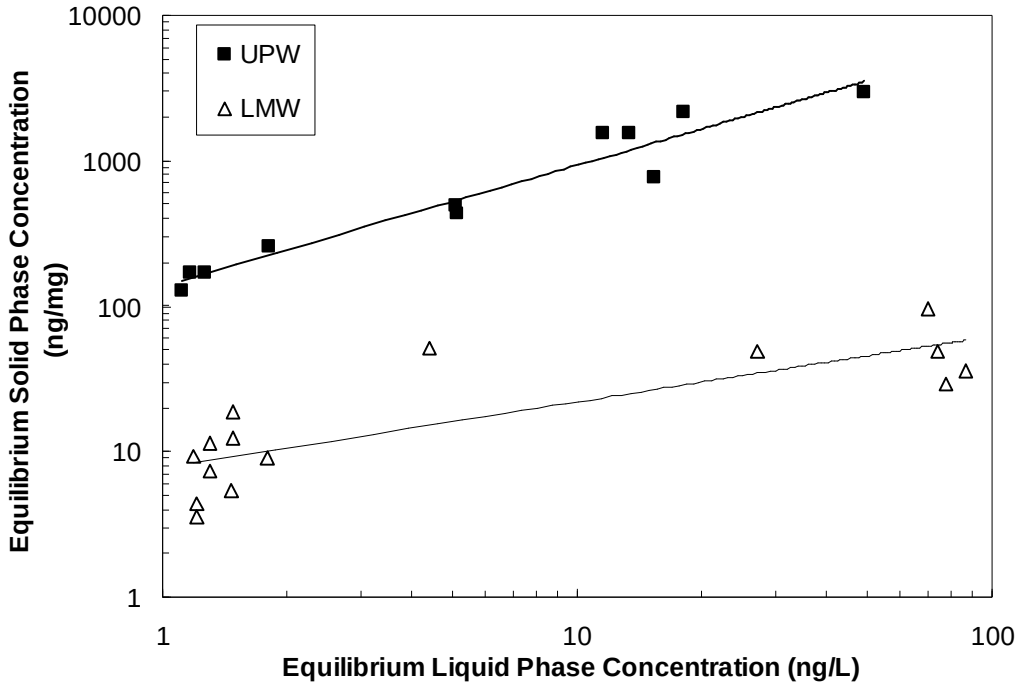

Figure 4.26 Comparison of geosmin adsorption isotherms in UPW and LMW for activated carbon CC-602. Lines represent Freundlich isotherm model fits.

Table 4.5 Effect of background water constituents in LMW on geosmin uptake.

Adsorbent	q_{10} (ng/mg)*	
	UPW	LMW
WPH	815	18.62
CC-602	933	21.98
H-Mordenite-230	3.90	0.97

* solid phase concentration at an equilibrium liquid phase concentration of 10 ng/L

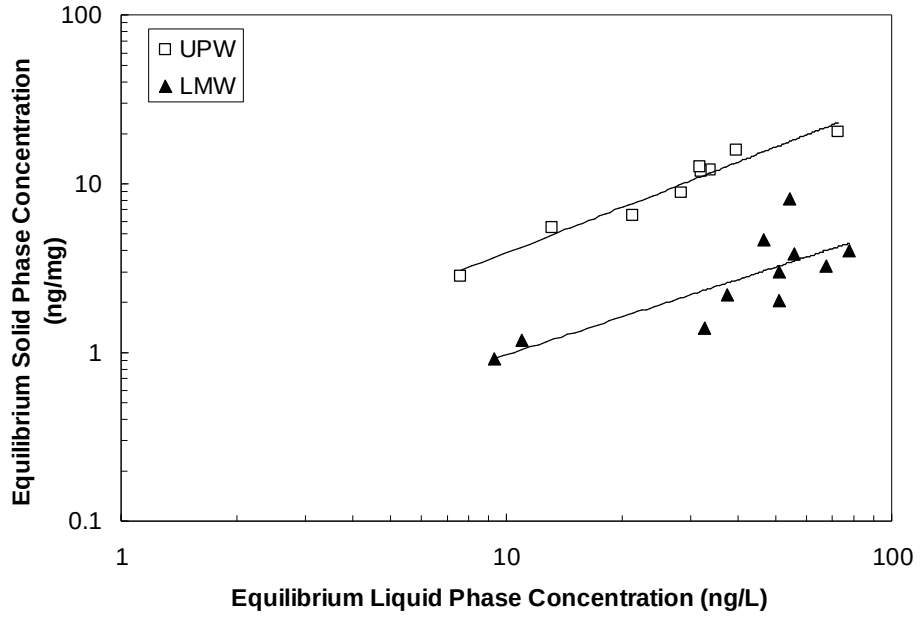

Figure 4.27 Comparison of geosmin adsorption isotherms in UPW and LMW for H-Mordenite-230. Lines represent Freundlich isotherm model fits.

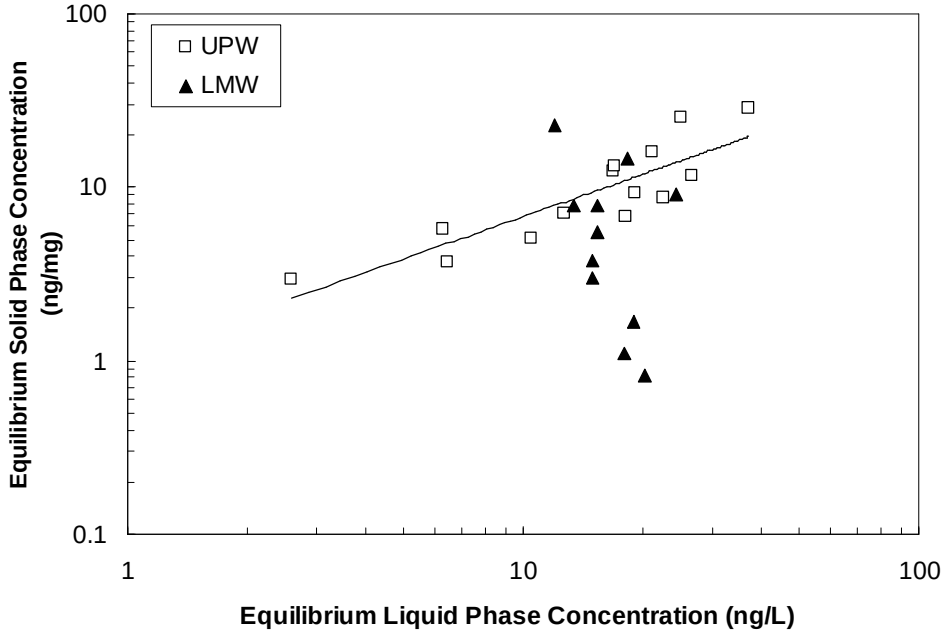

Figure 4.28 Comparison of geosmin adsorption isotherms in UPW and LMW for H-Y-810. Line represents Freundlich isotherm model fit.

4.5.3 Kinetic experiments

The ^{14}C-MIB isotherm results obtained with H-Mordenite-230 showed that MIB removal from TRW was higher than from LMW (Figure 4.19 and Table 4.4). Considering that the DOC concentration in LMW (1.8 mg/L) was only ~30% of that in TRW (~6 mg/L), the results shown in Figure 4.19 imply that apart from NOM, other background water constituents such as cations affect the MIB removal effectiveness of zeolites at conditions applicable to drinking water treatment. For example, ion exchange between aqueous cations such as Na^+ and the exchangeable H^+ ions on the zeolite surface may increase intraparticle diffusion resistance and reduce the acidity (or reactivity) of the zeolite. A suite of kinetic tests was therefore conducted to asses the effects of Na^+, Ca^{2+}, and cations in a salt mixture on MIB and geosmin removal. Results obtained with salt-amended UPW were compared to those obtained in UPW and LMW. Batch kinetic tests were conducted to determine MIB and geosmin removal rates as a function of time over a 2-hour period.

4.5.3.1 MIB removal kinetics

The first set of kinetic tests was conducted to determine the effects of LMW constituents on ^{12}C-MIB removal by WPH activated carbon and H-Mordenite-230, H-Mordenite-90-1 and H-Y-810 zeolites. Figure 4.29 compares MIB removal data obtained in UPW and LMW for

WPH activated carbon at doses of 2 and 15.5 mg/L. NOM adversely affected both the MIB adsorption capacity as well as MIB adsorption kinetics (Figure 4.29). The adverse effects of NOM on MIB removal were particularly pronounced at the lower PAC dose (2 mg/L); this result is consistent with a high solid-phase concentration of NOM constituents that compete with MIB for adsorption sites. At the higher PAC dose, the solid-phase concentration of NOM constituents that compete with MIB for adsorption sites was lower and thus did not affect MIB uptake as strongly.

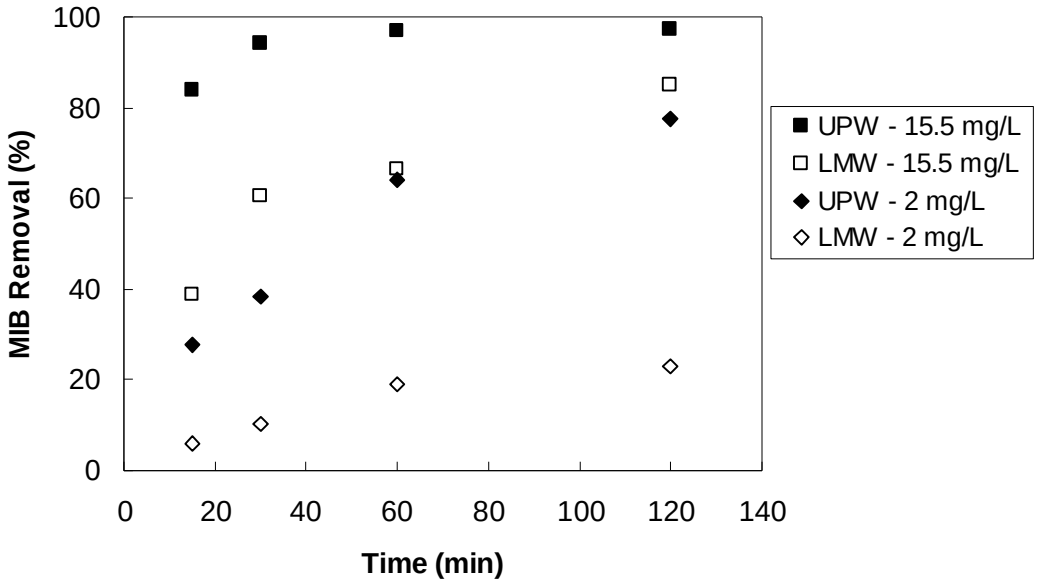

Figure 4.29 MIB removal kinetics for WPH activated carbon in UPW and LMW at PAC doses of 2 and 15.5 mg/L

Similar comparisons between MIB removal kinetics in UPW and LMW are shown in Figures 4.30, 4.31, and 4.32 for H-Mordenite-230, H-Mordenite-90-1 and H-Y-810, respectively. For both H-Mordenite-230 and H-Mordenite-90-1, the MIB removal effectiveness was markedly

reduced in LMW. This result can be explained by the presence of NOM in LMW and/or the displacement of framework H^+ ions by cations in LMW. The latter mechanism would have reduced the reactivity of the zeolite surface and/or increased the intraparticle diffusion resistance.

For H-Y-810, MIB removal was adversely affected by water matrix constituents in LMW at a zeolite dose of 15.5 mg/L. In contrast MIB removal was similar in UPW and LMW at a H-Y-810 dose of 2 mg/L. In long term isotherm experiments, no measurable MIB removal was obtained in LMW with H-Y-810 after 10 days (Figure 4.21). In contrast, MIB removal was approximately 50% and 30% at zeolite doses of 15.5 and 2 mg/L, respectively after two hours. These two contradicting results indicate displacement of MIB by NOM at longer contact times.

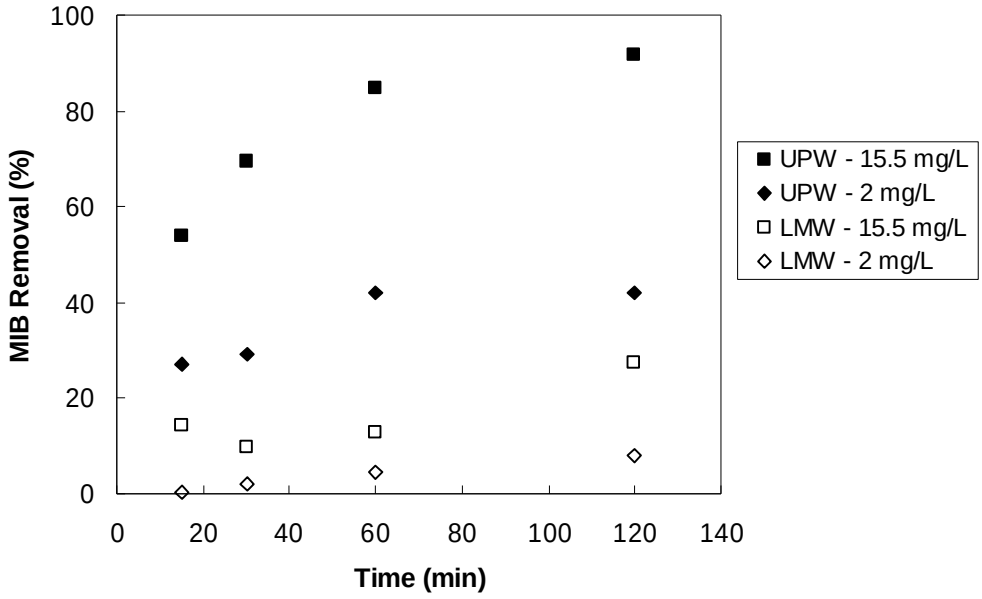

Figure 4.30 MIB removal kinetics for H-Mordenite-230 in UPW and LMW at zeolite doses of 2 and 15.5 mg/L

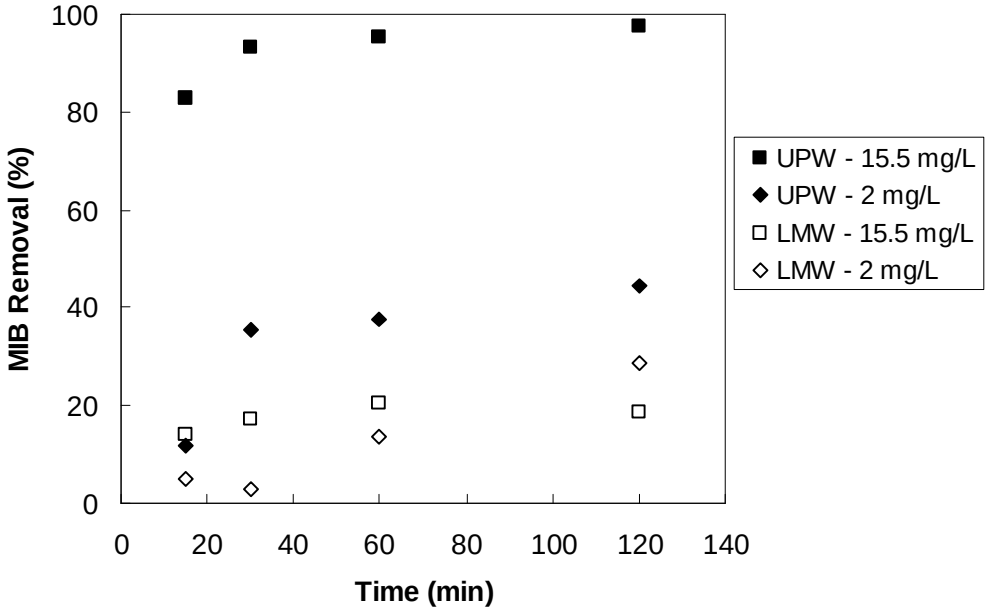

Figure 4.31 MIB removal kinetics for H-Mordenite-90-1 in UPW and LMW at zeolite doses of 2 and 15.5 mg/L

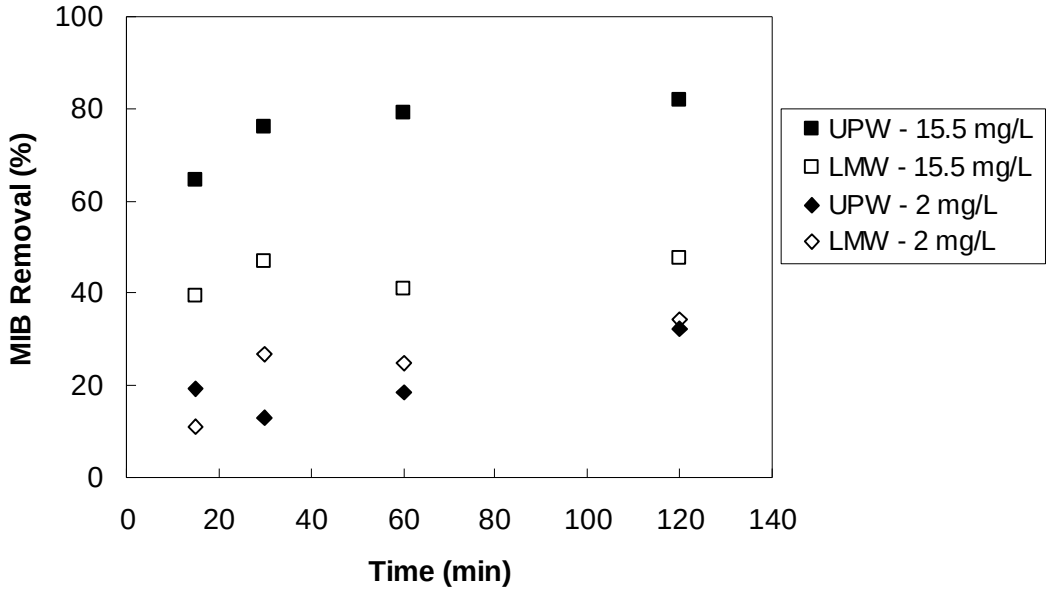

Figure 4.32 MIB removal kinetics for H-Y-810 in UPW and LMW at zeolite doses of 2 and 15.5 mg/L

To determine whether cations in the aqueous phase affect MIB removal, kinetic experiments were also conducted with UPW amended with 1 mM NaCl. Figures 4.33 and 4.34 compare MIB removal kinetics obtained with H-Mordenite-230 and H-Mordenite-90-1, respectively, in UPW, UPW amended with 1 mM NaCl, and LMW at a zeolite dose of 15.5 mg/L. The results in both figures show that the presence of NaCl markedly decreased the MIB removal percentage. Thus, dissolved salts in LMW are at least partly responsible for the compromised performance of H-Mordenite-230 and H-Mordenite-90-1 in LMW.

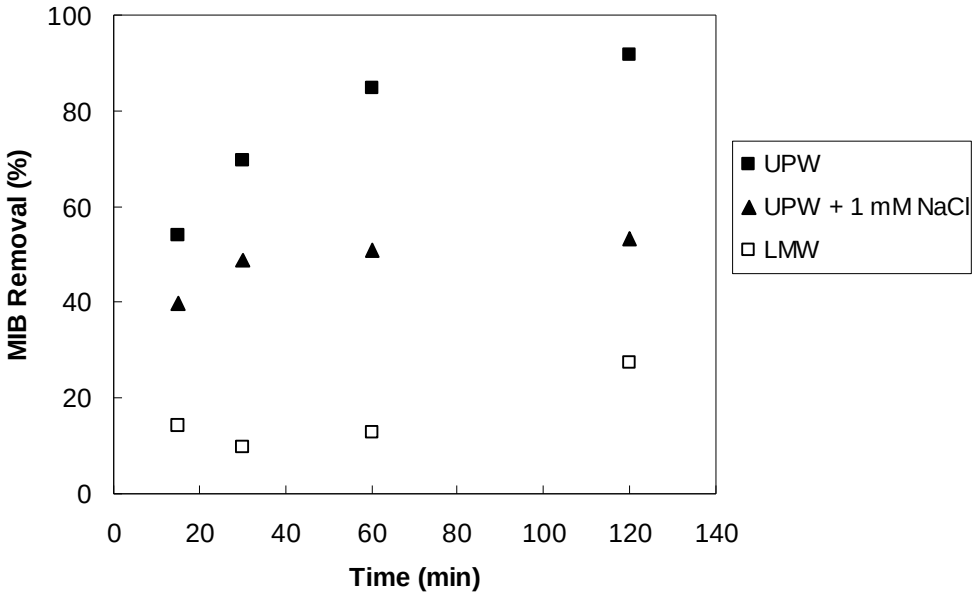

Figure 4.33 MIB removal kinetics for H-Mordenite-230 in UPW, UPW amended with 1 mM NaCl, and LMW at a zeolite doses of 15.5 mg/L

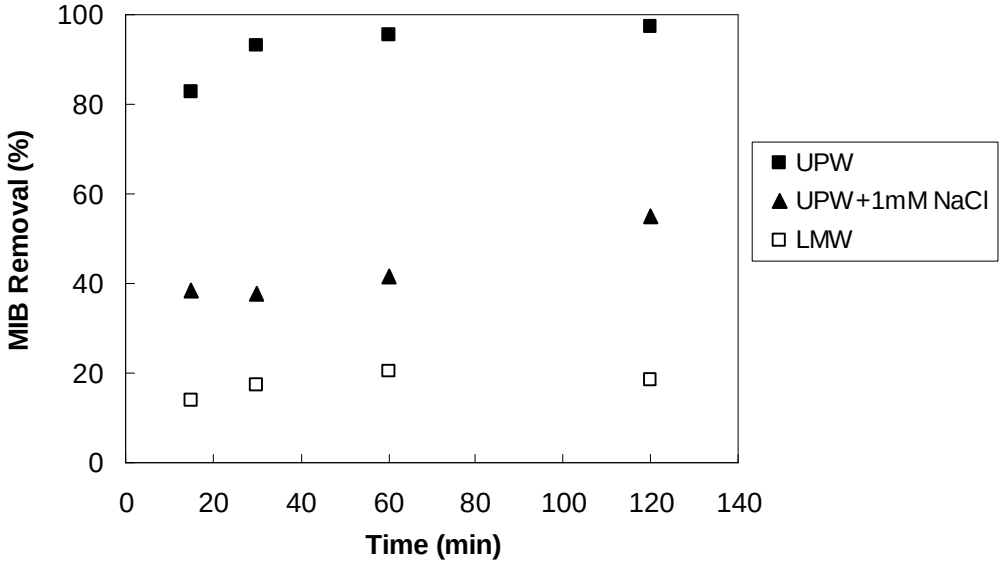

Figure 4.34 MIB removal kinetics for H-mordenite-90-1 in UPW, UPW amended with 1 mM NaCl, and LMW at a zeolite dose of 15.5 mg/L

Figure 4.35 compares the MIB removal effectiveness of H-Mordenite-230 and H-Mordenite-90-1 in UPW and UPW amended with 1 mM NaCl. In UPW, MIB removal was more rapid with H-Mordenite-90-1, a result that may be attributable to the higher reactivity of H-Mordenite-90-1. In the presence of NaCl, the MIB removal effectiveness of both zeolites was compromised, and similar levels of MIB removal were obtained. Ion exchange between framework H^+ and added Na^+ ions likely reduced or eliminated the reactivity of the zeolite surface. In addition, the presence of Na^+ ions in the zeolite channels likely hindered intraparticle MIB diffusion. Evidence for the latter mechanism is presented in section 4.5.3.2.

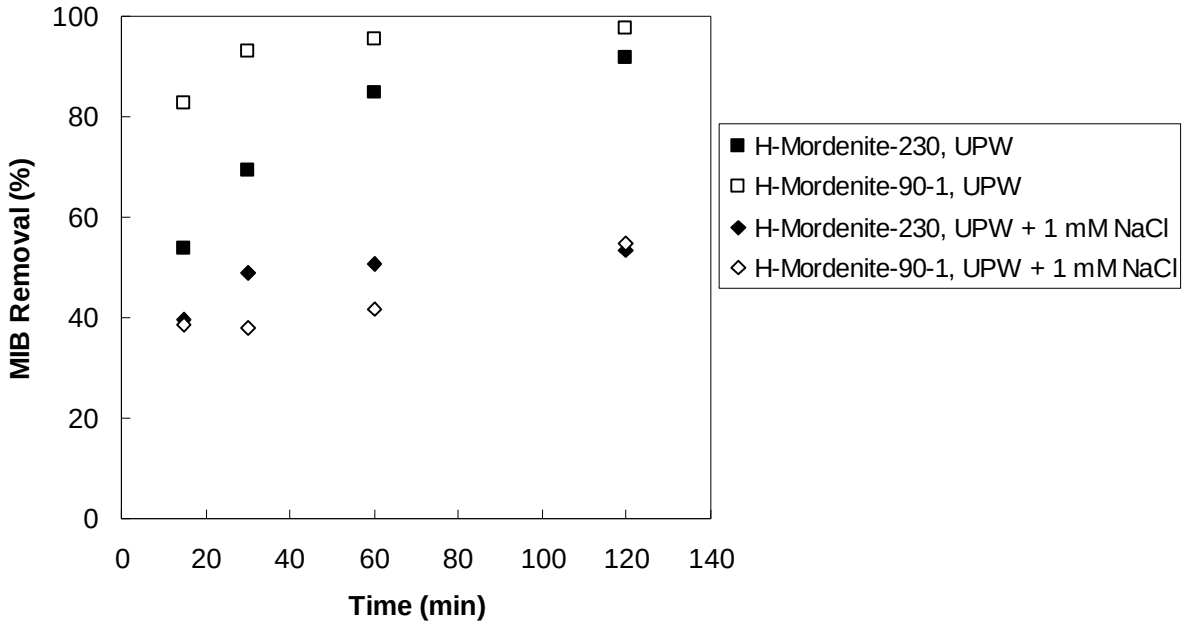

Figure 4.35 MIB removal kinetics for H-Mordenite-230 and H-Mordenite-90-1 in UPW and UPW amended with 1 mM NaCl at a zeolite dose of 15.5 mg/L

To evaluate the effectiveness of different mordenite zeolites, H-Y-810 and WPH PAC for MIB removal, batch kinetic data collected at a given adsorbent dose were compared for both UPW and LMW. In figures 4.36 and 4.37, MIB removal kinetics in UPW are compared for WPH PAC and for mordenite zeolites with SiO_2/Al_2O_3 ratios of 230, 90, and 40, and H-Y-810 at doses of 15.5 and 2 mg/L, respectively. Although MIB removal percentages obtained with 15.5 mg/L of H-Mordenite-230, H-Mordenite-90-1, and WPH activated carbon were similar after a contact time of 2 hr, the MIB removal rate obtained with H-Mordenite-230 was slower than that obtained with H-Mordenite-90-1 and WPH PAC (Figure 4.36). As discussed for Figure 4.35, the lower reactivity of H-Mordenite-230 relative to that of H-Mordenite-90-1 may be one factor that led to slower MIB removal kinetics. At an adsorbent dose of 2 mg/L, however, MIB removal was similar at SiO_2/Al_2O_3 ratios of 90 and 230 (Figure 4.37). Also, MIB removal kinetics obtained with 2 mg/L WPH activated carbon were similar to those obtained with H-Mordenite-230 and H-Mordenite-90-1 during the first 60 minutes, but the PAC was more effective at a contact time of 2 hours. Finally, both Figures 4.36 and 4.37 show that MIB removal improved as the SiO_2/Al_2O_3 ratio of mordenites increased from 40 to 90. This result is important because H-Mordenite-40 was the most reactive among the tested zeolites (see discussion related to Figures 4.11-4.14). A prerequisite for the dehydration reaction is that MIB adsorption takes place. Because of the hydrophilic nature of H-Mordenite-40, water can adsorb more strongly in its pores than in the pores of more hydrophobic zeolite, and MIB adsorption is therefore energetically less

favored on H-Mordenite-40 compared to more hydrophobic zeolites. The results of the short-term kinetic tests indicate that the more reactive surface of H-Mordenite-40 was not sufficiently accessible to MIB to effectively participate in dehydration reactions.

For H-Y-810, MIB removal percentages at both adsorbent doses were lower than those obtained with H-Mordenite-90-1, H-Mordenite 230, and WPH after 2 hours of contact time (Figures 4.36 and 4.37).

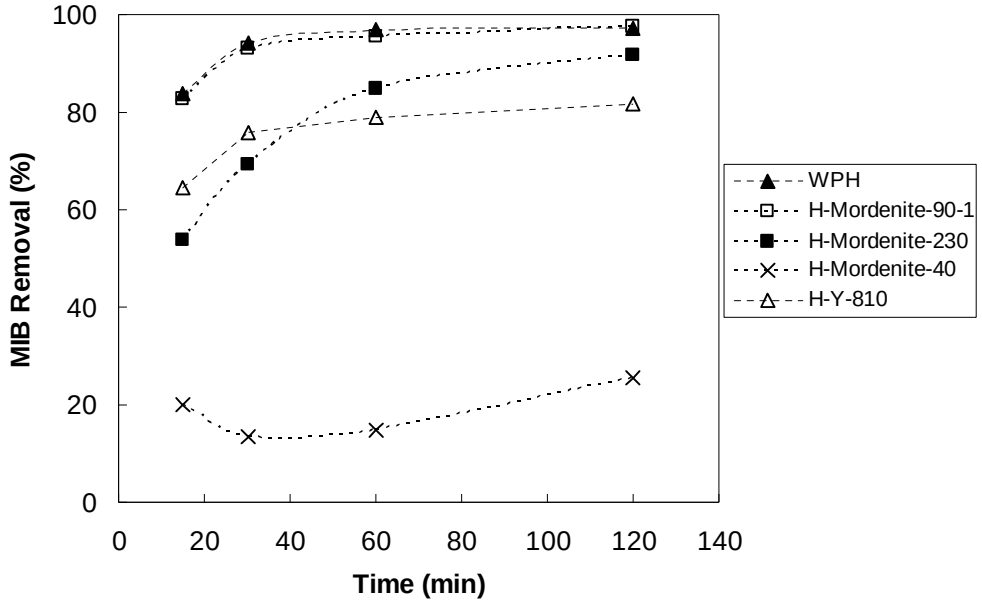

Figure 4.36 MIB removal kinetics for H-Mordenite-230, H-Mordenite-90-1, H-Mordenite- 40, H-Y-810 and WPH PAC in UPW at an adsorbent dose of 15.5 mg/L

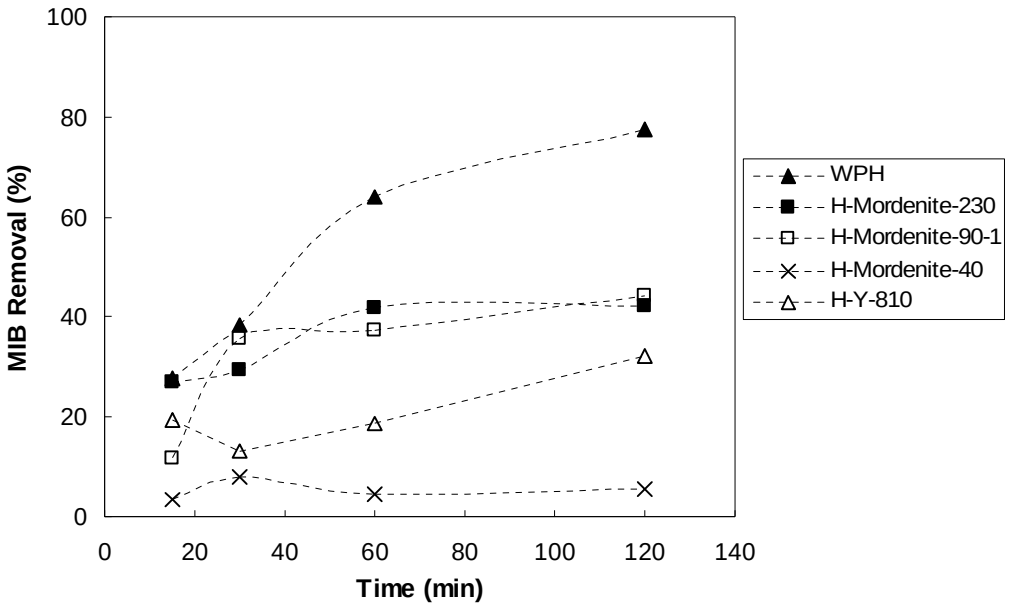

Figure 4.37 MIB removal kinetics for H-Mordenite-230, H-Mordenite-90-1, H-Mordenite-40, H-Y-810, and WPH PAC in UPW at an adsorbent dose of 2 mg/L

The performance of mordenite zeolites, H-Y-810 and WPH PAC for MIB removal from LMW are compared in Figure 4.38 and 4.39 at doses of 15.5 and 2 mg/L, respectively. As shown in Figure 4.38, WPH PAC was the most effective adsorbent for MIB removal from LMW. Relative to the results obtained in UPW (Figure 4.36), the performances of H-Mordenite-230, H-Mordenite-90-1 and H-Y-810 were adversely affected by background water matrix constituents such as NOM and cations in LMW. However, this adverse effect was less pronounced for H-Y-810 than for the two mordenite zeolites. Results in Figure 4.39 indicate that WPH and H-Mordenite-90-1 performed similarly at an adsorbent dose of 2 mg/L and that H-Y-810 performed slightly better, but MIB removal was low (~20% for WPH, ~25% for H-Mordenite-90-1, and ~30% for H-Y-810 after 2 hours). At an adsorbent

dose of 2 mg/L, H-Mordenite-230 performance was the worst among the tested adsorbents (8% MIB removal from LMW). As was the case for the higher adsorbent dose, background water matrix constituents in LMW more strongly affected MIB removal by mordenite zeolites than by H-Y-810 (Figures 4.36-4.39)

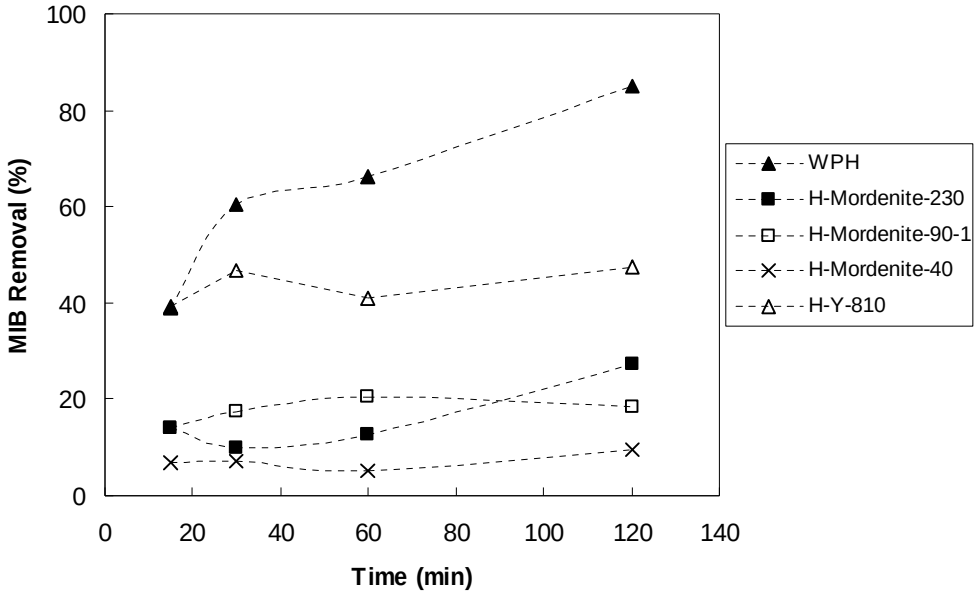

Figure 4.38 MIB removal kinetics for H-Mordenite-230, H-Mordenite-90-1, H-Mordenite-40, H-Y-810 and WPH PAC in LMW at an adsorbent dose of 15.5 mg/L

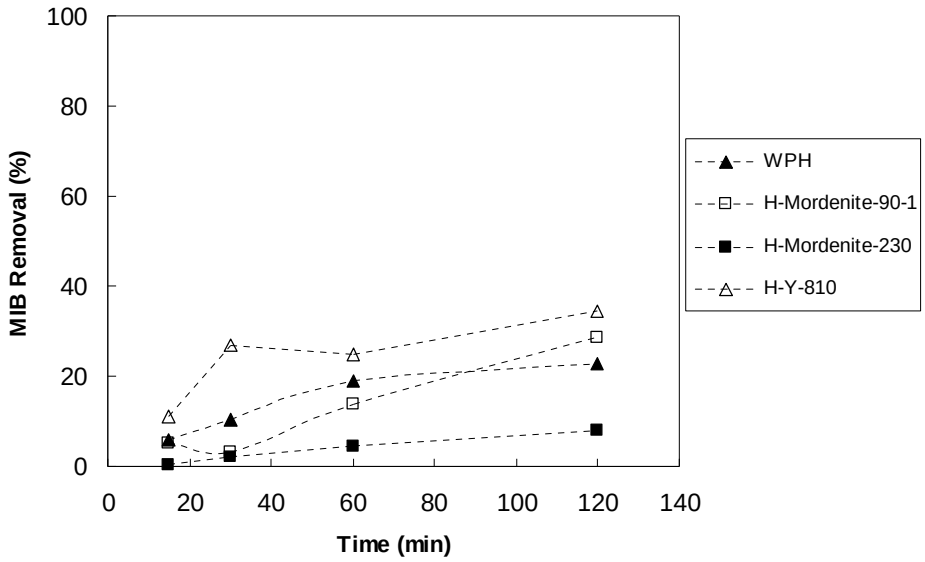

Figure 4.39 MIB removal kinetics for H-Mordenite-230, H-Mordenite-90-1, H-Y-810 and WPH PAC in LMW at an adsorbent dose of 2 mg/L

Finally, batch kinetic experiments were conducted with WPH PAC in its as-received form, its sub-micrometer diameter form (S-WPH S-PAC), and H-Y-810 zeolite in LMW at an adsorbent dose of 5mg/L. MIB removal efficiencies of WPH, S-WPH and H-Y-810 aer compared in Figure 4.40. Throughout the 2 hour test, MIB removal with S-WPH was higher than with WPH and H-Y-810. The superior performance of S-WPH was primarily related to its smaller particle size which leads to faster adsorption kinetics.

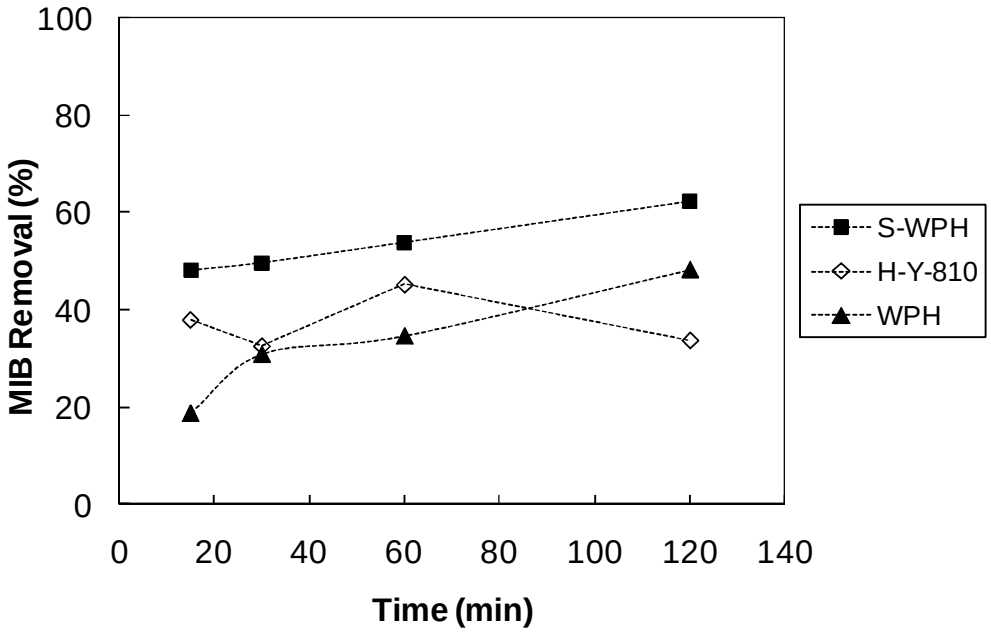

Figure 4.40 MIB removal kinetics for H-Y-810, WPH PAC and S-WPH S-PAC in LMW at an adsorbent dose of 5 mg/L

4.5.3 2 Geosmin Removal Kinetics

As was the case with MIB, the first set of kinetic tests was conducted to determine the effects of LMW constituents on geosmin removal by the adsorbents WPH, S-WPH, H-Mordenite-230, H-Mordenite-90-1, and H-Y-810. Geosmin removal kinetics obtained in UPW and LMW with WPH at doses of 15.5 and 2 mg/L are compared in Figure 4.41. Although geosmin adsorption kinetics were slower in LMW, geosmin removals after a contact time of 2 hours were similar in UPW and LMW at the 15.5 mg/L activated carbon dose. In contrast, geosmin removal after a contact time of 2 hours was more strongly affected by the presence

of NOM at an activated carbon dose of 2 mg/L. As was the case with MIB, this behavior was attributed to the higher surface loading of competing NOM fractions at the 2 mg/L activated carbon dose.

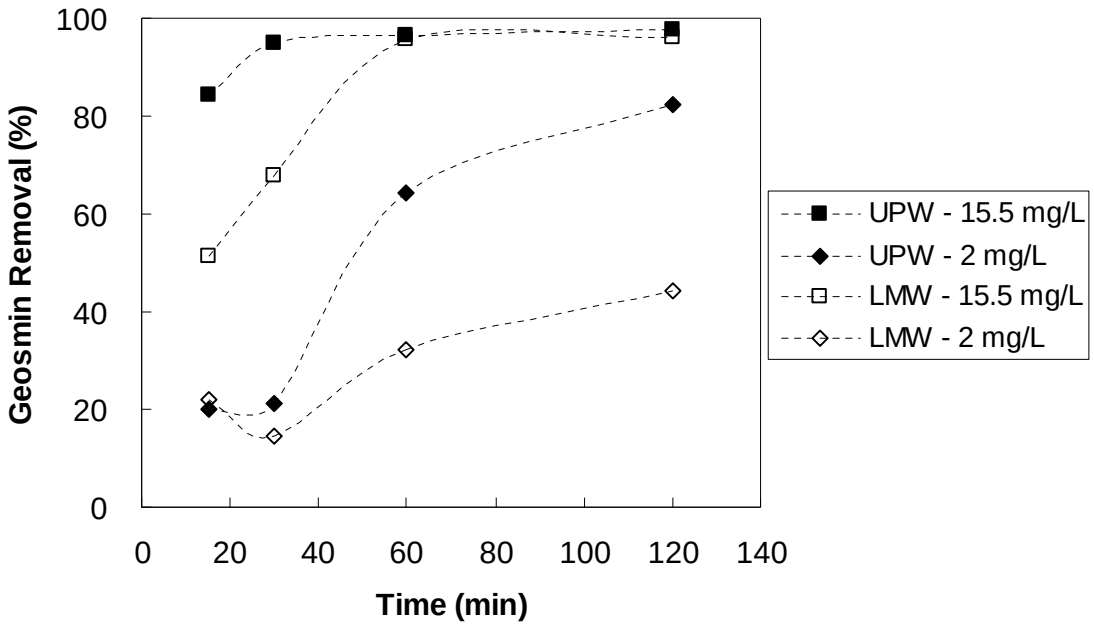

Figure 4.41 Geosmin removal kinetics for WPH PAC in UPW and LMW at carbon doses of 15.5 mg/L and 2 mg/L

Geosmin removal kinetics obtained with H-Mordenite-230 in UPW and LMW at doses of 15.5 and 2 mg/L are compared in Figure 4.42. At both zeolite doses, the results indicate that the performance of H-Mordenite-230 was markedly decreased by LMW constituents. Similar results are shown in Figure 4.43 for H-Mordenite-90-1; i.e., geosmin removal was strongly affected by LMW constituents. In contrast to mordenite zeolites, the H-Y-810 zeolite

produced similar geosmin removals in both UPW and LMW (Figure 4.44). Geosmin removal obtained in short term kinetic experiments was higher than that obtained in long term isotherm experiments, especially at 2 mg/L dose. This result suggests that geosmin was displaced by competing LMW constituents at longer contact times, but the displacement was not as complete as that observed for MIB.

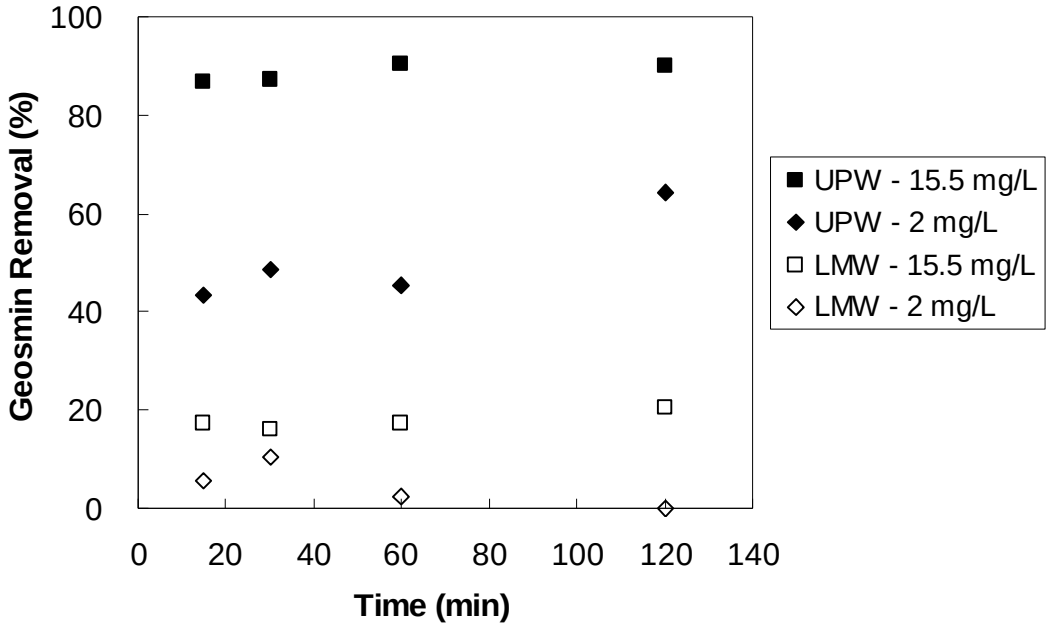

Figure 4.42 Geosmin removal kinetics for H-Mordenite-230 in UPW and LMW at zeolite doses of 15.5 mg/L and 2 mg/L

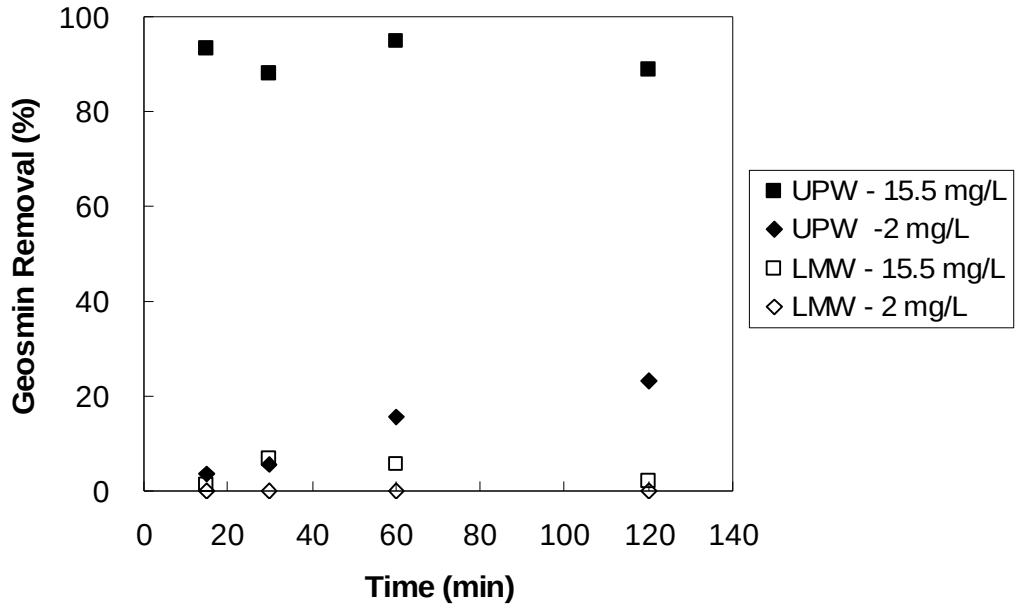

Figure 4.43 Geosmin removal kinetics for H-Mordenite-90-1 in UPW and LMW at zeolite doses of 15.5 mg/L and 2 mg/L

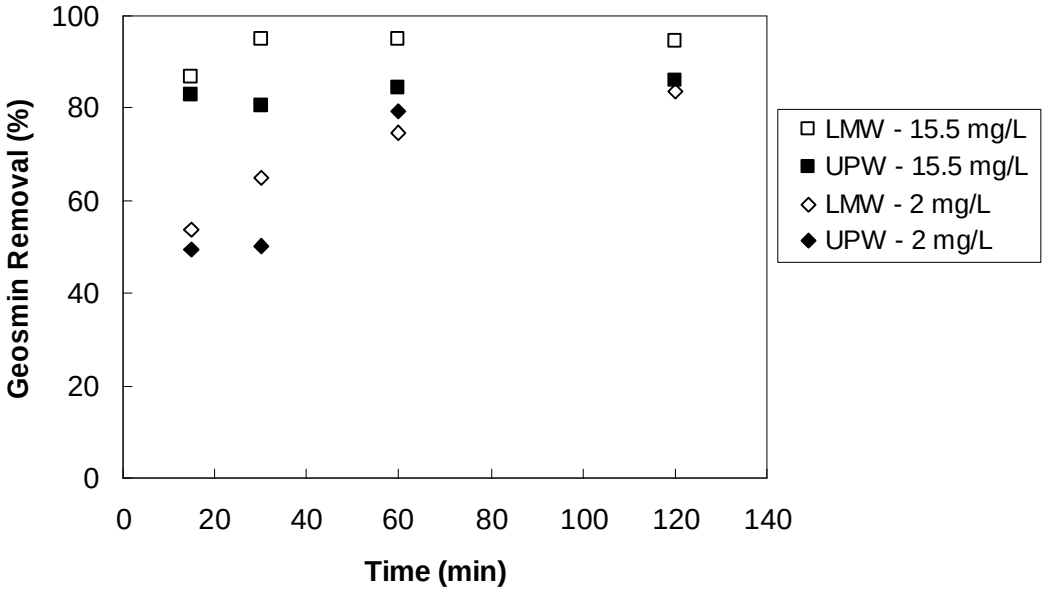

Figure 4.44 Geosmin removal kinetics for H-Y-810 in UPW and LMW at zeolite doses of 15.5 mg/L and 2 mg/L

To investigate the effects of cations on geosmin removal by mordenite zeolites, kinetic tests were performed with UPW amended with the following salts:

- 1 mM NaCl
- 1 mM $CaCl_2$
- Salt mixture consisting of 1 mM $CaCl_2$, 0.4 mM $MgCl_2$, 0.28 mM NaCl, and 0.03 mM KCl. This mixture approximates the cation composition of the tested LMW.

Figure 4.45 shows the effect of calcium and the cation mixture on geosmin removal by H-Mordenite-230. The results show that 1 mM Ca^{2+} lowered the geosmin removal effectiveness of H-Mordenite-230 from ~90% in UPW to ~65%. The addition of other cations (Mg^{2+}, Na^{+}, and K^{+}) did not measurably reduce geosmin removal beyond the levels obtained with 1 mM Ca^{2+} only (Figure 4.45). Given that the geosmin isotherm data (e.g., Figure 4.7) suggested that geosmin removal by mordenite zeolites occurs principally by adsorption, the effect of cations on geosmin removal appears to be one of exerting increased intraparticle diffusion resistance. Further evidence for this mechanism is provided below. Figure 4.45 further shows that the geosmin removal efficiency in LMW was lower than that in salt-amended UPW. The additional decrease suggests that NOM, in addition to cations, negatively affected geosmin removal from LMW.

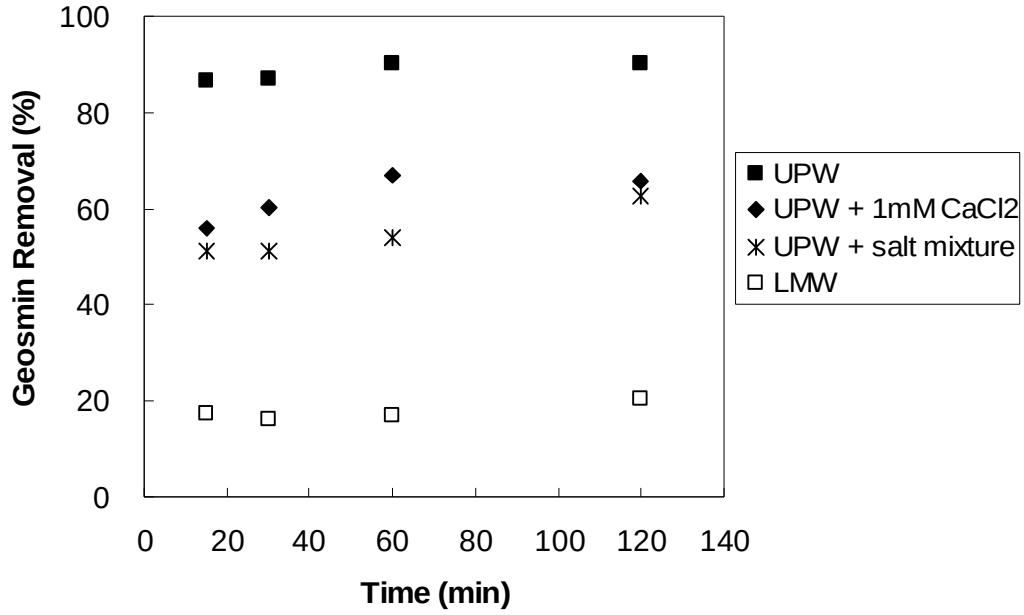

Figure 4.45 Effects of calcium and cations in a salt mixture on geosmin removal kinetics for H-mordenite-230. Zeolite dose: 15.5 mg/L.

As illustrated in Figure 4.46, geosmin removal by H-Mordenite-90 was similarly affected by the presence of NaCl, $CaCl_2$, and the salt mixture. The hydrated ionic radii of Ca^{2+} and Na^{+} are similar (4.12 and 3.58 Å, respectively, Volkov et al. 1997), which may explain why the presence of Na^{+} or Ca^{2+} in the zeolite pores led to a similar level of diffusion resistance.

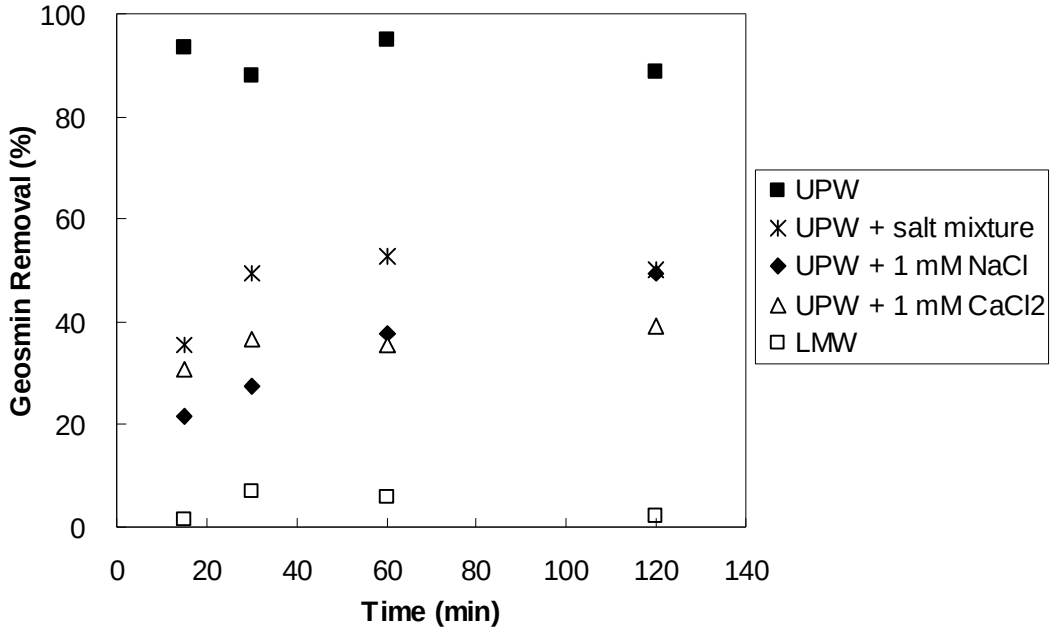

Figure 4.46 Effects of sodium, calcium, and cations in a salt mixture on geosmin removal kinetics for H-mordenite-90-1. Zeolite dose: 15.5 mg/L.

Figure 4.47 compares the effect of calcium cations on geosmin removal by H-Mordenite-230 and H-Mordenite-90-1. Geosmin removal by H-Mordenite-90-1 was more strongly affected by the presence of $CaCl_2$ than geosmin removal by H-Mordenite-230. This result suggests that the ion exchange capacity, which increases with decreasing SiO_2/Al_2O_3 ratio, affected the degree to which cations increased the intraparticle diffusion resistance. In other words, more Ca^{2+} was exchanged for H^+ on H-Mordenite-90-1 than on H-Mordenite-230, and the higher Ca^{2+} loading on H-Mordenite-90 imparted a greater diffusion resistance for geosmin. This effect was not as clearly seen with MIB (Figure 4.35) because MIB removal by zeolites

can occur by both reaction and adsorption mechanisms while geosmin removal occurs predominantly by adsorption.

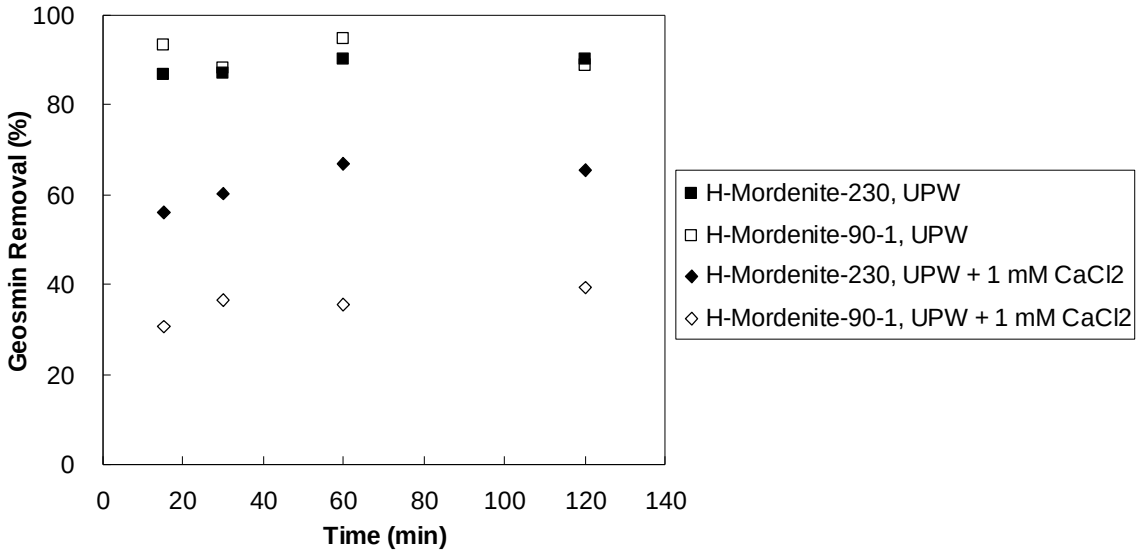

Figure 4.47 Effect of calcium on geosmin removal kinetics for H-Mordenite-230 and H-Mordenite-90-1. Zeolite dose: 15.5 mg/L.

To determine whether the presence of cations affects adsorption kinetics or entirely blocks geosmin access to zeolite pores, three longer-term kinetic tests were conducted. Figure 4.48 illustrates that in all tests that were conducted in the presence of salts, geosmin uptake increased slowly over the 1-week test period. In contrast, geosmin removal in UPW did not change measurably after a contact time of 15 minutes.

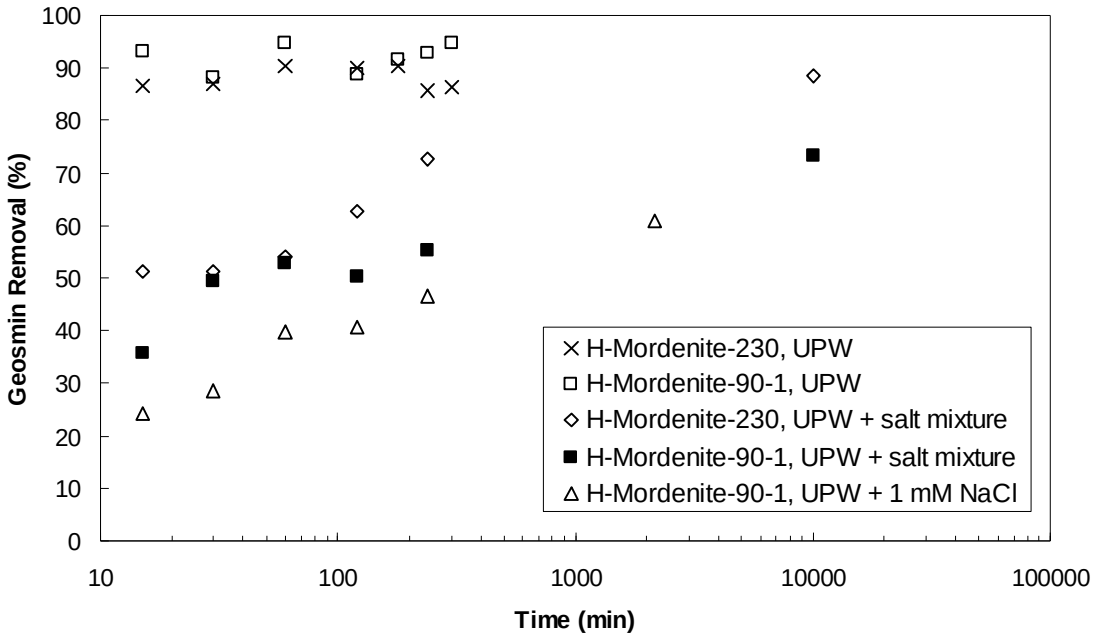

Figure 4.48 Effect of sodium and cations in a salt mixture on geosmin removal kinetics for H-Mordenite-230 and H-Mordenite-90-1. Zeolite dose: 15.5 mg/L. The last data point corresponds to a contact time of 1 week.

The strong effect of cations on geosmin uptake kinetics by mordenite zeolites is likely related to the essentially one-dimensional channel framework of mordenite. Only the larger channels (6.5 × 7.0 Å) of the mordenite framework (see Figure 2.5) are accessible to geosmin. A cation that is ion exchanged to an acidic surface sites in the zeolite pore may therefore block the pore such that geosmin diffusion is only possible when the ion migrates to another site.

To determine whether geosmin uptake kinetics are a function of the salt concentration, geosmin uptake after a 2-hour contact time with 15.5 mg/L H-Mordenite-90-1 was compared for UPW amended with NaCl at concentrations of 0.1 mM, 0.25 mM, 0.5 mM, and 1 mM. As

shown in Figure 4.49, geosmin uptake was similar at the 4 salt concentrations, suggesting that even small quantities of salt greatly affect geosmin uptake kinetics. If each aluminum site on H-Mordenite-90-1 represents one ion exchange site, then the addition of 15.5 mg H-Mordenite-90-1 would have provided ion exchange sites for 5.6 µmol of Na^+. Given that the tested salt concentrations greatly exceeded the concentration of ion exchange sites, it is reasonable that no effect of salt concentration on geosmin uptake kinetics was observed. For reference, Figure 4.49 includes geosmin uptake data obtained after 2 hours in UPW and LMW. These results reiterate that cations were one important factor, but not the only factor, that affected geosmin uptake kinetics from LMW.

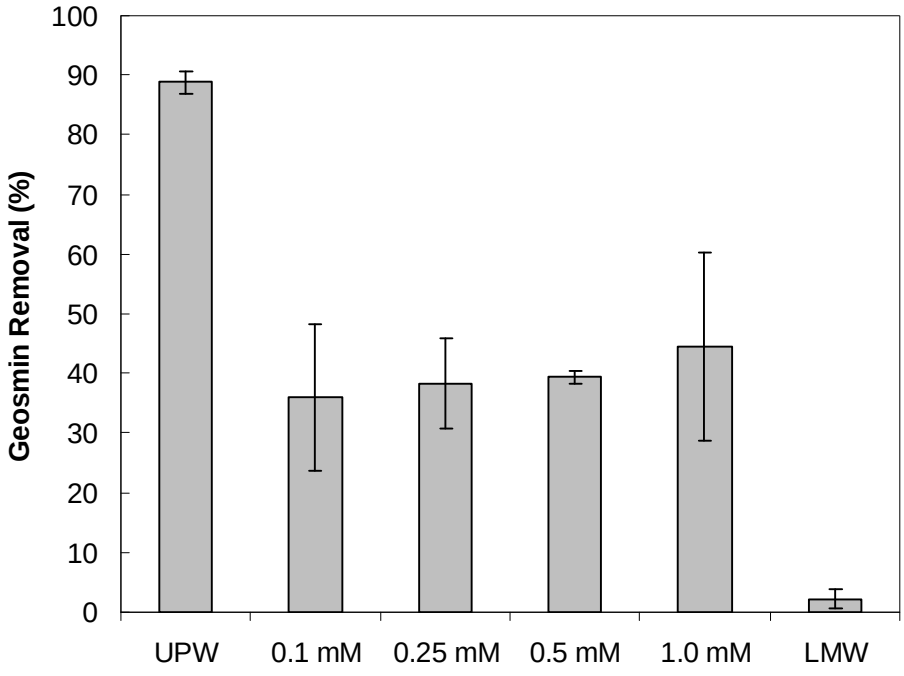

Figure 4.49 Effect of NaCl concentration on geosmin removal by H-Mordenite-90-1 at a zeolite dose of 15.5 mg/L. Contact time: 2 hours. Data for UPW and LMW are shown for reference.

To evaluate the effectiveness of different mordenite zeolites, Y-zeolite and WPH PAC for geosmin removal, batch kinetic data collected at a given adsorbent dose were compared for both UPW and LMW. In Figures 4.50 and 4.51, geosmin uptake kinetics from UPW are compared for three mordenite zeolites, H-Y-810 and WPH PAC at doses of 15.5 and 2 mg/L, respectively.

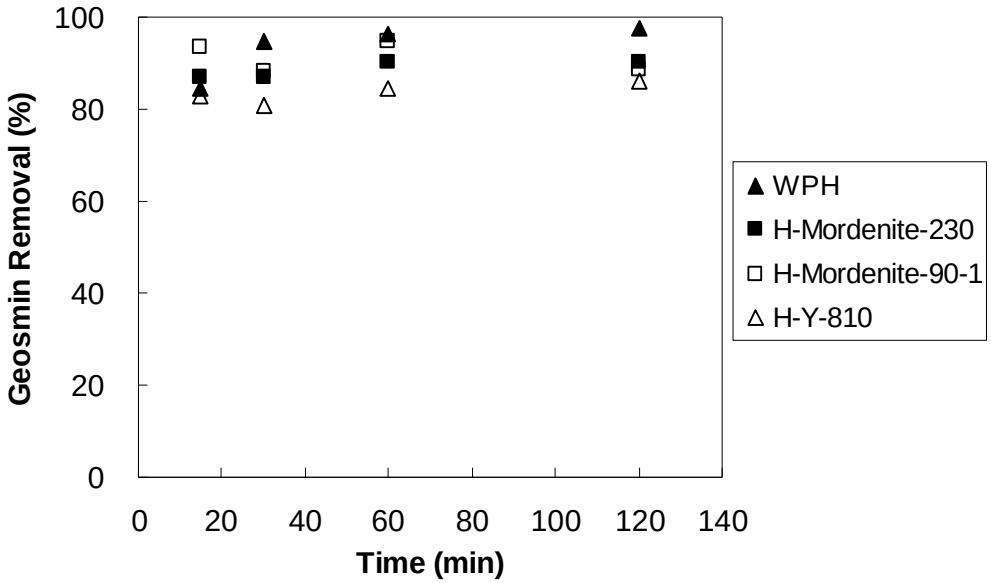

Figure 4.50 Geosmin removal kinetics for H-Mordenite-230, H-Mordenite-90-1, H-Y-810, and WPH PAC in UPW at an adsorbent dose of 15.5 mg/L

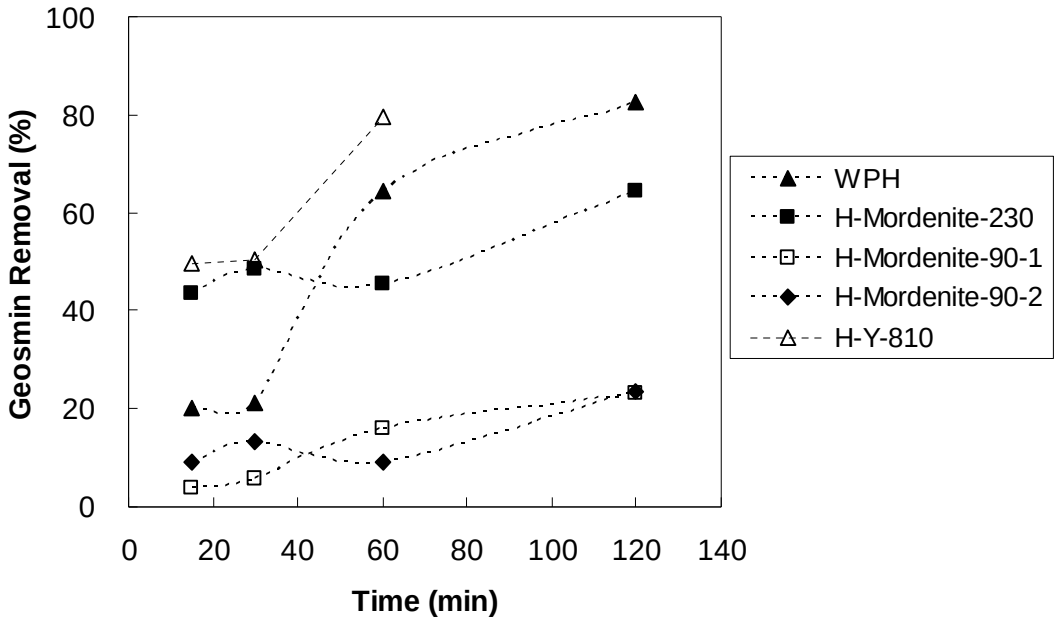

Figure 4.51 Geosmin removal kinetics for H-Mordenite-230, H-Mordenite-90-1, H-Mordenite-90-2, H-Y-810, and WPH PAC in UPW at an adsorbent dose of 2 mg/L

At an adsorbent dose of 15.5 mg/L, geosmin removal exceeded 85% for all adsorbents (Figure 4.50). At an adsorbent dose of 2 mg/L, H-Y-810 was the most effective adsorbent for geosmin removal from LMW after a contact time of 1hour.. H-Mordenite-230 removed geosmin as effectively as H-Y-810 during the first 30 minutes while WPH PAC yielded higher geosmin removals than H-Mordenite-230 after contact times of 1 and 2 hours. At the 2 mg/L dose, H-Mordenite-230 was more effective than the H-Mordenite-90 zeolites (Figure 4.51). It is unclear why geosmin removal was independent of the mordenite SiO_2/Al_2O_3 ratio at the higher adsorbent dose while it was affected by the SiO_2/Al_2O_3 ratio at the lower adsorbent dose.

Comparisons of gesomin removal kinetics obtained with mordenite zeolites, H-Y-810 and WPH PAC in LMW at adsorbent doses of 15.5 and 2 mg/L are presented in Figures 4.52 and 4.53, respectively. At the higher adsorbent dose, the geosmin removal rate obtained with WPH PAC was slower than that obtained with H-Y-810 zeolite, but geosmin removal percentages obtained with H-Y-810 and WPH were similar after contact times of 1 and 2 hours. At an adsorbent dose of 2 mg/L, geosmin removal with H-Y-810 was considerably higher than with WPH. Geosmin uptake by the mordenite zeolites was dramatically lower in LMW than in UPW and did not match the performance of the WPH PAC or H-Y-810 zeolite at either adsorbent dose (Figures 4.52 and 4.53).

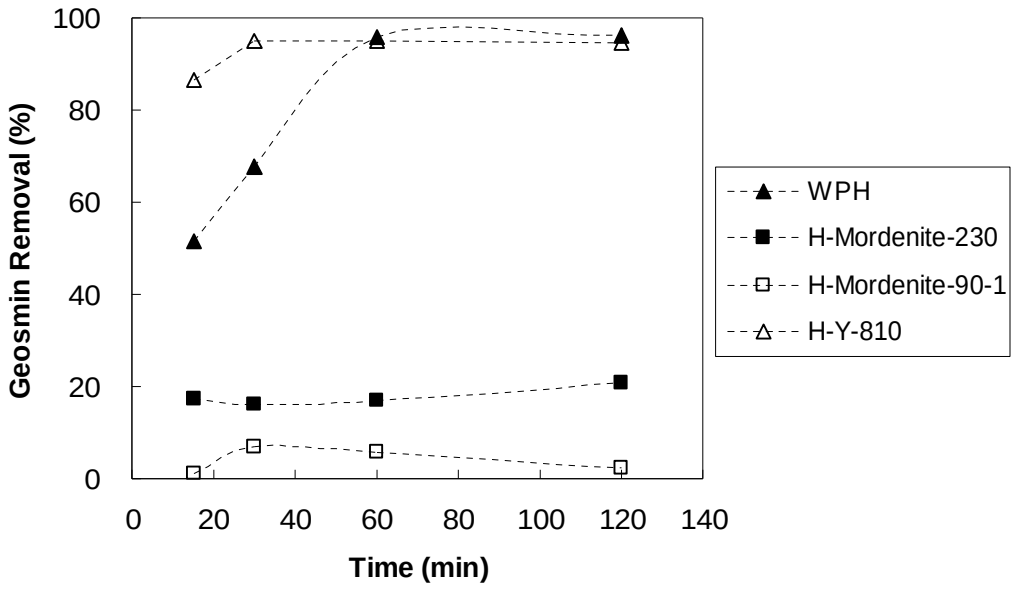

Figure 4.52 Geosmin removal kinetics for H-Mordenite-230, H-Mordenite-90-1, H-Y-810, and WPH PAC in LMW at an adsorbent dose of 15.5 mg/L

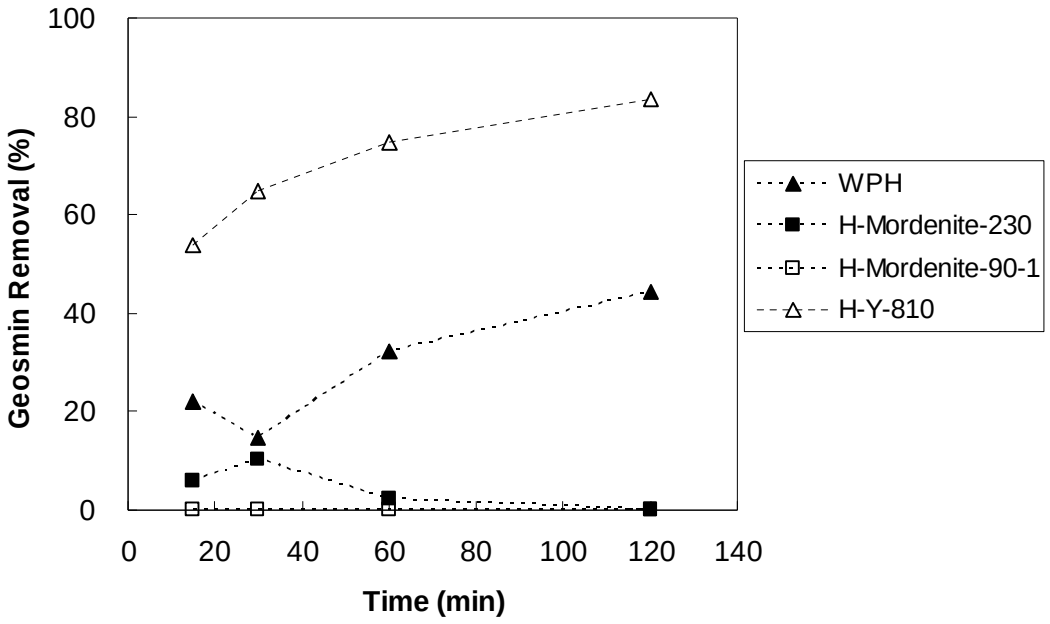

Figure 4.53 Geosmin removal kinetics for H-Mordenite-230, H-Mordenite-90-1, and WPH PAC in LMW at an adsorbent dose of 2 mg/L

Batch kinetic experiments with WPH, S-WPH, and H-Y-810 were also conducted for geosmin removal from LMW at an adsorbent dose of 5 mg/L. As was the case for MIB, geosmin removal with S-WPH was higher than with H-Y-810 and WPH. The difference in geosmin uptake rates between WPH and S-WPH was more pronounced than that obtained with MIB (Figures 4.40 and 4.54). Higher geosmin removal efficiencies and faster uptake rates on S-PAC than on PAC was also reported by Matsui et al. (2007, 2008, 2009). By comparing geosmin removal from ultrapure water with a wood-based PAC and its corresponding S-PAC, Matsui et al (2009) found that after a contact time of 30 minutes,

geosmin removal obtained with S-PAC adsorption was ~90%, while geosmin removal with the same dose of PAC reached only ~30% .

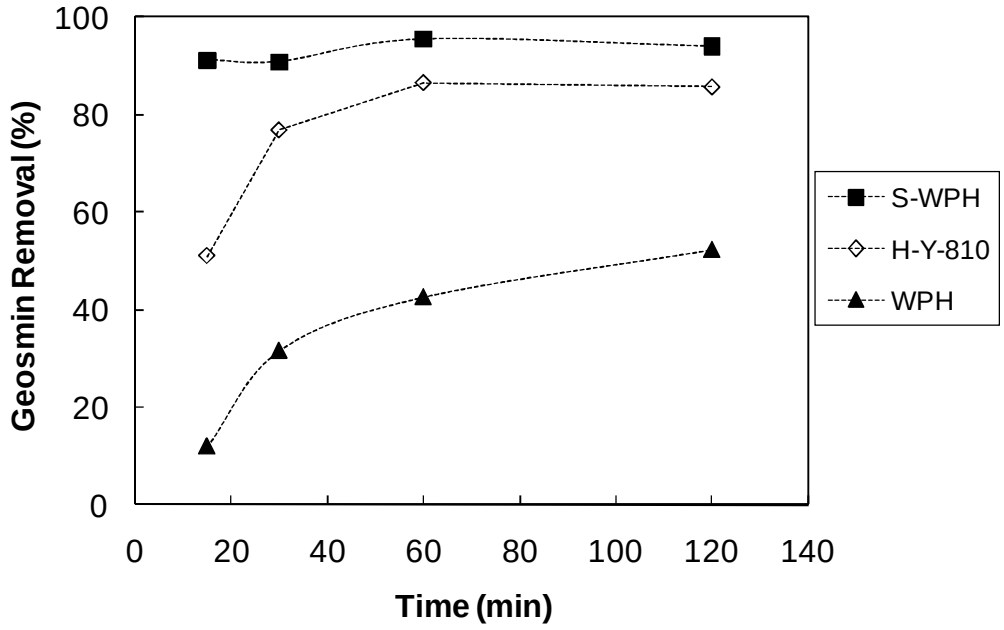

Figure 4.54 Geosmin removal kinetics for H-Y-810, WPH PAC and S- WPH S-PAC in LMW at an adsorbent dose of 5 mg/L

CHAPTER 5

REMOVAL OF MIB AND GEOSMIN BY HIGH-SILICA ZEOLITES AND POWDERED ACTIVATED CARBON IN THE PRESENCE OF OZONE

This chapter summarizes results of experiments that were conducted (1) to measure the adsorption capacity of mordenite and Y zeolites for ozone and (2) to quantify whether the oxidative removal of MIB and geosmin can be enhanced by the addition of zeolites or PAC.

5.1 OZONE ADSORPTION BY HIGH-SILICA ZEOLITES

Batch ozone uptake experiments were performed in ozone-demand free UPW with H-Mordenite-40, H-Mordenite-90-1, H-Mordenite-230, and H-Y-810 zeolites. Experiments were conducted at pH 2 to minimize ozone decomposition in the aqueous phase. Initial ozone concentrations in batch uptake experiments were approximately 1.5 mg/L and 0.75 mg/L. To calculate the quantity of adsorbed ozone (via equation 3.1), ozone concentration profiles in the presence of zeolite were compared to those obtained in the absence of zeolite.

Figures 5.1 and 5.2 summarize ozone concentration profiles obtained in the absence of zeolite and in the presence of 2000 mg/L H-Mordenite-230 and H-Mordenite-90-1, respectively.

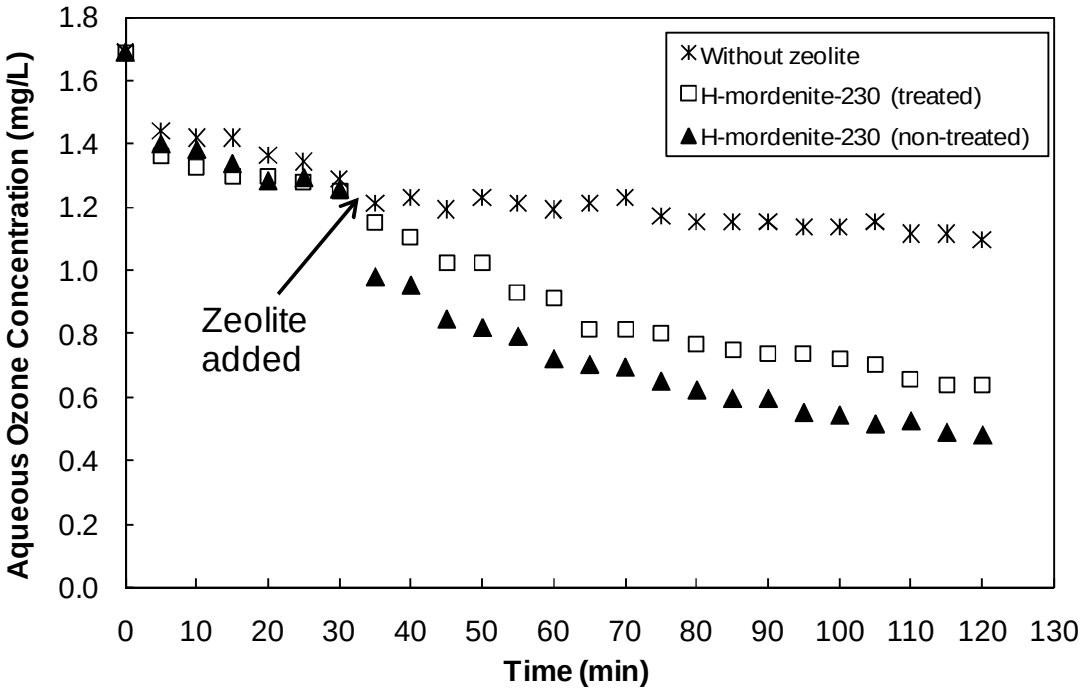

Figure 5.1 Results of ozone uptake experiment conducted with NH_4Cl-treated and non-treated H-Mordenite-230. Zeolite dose: 2 g/L, ozone dose: 1.5 mg/L.

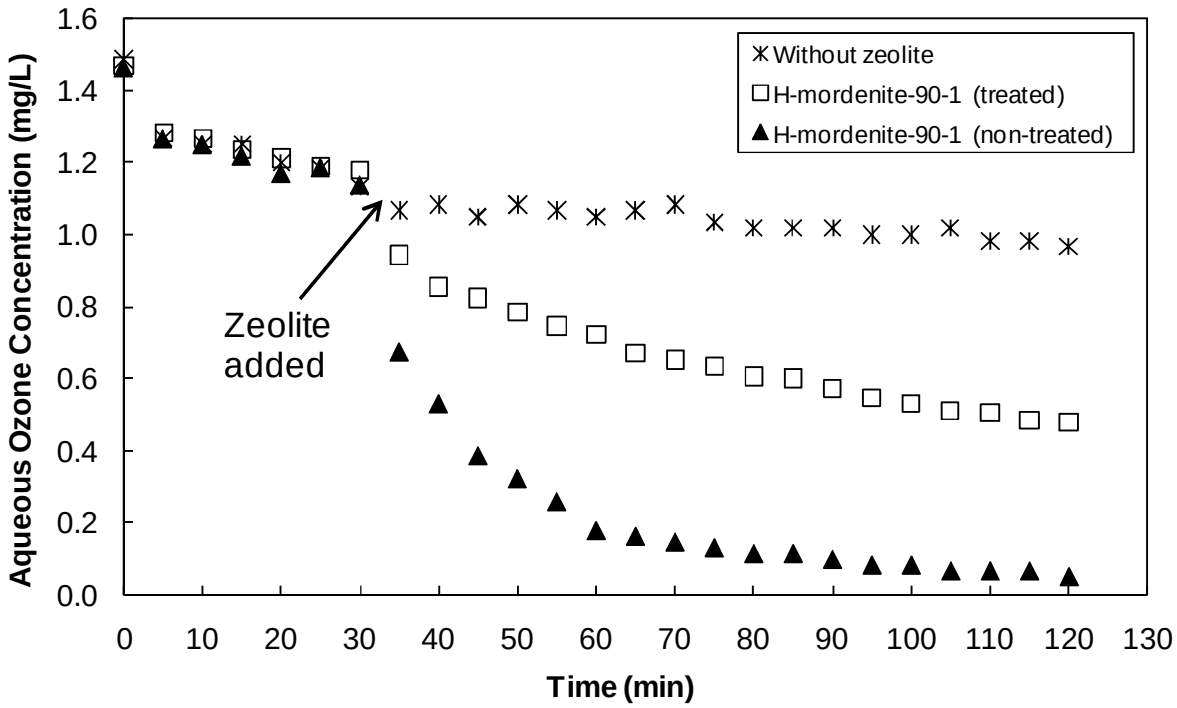

Figure 5.2 Results of ozone uptake experiment conducted with NH_4Cl-treated and non-treated H-Mordenite-90-1. Zeolite dose: 2 g/L, ozone dose: 1.5 mg/L.

Figures 5.1 and 5.2 also illustrate the effect of NH_4Cl treatment to remove exchangeable H^+ ions from the zeolite prior to ozone uptake experiments. For both H-Mordenite-230 and H-Mordenite-90-1, ozone decayed more rapidly when non-treated zeolite was added, and the difference between ozone concentration profiles obtained with treated and non-treated zeolites was larger for H-Mordenite-90-1. Compared to H-Mordenite-230, H-Mordenite-90-1 has a higher acidity (i.e. lower SiO_2/Al_2O_3), which means that it has more exchangeable H^+ ions, and the higher surface acidity leads to an elevated concentration of OH^- ions in the zeolite pore (Fujita et al. 2004a). Since ozone decomposition is higher in the presence of OH^-

ions, the difference in ozone concentration profiles between treated and non-treated zeolites was smaller for H-Mordenite-230 and larger for H-Mordenite-90-1.

Using NH_4Cl-treated zeolites, ozone uptake experiments were completed with H-Mordenite-40, H-Mordenite-90-1, H-Mordenite-230, and H-Y-810 at zeolite concentrations ranging from 500 to 4000 mg/L. Figure 5.3, which summarizes results in form of an isotherm plot, suggests that ozone uptake was highest by H-Mordenite-90-1 and lowest by H-Mordenite-40. Partition coefficients (K_p) were calculated for individual data points shown in Figure 5.3 by using the equation $K_p=q/C$, where q and C are the amount adsorbed (mg/g) and the aqueous ozone concentration (mg/L), respectively. Comparing partition coefficients that describe the partitioning of ozone between the zeolite and aqueous phases, results obtained in this study were higher than those reported by Fujita et al. (2004a). K_p values obtained here were in the range of 0.2 to 1.6 L/g, whereas the largest partition coefficient obtained by Fujita et al. (2004a) was ~0.125 L/g at an aqueous ozone concentration of approximately 5 mg/L. It is also important to note that the use of partition coefficients assumes that isotherms are linear; however, isotherm plots presented in Figure 5.3a suggest that this assumption is not likely valid at the conditions tested (i.e., constant initial ozone concentration, variable zeolite dose) The Freundlich isotherm model ($q = K \cdot C^{1/n}$) could not describe the ozone adsorption data obtained for H-Mordenite-230, H-Mordenite-90-1 and H-Y-810, as evidenced by the nonlinearity of the data when plotted in log-log format (Figure 5.3b).

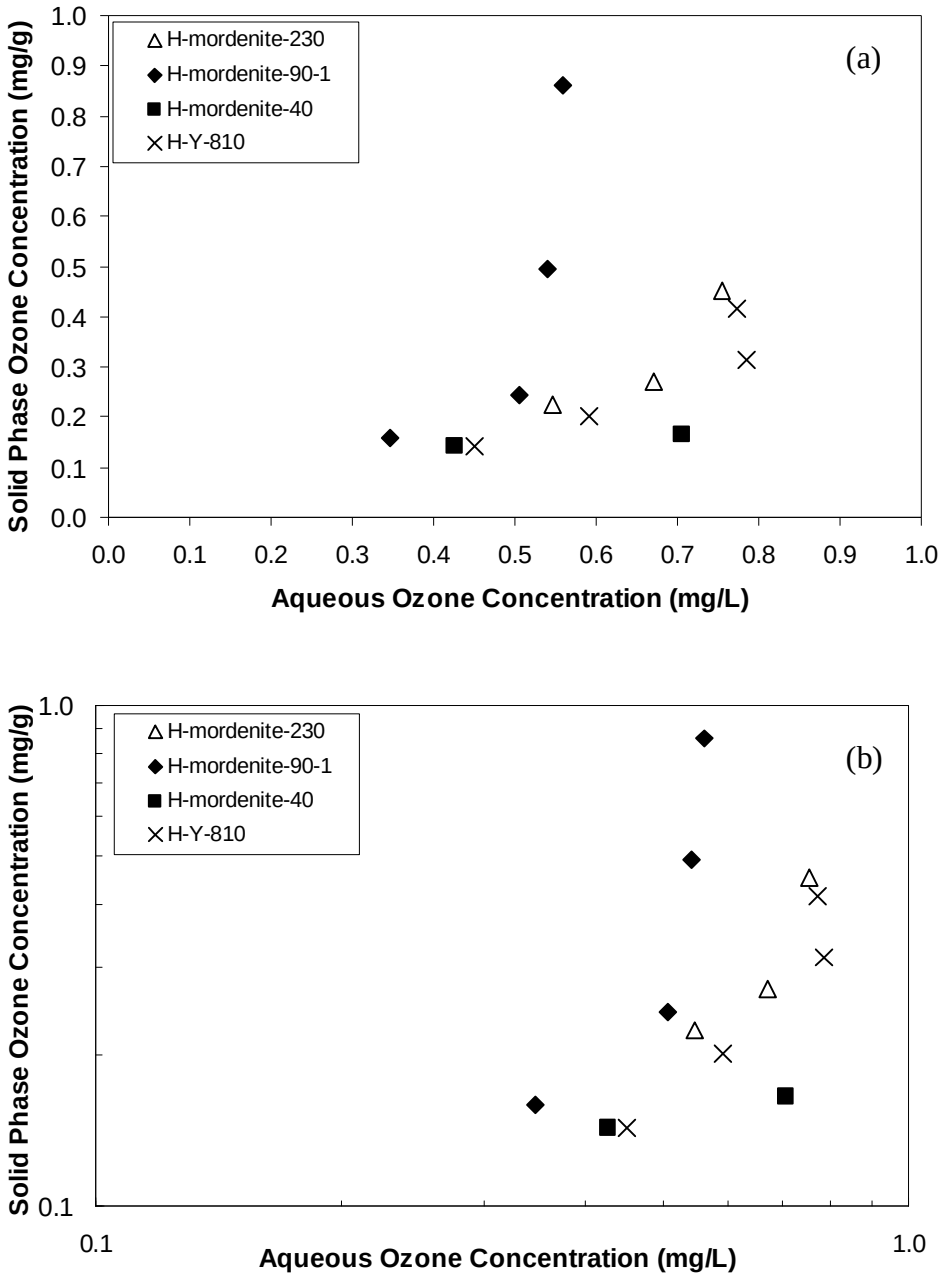

Figure 5.3 Relationship between solid- and aqueous-phase ozone concentrations for NH_4Cl-treated three mordenite zeolites and one Y zeolite.

While the partition coefficient describing ozone adsorption on zeolites was relatively low, it is interesting to calculate the concentration of ozone inside of the zeolite pores. Results from a prior Water Research Foundation study (Knappe et al. 2007) showed that the pore volume of mordenite zeolites is approximately 0.25 mL/g. If one assumes a partition coefficient of 0.5 L/g at an aqueous ozone concentration of 0.5 mg/L, then the solid-phase ozone concentration at this condition would be 0.25 mg/g ($q = K_p \cdot C$). Then, the ozone concentration in the zeolite pores will be (0.25 mg/g)/(0.25 mL/g) = 1 mg/mL = 1000 mg/L or a factor of 2000 higher than in the bulk solution. This result suggests that mordenite zeolites and Y zeolite are indeed effective for elevating intraparticle ozone concentrations by several orders of magnitude over those in the bulk solution.

Isotherm plots and partition coefficients (K_p) obtained with H-Y-810 zeolite at two different initial ozone concentrations are presented in Figures 5.4 and 5.5, respectively. Similar K_p values in Figure 5.5 suggest that ozone uptake isotherms may be linear when the zeolite dose is kept constant and the initial ozone concentration is varied.

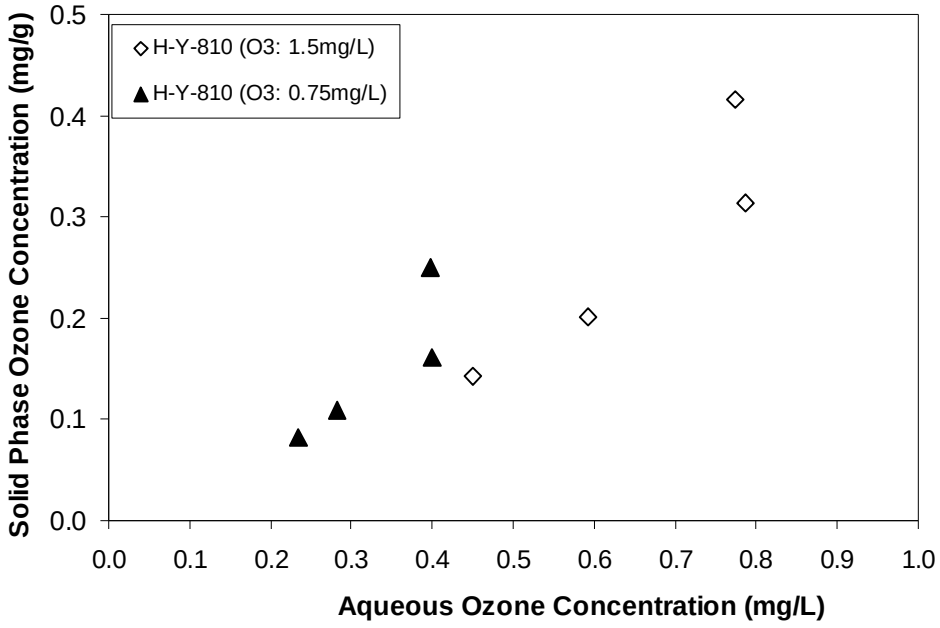

Figure 5.4 Relationship between solid- and aqueous-phase ozone concentrations for NH_4Cl-treated Y zeolite at two different initial ozone concentrations.

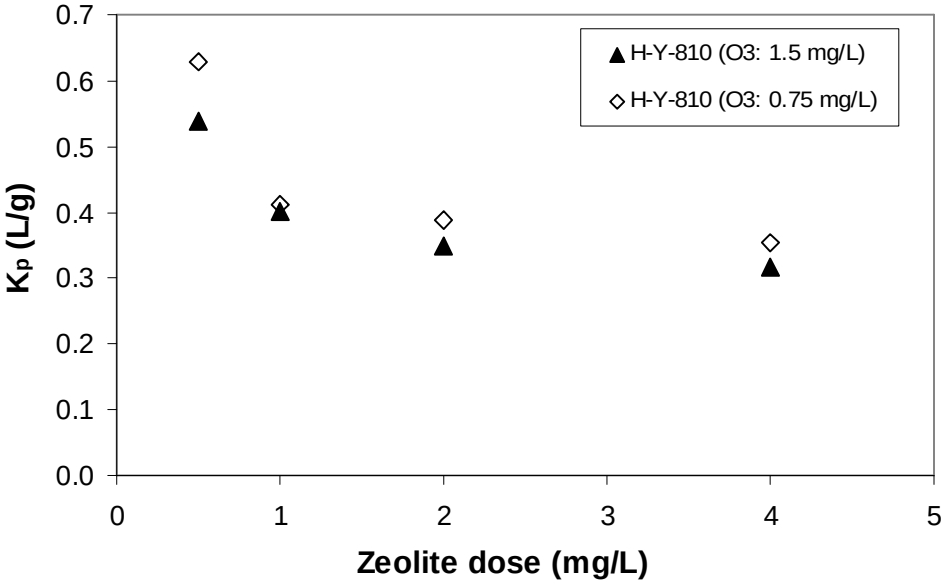

Figure 5.5 Partition coefficients obtained with NH_4Cl-treated Y zeolite at two different initial ozone concentrations.

5.2 MIB AND GEOSMIN REMOVAL BY H-MORDENITE-90-1 IN THE PRESENCE OF OZONE

Batch experiments for MIB removal were performed in both ozone-demand free UPW and LMW. Three sets of experiments were completed in duplicate for each water:

- MIB removal by ozone only
- MIB removal by zeolite only
- MIB removal by zeolite and ozone

For experiments involving zeolite, NH_4Cl-treated H-Mordenite-90-1 was added at a dose of 2 mg/L. Ozone was dosed at an initial concentration of ~1.5 mg/L in experiments involving ozone.

Figure 5.6 summarizes percent MIB removal results that were obtained in UPW as a function of zeolite and/or ozone contact time. MIB removal was similar when comparing results obtained with ozone only to those obtained with the combined addition of ozone and zeolite. In contrast, the application of zeolite alone yielded MIB removal percentages that were lower than those obtained in the presence of ozone (<40% removal with zeolite only compared to ~80% removal with ozone and zeolite plus ozone after a contact time of 60 minutes). After a contact time of 10 minutes, MIB transformation by ozone only was ~25% (Figure 5.6),

which closely matches the results obtained by Lalezary et al. (1986) for an ozone dose of 2 mg/L and a contact time of 10 minutes.

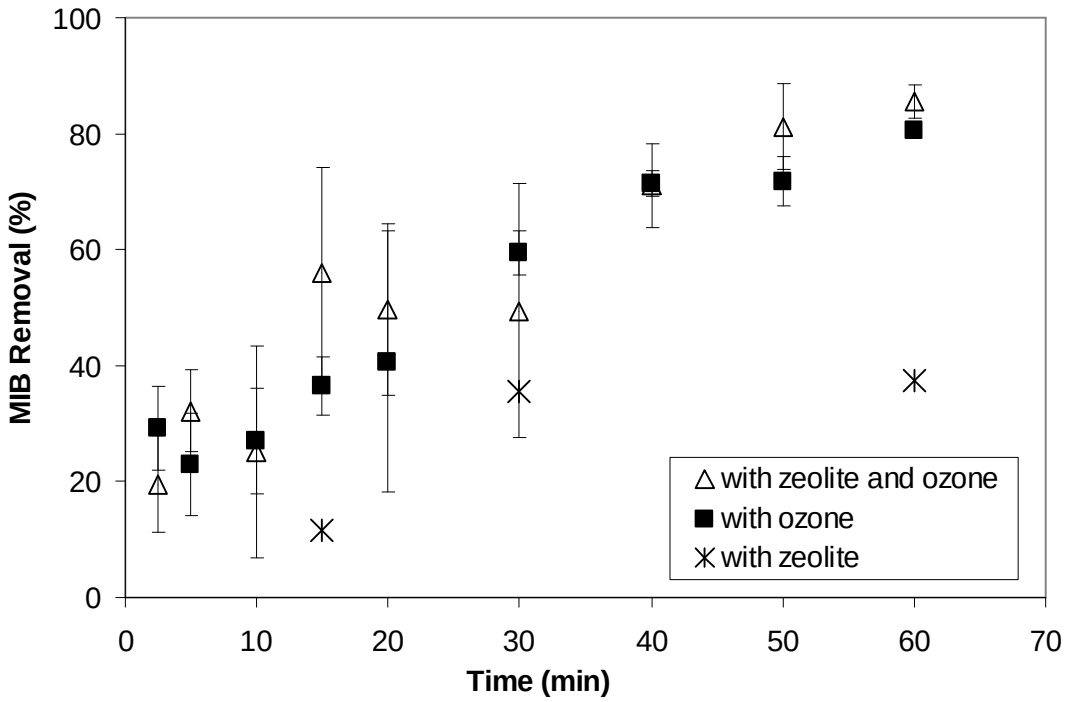

Figure 5.6 MIB removal from UPW by zeolite-enhanced ozonation as well as by ozone and zeolite alone. Zeolite: NH_4Cl-treated H-Mordenite-90-1 at a dose of 2 mg/L. Ozone dose: 1.5 mg/L. Error bars represent one standard deviation of duplicate experiments.

Figure 5.7 summarizes MIB removal data obtained in LMW. As was the case with UPW, the addition of zeolite did not measurably improve MIB removal. While some of the MIB removal percentages during the first 20 minutes of contact appear to be higher for the zeolite-enhanced ozonation process, the removal percentages were in most cases statistically similar. MIB removal with H-Mordenite-90-1 alone reached ~15% in LMW while the addition of

ozone with and without zeolite transformed about 80% of the initially added MIB. MIB removal was slower in UPW (Figure 5.6) than in LMW (Figure 5.7), an expected result because NOM promotes the decomposition of ozone and enhances the formation of hydroxyl radicals (e.g., Glaze et al. 1990, Peter and von Gunten 2007).

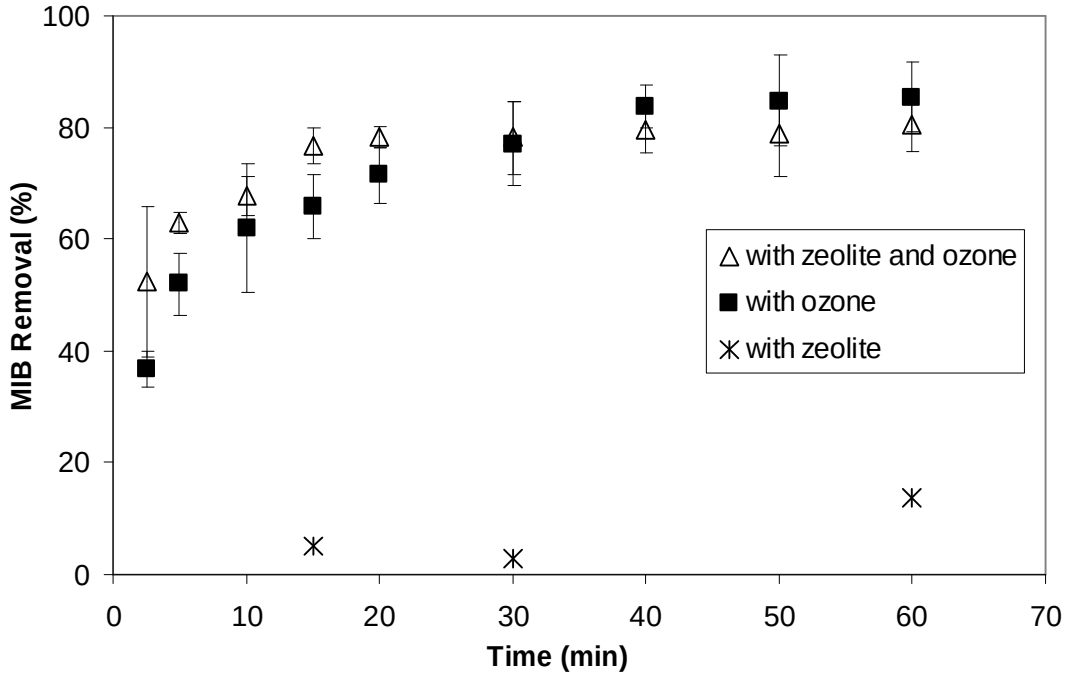

Figure 5.7 MIB removal from LMW by zeolite-enhanced ozonation as well as by ozone and zeolite alone. Zeolite: NH_4Cl-treated H-Mordenite-90-1 at a dose of 2 mg/L. Ozone dose: 1.5 mg/L. Error bars represent one standard deviation of duplicate experiments.

Experiments identical to those described for MIB were conducted to evaluate the effectiveness of the zeolite-enhanced ozonation process for geosmin removal. Figure 5.8 summarizes percent geosmin removal results that were obtained in UPW with H-Mordenite-

90-1 zeolite as a function of zeolite and/or ozone contact time. A comparison of the data obtained with ozone only and those obtained with the combined addition of ozone and H-Mordenite-90-1 shows that geosmin removal was similar and that the added zeolite did not enhance geosmin removal. As was the case with MIB, the application of zeolite alone yielded geosmin removal percentages that were substantially lower than those obtained in the presence of ozone (~ 5% removal with zeolite only, compared to ~95% removal with ozone and with zeolite plus ozone after 30 minutes contact time).

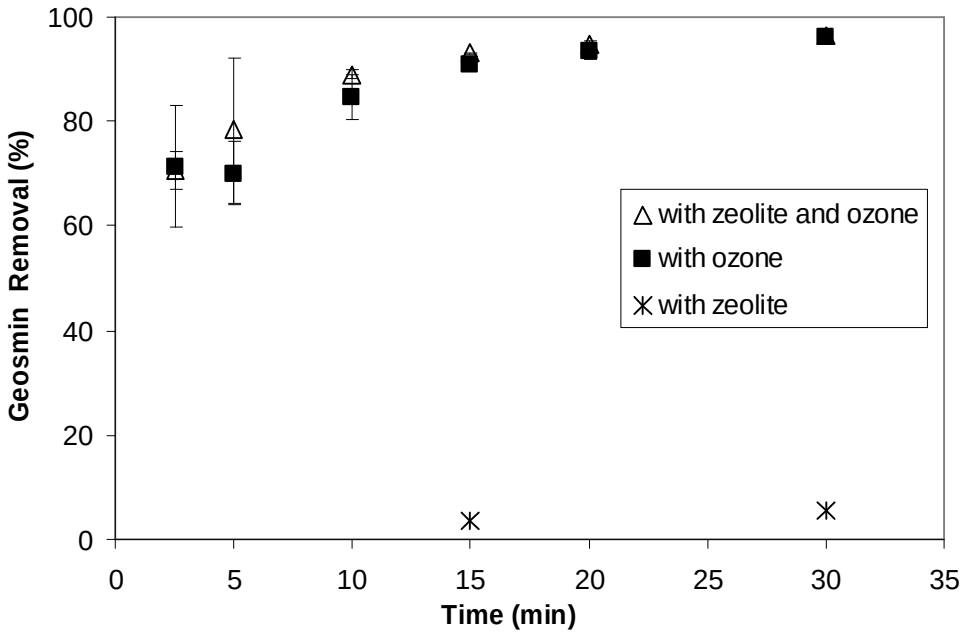

Figure 5.8 Geosmin removal from UPW by zeolite-enhanced ozonation as well as by ozone and zeolite alone. Zeolite: NH_4Cl-treated H-Mordenite-90-1 at a dose of 2 mg/L. Ozone dose: 1.5 mg/L. Error bars represent one standard deviation of duplicate experiments.

Figure 5.9 summarizes geosmin removal data obtained in LMW with H-Mordenite-90-1. Again, the zeolite-enhanced ozonation process did not yield measurably improved geosmin removal from LMW relative to ozonation only. Geosmin removal by H-Mordenite-90-1 alone was negligible in LMW while the addition of ozone with and without zeolite transformed about 90% of the initially added geosmin after 30 minutes contact time. One reason why the zeolite-enhanced ozonation process did not offer a significant advantage over conventional ozonation was that geosmin adsorption by H-Mordenite-90-1 was negligible in LMW. Compared to MIB, geosmin removal rates in the presence of ozone were faster and did not differ measurably between UPW and LMW.

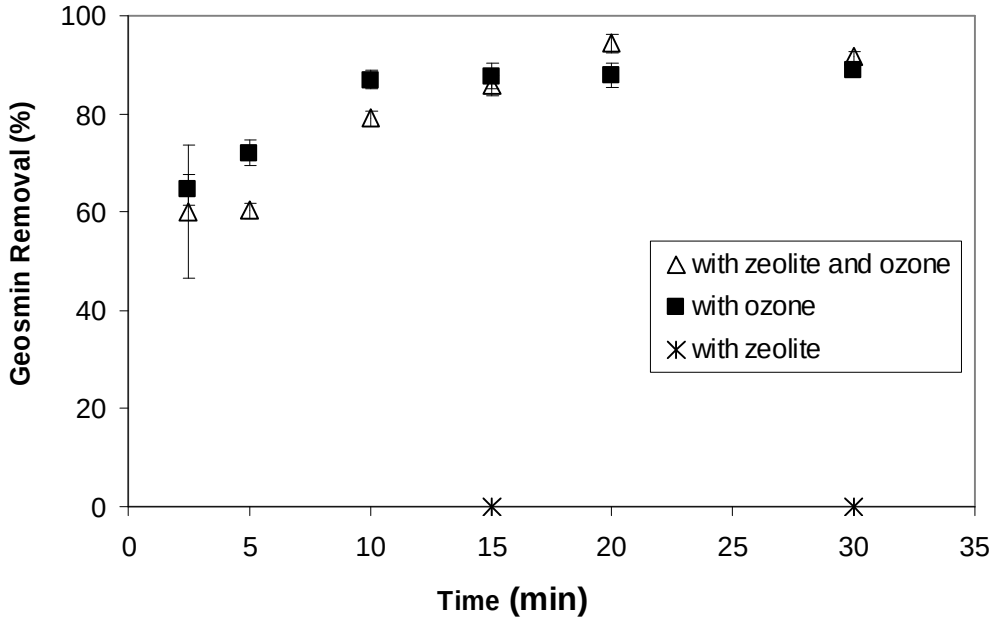

Figure 5.9 Geosmin removal from LMW by zeolite-enhanced ozonation as well as by ozone and zeolite alone. Zeolite: NH_4Cl-treated H-Mordenite-90-1 at a dose of 2 mg/L. Ozone dose: 1.5 mg/L. Error bars represent one standard deviation of duplicate experiments.

Figure 5.10 compares the ozone depletion curves obtained during the MIB and geosmin removal experiments in UPW and LMW with and without H-Mordenite-90-1 zeolite. Aqueous ozone concentrations (C, mg/L) were divided by the initial ozone concentrations (C_0, mg/L) of each experiment to normalize for small differences in the initial ozone concentration. Results in Figures 5.10 show that aqueous ozone concentrations in UPW decreased more slowly than those in LMW. This result supports that the NOM in LMW enhanced ozone decomposition and promoted the formation of hydroxyl radicals. While the slower depletion of ozone in UPW translated into a greater ozone exposure relative to that in LMW, the higher ozone exposure in UPW did not benefit the removal of MIB and geosmin because the second order rate constant describing the oxidation of MIB and geosmin by molecular ozone is very small (0.35 M^{-1} s^{-1} for MIB and 0.1 M^{-1} s^{-1} for geosmin) (Peter and von Gunten 2007). Thus, oxidation of MIB and geosmin in ozonation processes occurs primarily via the hydroxyl radical that forms during the decomposition of ozone.

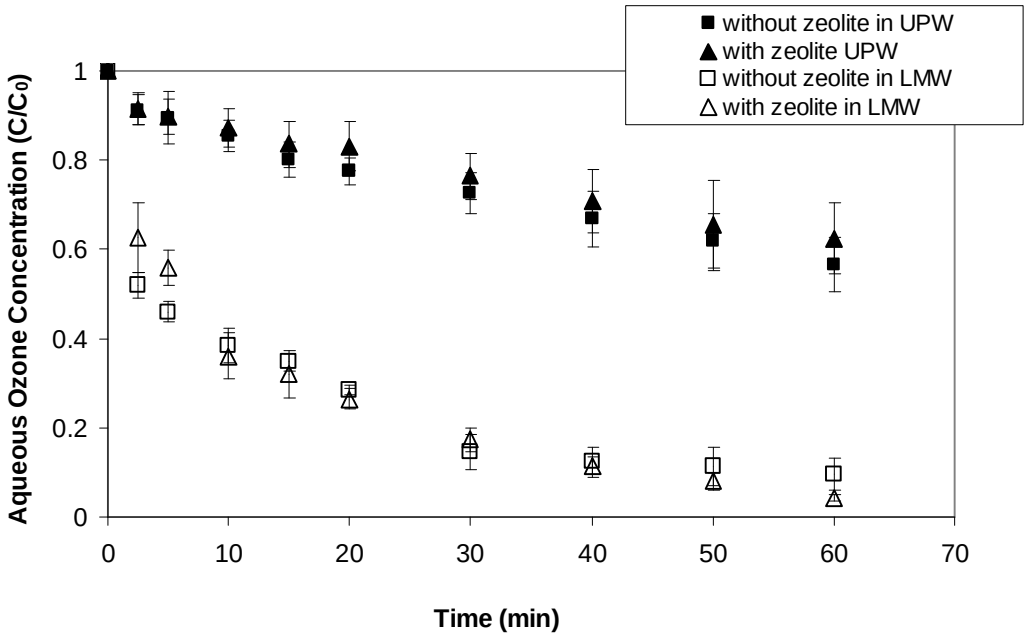

Figure 5.10 Ozone residual concentration profiles in UPW and LMW during MIB/geosmin removal experiments. Zeolite: H-Mordenite-90-1 at a dose of 2 mg/L. Ozone dose: 1.5 mg/L. Error bars represent one standard deviation of duplicate experiments.

5.3 MIB AND GEOSMIN REMOVAL BY H-Y-810 IN THE PRESENCE OF OZONE.

In addition to H-Mordenite-90, H-Y-810, a zeolite with slightly larger pore openings (Table 3.1), was evaluated. MIB removal data were obtained in UPW and LMW with an initial ozone concentration of ~1.5 mg/L and with a H-Y-810 zeolite dose of 2 mg/L. MIB removal data obtained with H-Y-810 in UPW are summarized in Figure 5.11. Although removal percentages are slightly higher in the first 20 minutes of the experiment, a significant improvement in MIB removal from UPW was not observed with the zeolite-enhanced

ozonation process relative to ozonation alone. The addition of ozone with and without zeolite transformed about 80% of the initially added MIB after 60 minutes of contact time. MIB removal by H-Y-810 alone was around 20% after 60 minutes of contact time in UPW. In LMW, MIB removal with ozone alone and with the zeolite-enhanced ozonation process was again similar (Figure 5.12). In LMW, MIB removal with H-Y-810 alone reached ~25%, while the addition of ozone with and without zeolite transformed about 70% of the initially added MIB after 30 minutes of contact time.

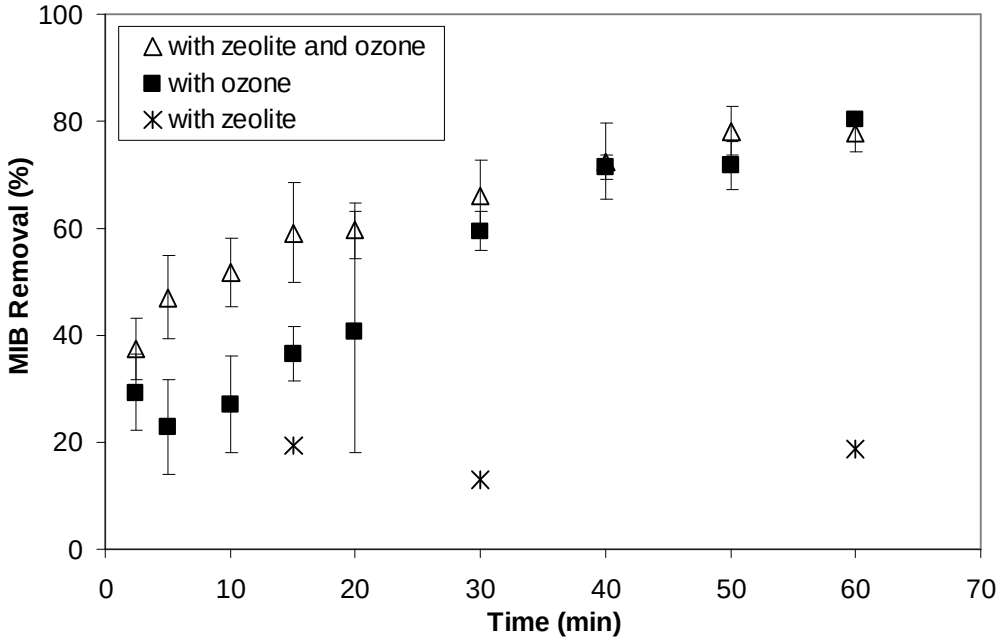

Figure 5.11 MIB removal from UPW by zeolite-enhanced ozonation as well as by ozone and zeolite alone. Zeolite: NH_4Cl-treated H-Y-810 at a dose of 2 mg/L. Ozone dose: 1.5 mg/L. Error bars represent one standard deviation of duplicate experiments

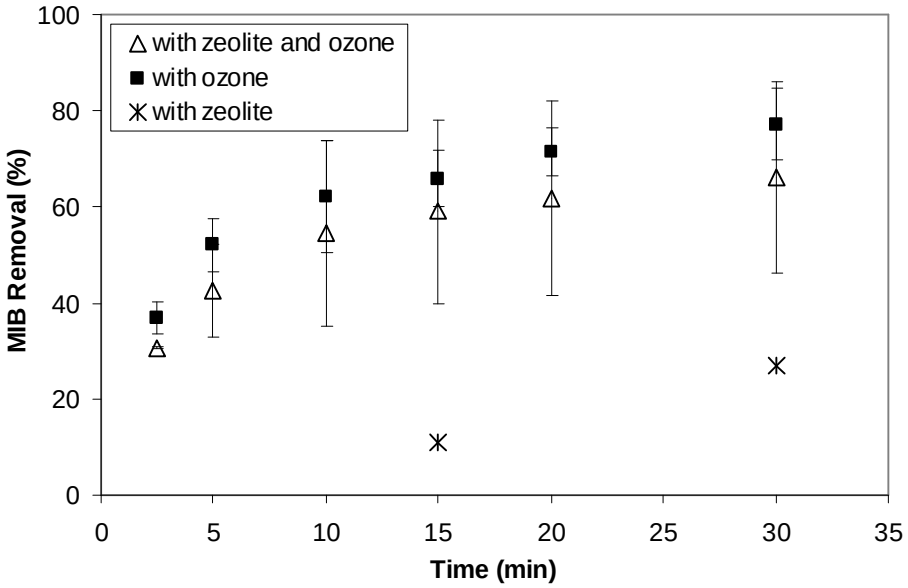

Figure 5.12 MIB removal from LMW by zeolite-enhanced ozonation as well as by ozone and zeolite alone. Zeolite: NH_4Cl-treated H-Y-810 at a dose of 2 mg/L. Ozone dose: 1.5 mg/L. Error bars represent one standard deviation of duplicate experiments

Figures 5.13 and 5.14 represent geosmin removal data obtained with H-Y-810 in UPW and LMW, respectively. Although geosmin removal percentages in LMW are slightly higher, especially in the first 10 minutes of the experiment, the zeolite-enhanced ozonation process did not yield a dramatic improvement in geosmin removal from both UPW and LMW relative to ozonation. The addition of ozone with and without zeolite transformed about 95% and 90% of the initially added geosmin after 30 minutes contact time in UPW and LMW, respectively, whereas geosmin removal by H-Y-810 alone in UPW and LMW was 50% and 65%, respectively after 30 minutes of contact time.

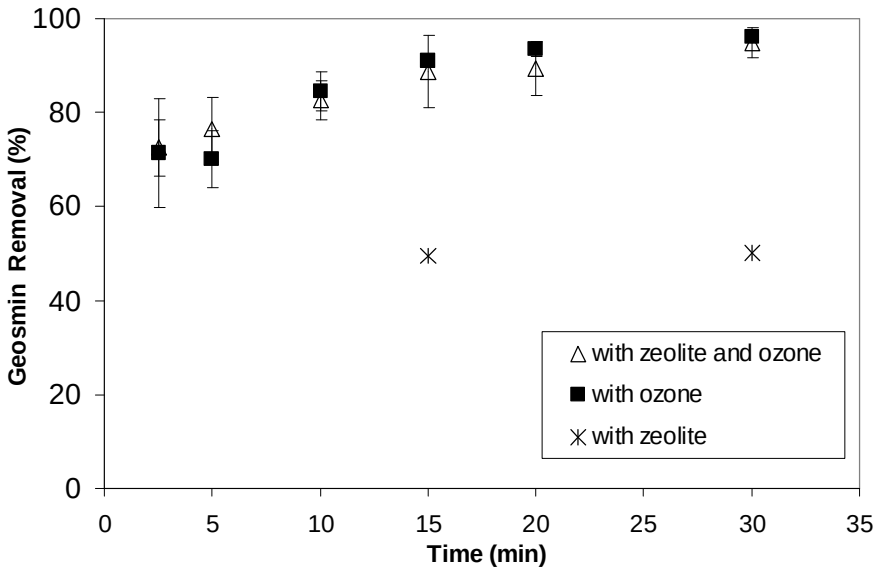

Figure 5.13 Geosmin removal from UPW by zeolite-enhanced ozonation as well as by ozone and zeolite alone. Zeolite: NH_4Cl-treated H-Y-810 at a dose of 2 mg/L. Ozone dose: 1.5 mg/L. Error bars represent one standard deviation of duplicate experiments.

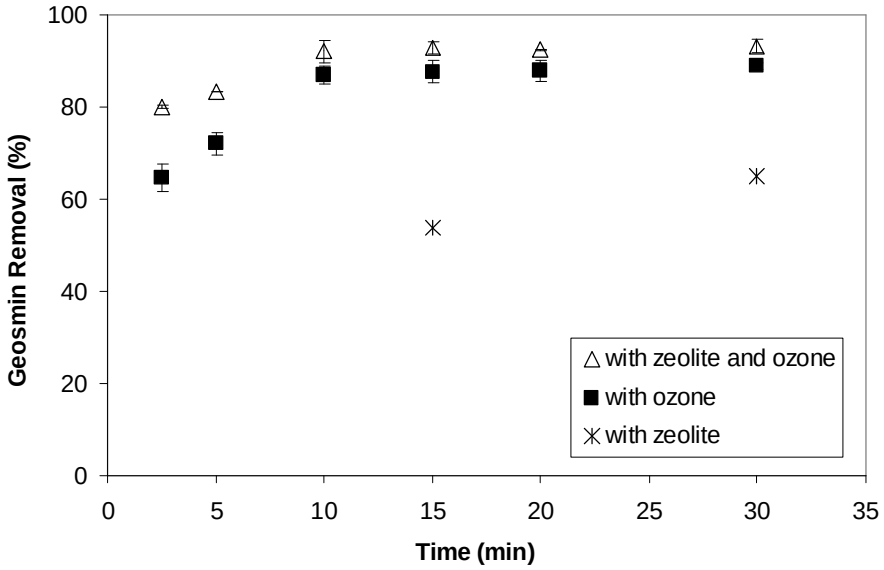

Figure 5.14 Geosmin removal from LMW by zeolite-enhanced ozonation as well as by ozone and zeolite alone. Zeolite: NH_4Cl-treated H-Y-810 at a dose of 2 mg/L. Error bars represent one standard deviation of duplicate experiments.

The ozone depletion curves obtained during the MIB and geosmin removal experiments in UPW and LMW with and without H-Y-810 zeolite are presented in Figure 5.15. As was the case with H-Mordenite-90-1, ozone decay was slower in UPW than in LMW. In LMW, the addition of H-Y-180 may have accelerated the disappearance of ozone from the aqueous phase. As will be shown below, a similar result was not observed when the ozone dose was ~0.75 mg/L.

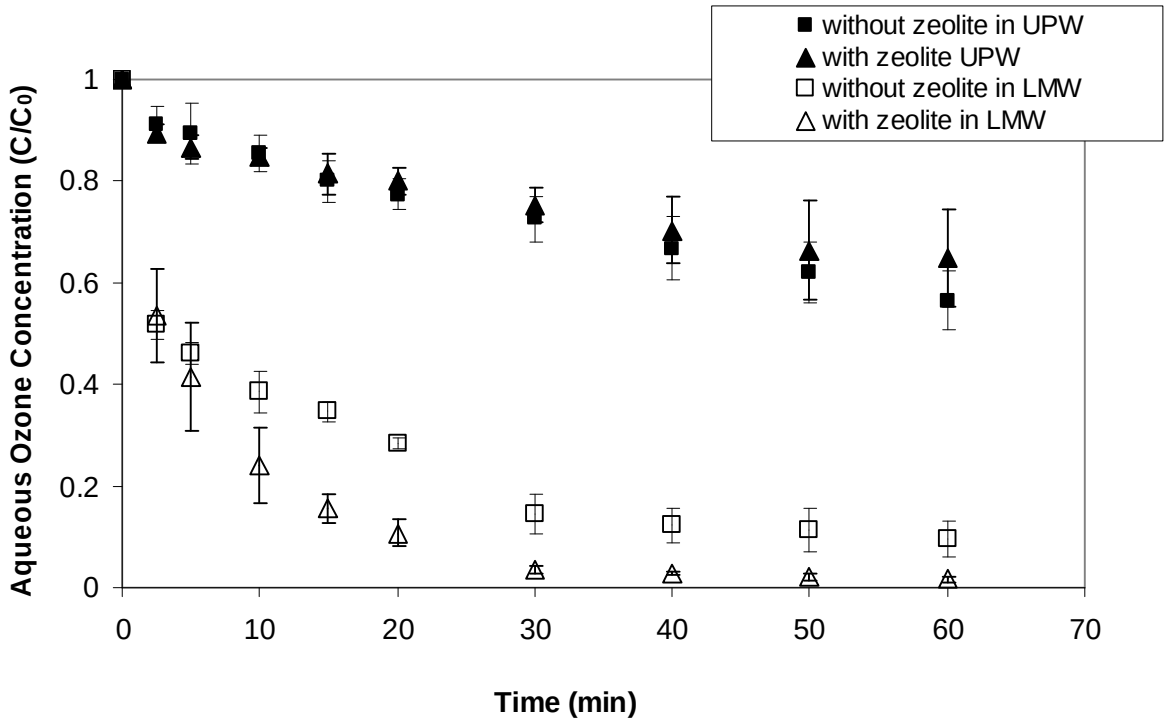

Figure 5.15 Ozone residual concentration profiles in UPW and LMW during MIB/geosmin removal experiments. Zeolite: H-Y-810 at a dose of 2 mg/L. Ozone dose: 1.5 mg/L. Error bars represent one standard deviation of duplicate experiments.

Additional experiments were conducted in LMW with H-Y-810 at a lower initial ozone concentration of 0.75 mg/L and a higher zeolite dose of 5 mg/L. MIB and geosmin removal data obtained with 2 mg/L and 5 mg/L H-Y-810 and/or 0.75 mg/L ozone are summarized in Figures 5.16 and 5.17. As was the case with the 1.5 mg/L ozone dose, MIB removal was not significantly different between zeolite-enhanced ozonation and ozone alone when the zeolite dose was 2 mg/L. After 30 minutes of contact time, MIB removal was approximately 50% in both cases (Figure 5.16). In contrast, geosmin removal was higher for zeolite-enhanced ozonation than for ozonation or zeolite addition alone at a zeolite dose of 2 mg/L. After a contact time of 30 minutes, geosmin removals were around 80% for zeolite-enhanced ozonation and ~65% for conventional ozonation and zeolite addition alone (Figure 5.17).

Figures 5.16 and 5.17 also compare MIB and geosmin removals, respectively, with H-Y-810 doses of 2 and 5 mg/L. MIB removal was slightly higher with the 5 mg/L zeolite dose compared to the 2 mg/L zeolite dose both in the presence and absence of ozone. After 30 minutes of contact time, and with 5 mg/L H-Y-810, MIB removals were approximately 60% and 30% in the presence and absence of ozone, respectively.

For contact times of 10 minutes and longer, the zeolite-enhanced ozonation process yielded ~75% geosmin removal at both zeolite doses. In the case of zeolite addition alone, geosmin removals, after a contact time of 30 minutes, were 65% and 75% at zeolite doses of 2 and 5

mg/L, respectively. A comparison of the ozone depletion curves for the two zeolite doses suggests that increasing the zeolite dose from 2 mg/L to 5 mg/L did not have a measurable effect on ozone decay (Figure 5.18).

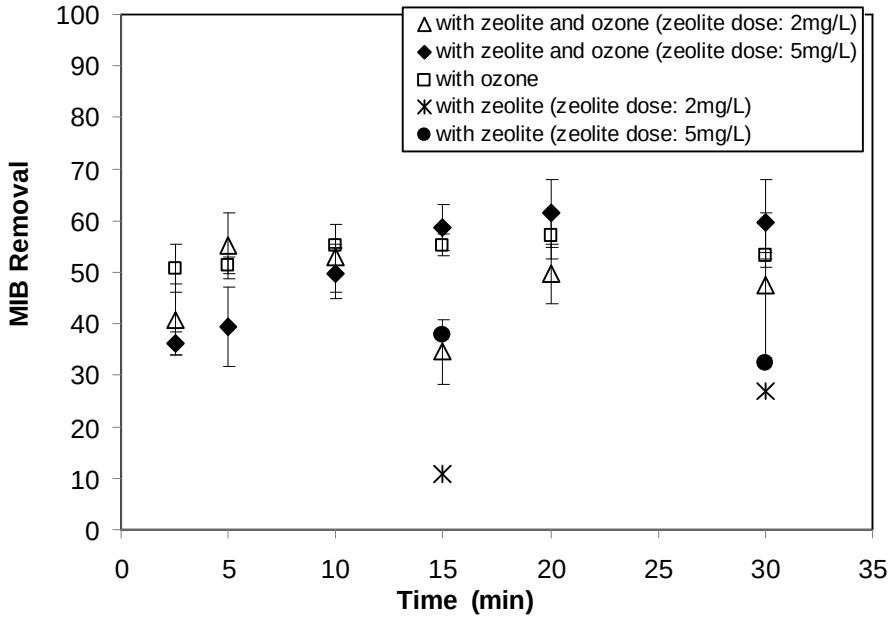

Figure 5.16 MIB removal from LMW by zeolite-enhanced ozonation as well as by ozone and zeolite alone. Zeolite: H-Y-810 at doses of 2 mg/L and 5 mg/L. Ozone dose: 0.75 mg/L. Error bars represent one standard deviation of duplicate experiments.

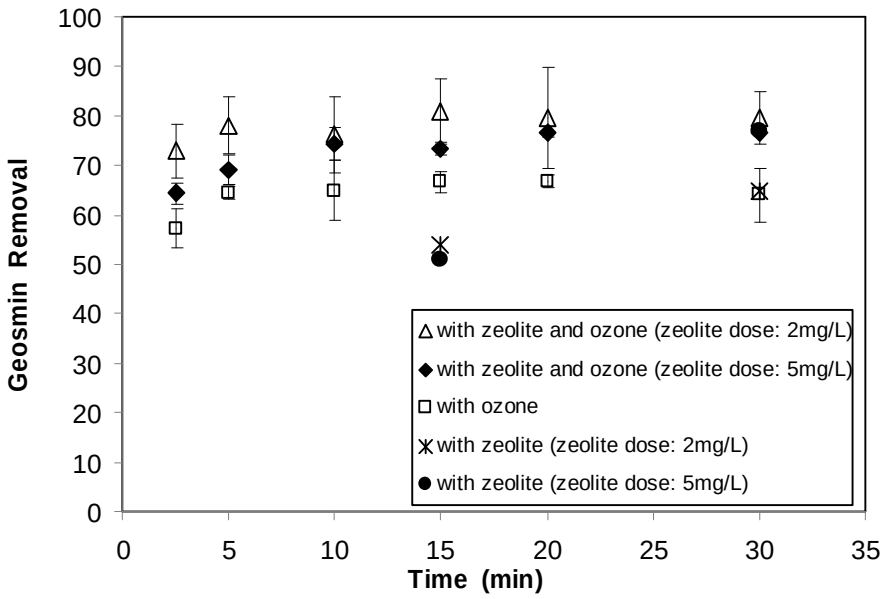

Figure 5.17 Geosmin removal from LMW by zeolite-enhanced ozonation as well as by ozone and zeolite alone. Zeolite: H-Y-810 at doses of 2 mg/L and 5 mg/L. Ozone dose: 0.75 mg/L. Error bars represent one standard deviation of duplicate experiments.

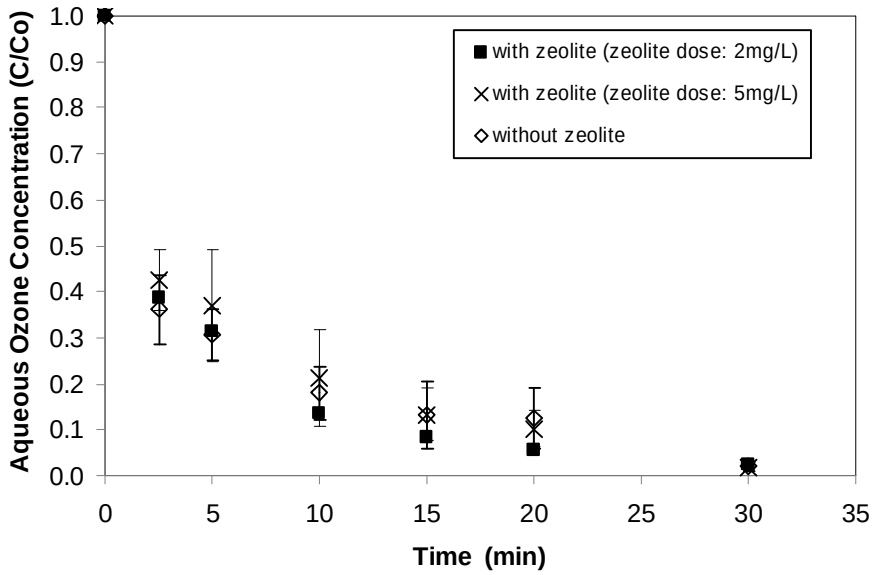

Figure 5.18 Ozone residual concentration profiles in LMW during MIB/geosmin removal experiments. Zeolite: H-Y-810 at doses of 2 and 5 mg/L. Ozone dose: 0.75 mg/L. Error bars represent one standard deviation of duplicate experiments.

5.4 MIB AND GEOSMIN REMOVAL BY NON-TREATED H-Y-810 IN THE PRESENCE OF OZONE.

The effect of NH_4Cl treatment on MIB and geosmin removal was also evaluated by conducting experiments with 2 mg/L non-treated H-Y-810 at an initial ozone concentration of 0.75 mg/L. Figure 5.19 and 5.20 summarize removal data obtained from LMW with treated and non-treated H-Y-810 zeolite for MIB and geosmin, respectively. As the data suggest, zeolite treatment with NH_4Cl did not measurably change MIB removal in the presence of ozone.

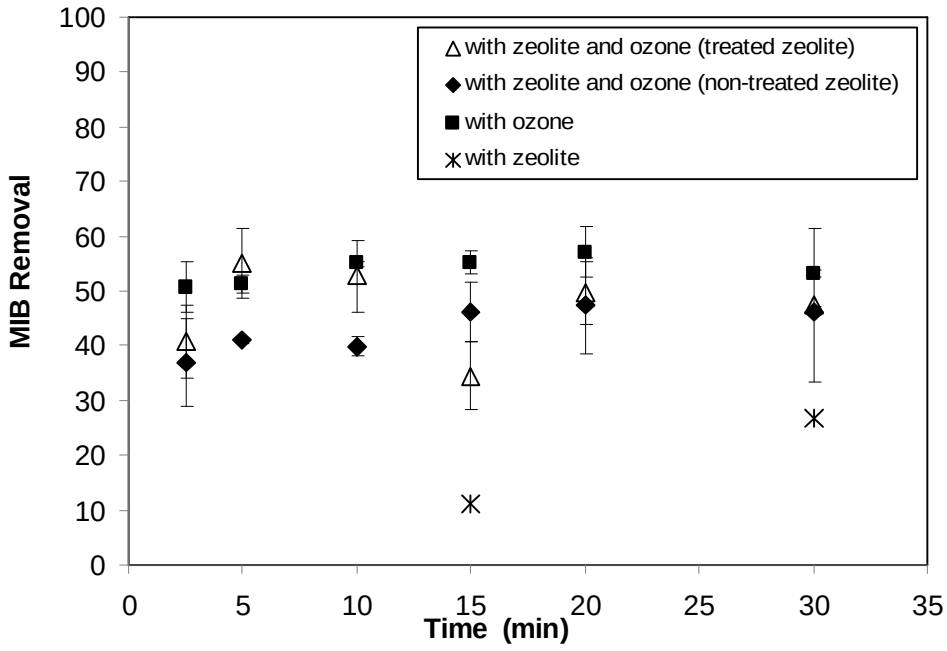

Figure 5.19 MIB removal from LMW by zeolite-enhanced ozonation as well as by ozone and zeolite alone. Zeolite: treated and non-treated H-Y-810 at a dose of 2 mg/L. Ozone dose: 0.75 mg/L. Error bars represent one standard deviation of duplicate experiments.

As was the case with MIB, the NH_4Cl treatment of H-Y-810 did not affect the removal of geosmin in the presence of ozone. On the other hand, ozone decay was faster when non-treated zeolite was added than when NH_4Cl treated zeolite was added (Figure 5.21). The latter result is in agreement with the results of ozone uptake experiments conducted with treated and non-treated zeolites (Figures 5.1 and 5.2).

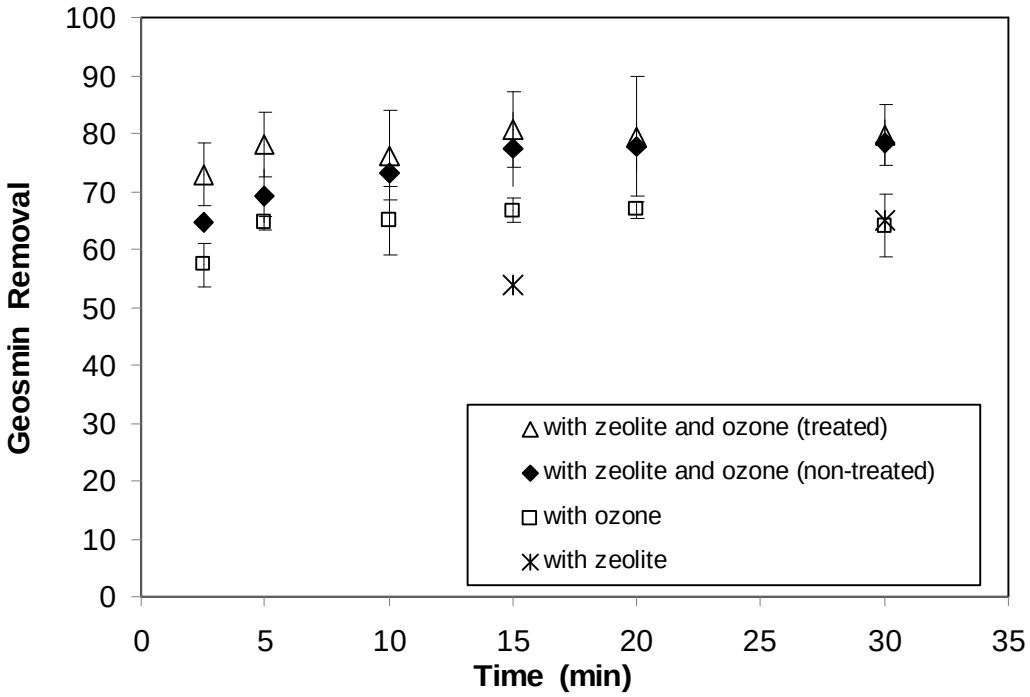

Figure 5.20 Geosmin removal from LMW by zeolite-enhanced ozonation as well as by ozone and zeolite alone. Zeolite: treated and non-treated H-Y-810 at a dose of 2 mg/L. Ozone dose: 0.75 mg/L. Error bars represent one standard deviation of duplicate experiments.

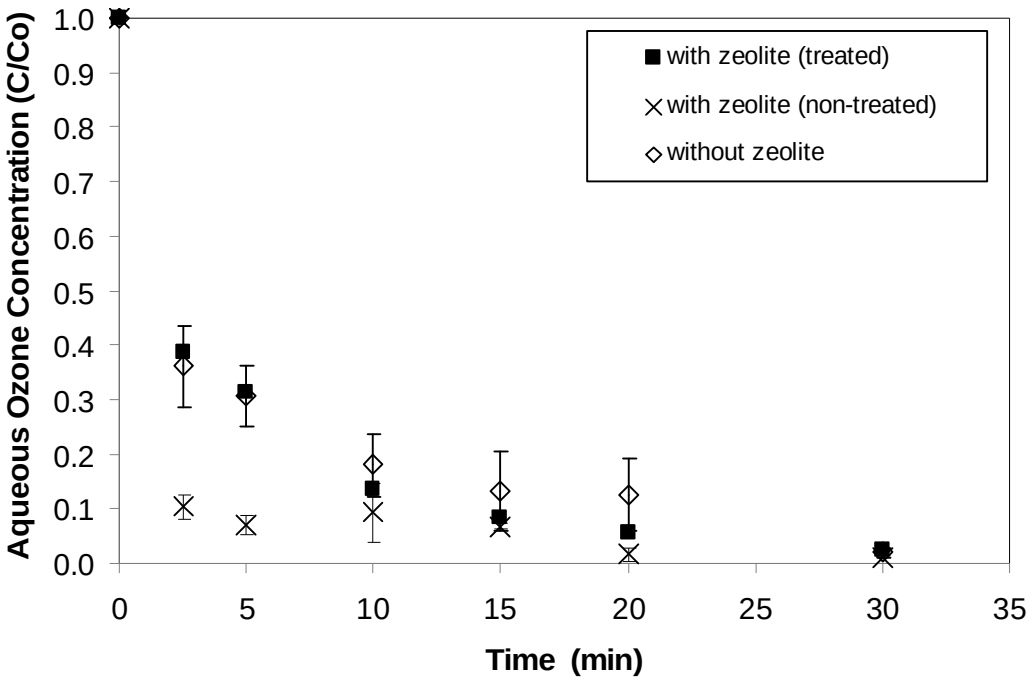

Figure 5.21 Ozone residual concentration profiles in LMW during MIB/geosmin removal experiments. Zeolite: treated and non-treated H-Y-810 at a dose of 2 mg/L. Ozone dose: 0.75 mg/L. Error bars represent one standard deviation of duplicate experiments.

5.5 MIB AND GEOSMIN REMOVAL BY POWDERED ACTIVATED CARBON IN THE PRESENCE OF OZONE.

In addition to zeolites, a coal-based powdered activated carbon (PAC) in its as-received form (WPH) and in its sub-micrometer diameter form (S-WPH) was tested to determine whether the presence of PAC or S-PAC during ozonation processes affects the removal of MIB and geosmin. As illustrated in Figure 5.22, for both ozone alone and the combination of PAC and ozone, MIB removals were about 50% after a contact time of 2.5 minutes and reached about

60% after a contact time of 20 minutes. Differences between ozone only and the combination of PAC and ozone were also small for geosmin, but geosmin removals were about 10% above those measured for MIB (Figures 5.22). After 60 minutes of contact with WPH alone, MIB and geosmin removals were approximately 35% and 40%, respectively (Figures 5.22 and 5.23).

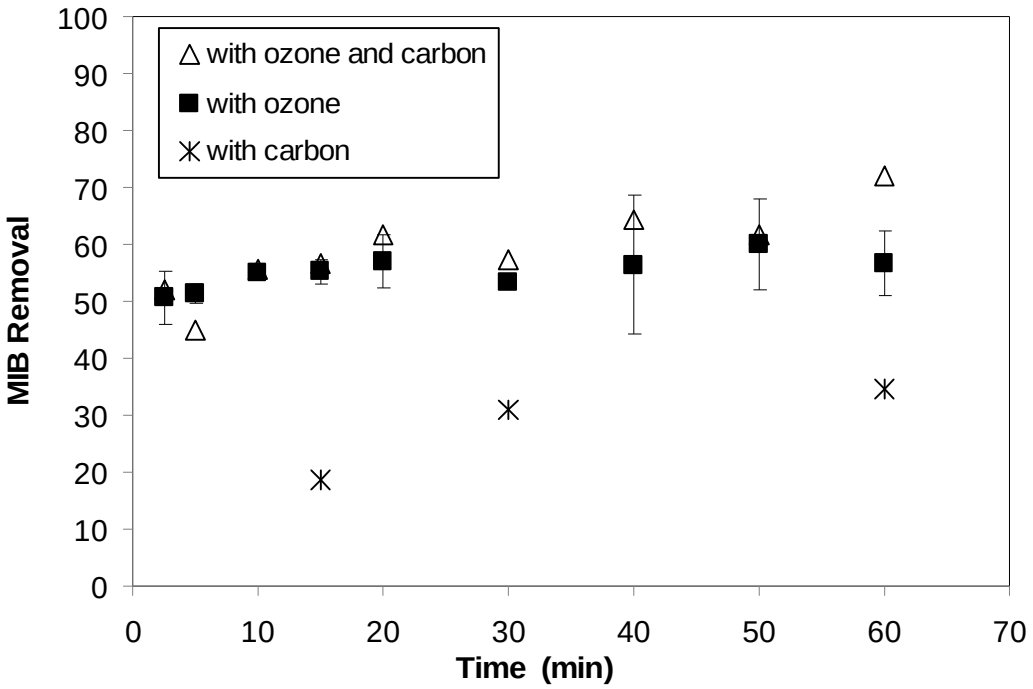

Figure 5.22. MIB removal from LMW by ozone and carbon as well as by ozone and carbon alone. Carbon: WPH at a dose of 5 mg/L. Ozone dose: 0.75 mg/L. Error bars represent one standard deviation of duplicate experiments.

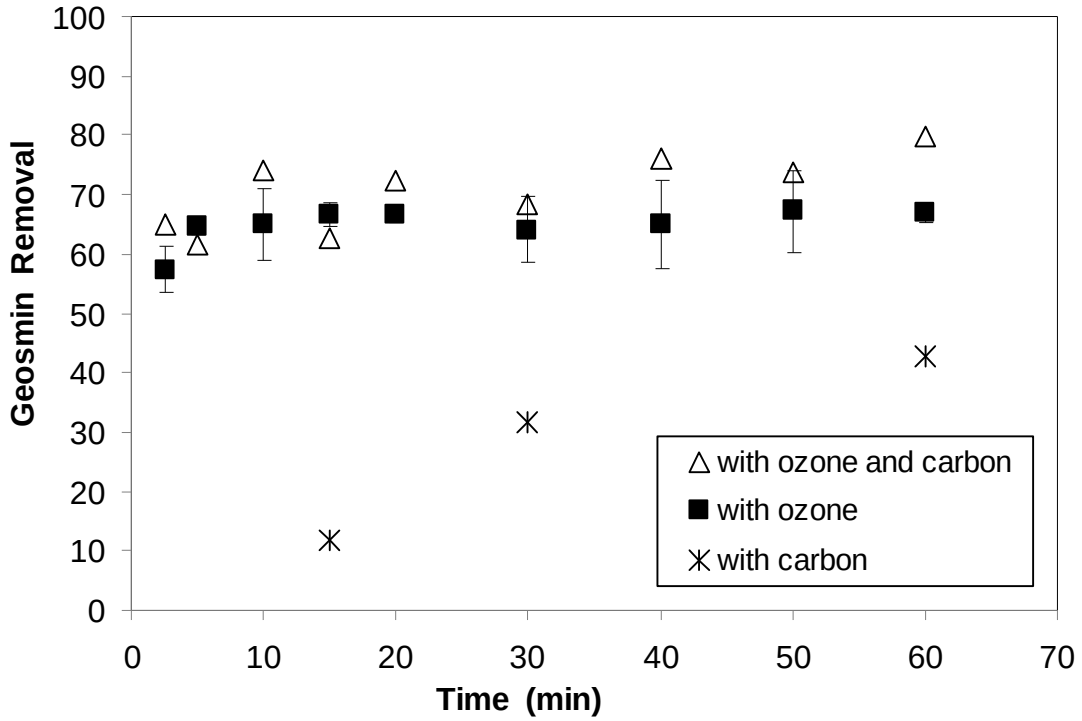

Figure 5.23. Geosmin removal from LMW by ozone and carbon as well as by ozone and carbon alone. Carbon: WPH at a dose of 5 mg/L. Ozone dose: 0.75 mg/L. Error bars represent one standard deviation of duplicate experiments.

Comparing MIB removal results for ozone only and the combination of S-WPH and ozone, there was again no measurable difference in MIB removal (Figure 5.24). As was the case for WPH, both ozone alone and the combination of ozone and S-WPH yielded MIB removals of ~50% after a contact time of 2.5 minutes and ~60% after a contact time of 20 minutes. The addition of S-WPH alone yielded ~55% MIB removal after a contact time of 60 minutes (Figure 5.24), which was substantially higher than that obtained with WPH alone.

In contrast to MIB, the addition of S-WPH greatly increased geosmin removal over that obtained with ozone alone (Figure 5.25). The geosmin removal with S-WPH and ozone was ~98% whereas only ~65% removal could be obtained with ozone alone. However, the increase in geosmin removal was mostly associated with the presence of S-WPH instead of a combined effect of ozone and carbon. S-WPH alone adsorbed about 95% of the initially added geosmin after a contact time of 60 minutes (Figure 5.25), and the geosmin removal data obtained with S-WPH closely matched the results obtained with the combination of S-WPH and ozone.

A comparison of the WPH and S-WPH data shows that faster adsorption kinetics were obtained with S-WPH. MIB removal after a 15 minutes contact time was ~20% for WPH and ~50% for S-WPH and geosmin removal after a 15 minutes contact time was ~15% for WPH and >90% for S-WPH. For S-WPH, MIB and geosmin adsorption had almost reached equilibrium after a contact time of 15 minutes, as evidenced by the small changes in MIB and geosmin removals with increasing contact times. In contrast, MIB and geosmin removals obtained with WPH PAC after contact times of 15 and 60 minutes differed substantially (Figures 5.22-25).

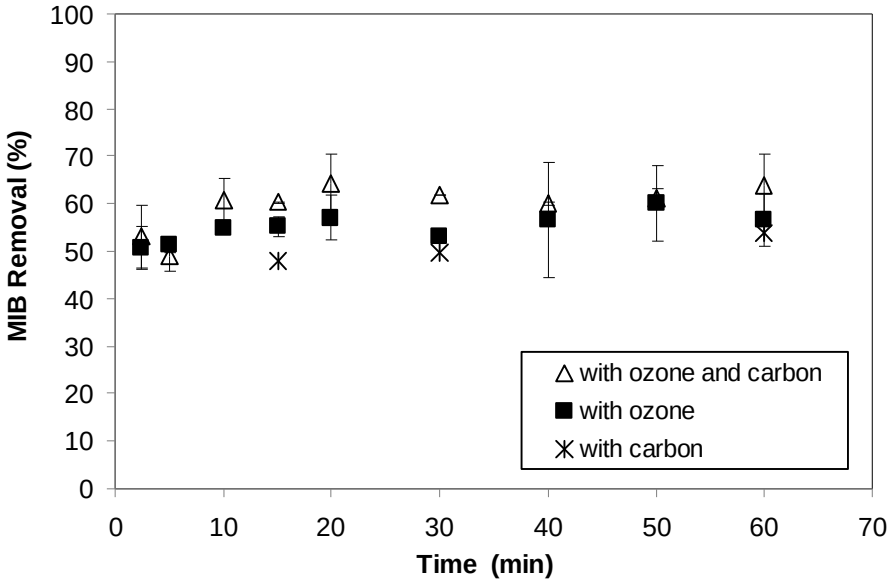

Figure 5.24. MIB removal from LMW by ozone and carbon as well as by ozone and carbon alone. Carbon: S-WPH at a dose of 5 mg/L. Ozone dose: 0.75 mg/L. Error bars represent one standard deviation of duplicate experiments.

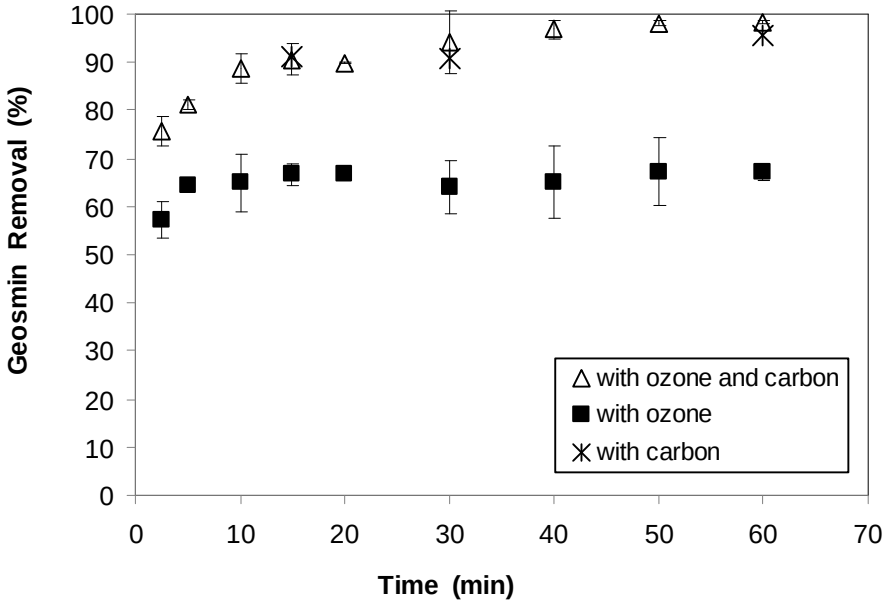

Figure 5.25. Geosmin removal from LMW by ozone and carbon as well as by ozone and carbon alone. Carbon: S-WPH at a dose of 5 mg/L. Ozone dose: 0.75 mg/L. Error bars represent one standard deviation of duplicate experiments.

Activated carbon can catalyze the transformation of ozone into stronger oxidative species such as hydroxyl radicals (Faria et. al. 2006, Ma et. al. 2004, Oh et. al. 2004, Jans et. al., 1998). Also, the presence of activated carbon during ozonation can significantly increase the removal rate of organic pollutants compared to conventional ozonation (Beltran et. al., 2002, Ma et. al. 2004, Oh et. al. 2004). Comparing the ozone depletion curves in the presence and absence of WPH and S-WPH (Figure 5.26), the addition of 5 mg/L WPH had little effect on ozone decomposition in LMW, which may explain why the addition of WPH did not produce a significant change in MIB or geosmin removal. In the presence of S-WPH, ozone depletion was more rapid which may have translated into higher hydroxyl radical concentrations in solution. It was expected that with a high concentration of hydroxyl radicals, the removal of MIB or geosmin would be higher in the presence of S-WPH compared to ozone alone or carbon alone but such a result was not obtained for either MIB or geosmin. Even though the ozone depletion was faster in presence of S-PAC and may have resulted in a higher generation rate of hydroxyl radicals, S-PAC may also be oxidized by the hydroxyl radicals, thus limiting the availability of hydroxyl radicals for the oxidation of MIB and geosmin. In other words, S-PAC may have served as a hydroxyl radical scavenger. Further study is required to explore the radical formation and fate mechanisms associated with the reaction between ozone and PAC or S-PAC.

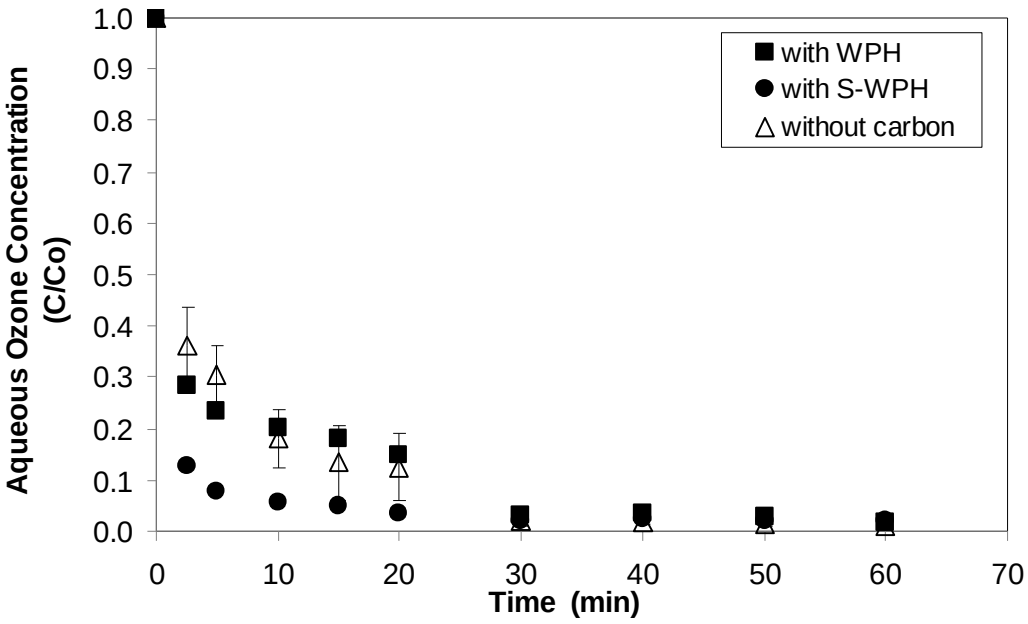

Figure 5.26 Ozone residual concentration profiles in LMW during MIB/geosmin removal experiments. Carbon: WPH and S-WPH at a dose of 5 mg/L. Ozone dose: 0.75 mg/L. Error bars represent one standard deviation of duplicate experiments.

CHAPTER 6

CONCLUSIONS AND RECOMMENDATIONS

The principal objective of this research was to investigate two innovative treatment methods for the control of earthy/musty odors associated with the presence of MIB and geosmin in drinking water. The first treatment method was an adsorption/reaction process based on the use of high-silica zeolites, a class of catalytic adsorbents that has not been studied extensively for water treatment applications. The second treatment method was an adsorption/oxidation process based on the combined use of high-silica zeolites and ozone (zeolite-enhanced ozonation).

Regarding MIB and geosmin removal by the first treatment method, the results of this study showed that:

- Among the studied zeolite framework types, mordenite was the most effective for MIB removal from UPW while both mordenite and Y were equally well suited for geosmin removal from UPW.
- The MIB and geosmin adsorption capacities of all tested zeolites were lower than those of a coal-based and a coconut-shell-based activated carbon.

- MIB and geosmin adsorption increased as the SiO_2/Al_2O_3 ratio of mordenite and Y zeolites increased. Data obtained with mordenite zeolites suggest that MIB/geosmin removal does not improve above SiO_2/Al_2O_3 ratios of about 90.
- MIB removal by mordenite zeolites was aided by a reactive removal mechanism. Most likely, MIB was transformed on acidic zeolite surfaces via a dehydration reaction that yielded non-odorous products. The results of isotherm-type tests (10-day contact time) showed that the contribution of the dehydration reaction to the overall MIB removal increased as the SiO_2/Al_2O_3 ratio of the zeolite decreased. A prerequisite for the dehydration reaction is that MIB adsorption takes place. Because of the hydrophilic nature of zeolites with low SiO_2/Al_2O_3 ratios, water adsorbs strongly in the pores of hydrophilic zeolites. As a result, MIB adsorption is energetically less favored than on more hydrophobic zeolites. The results of short-term kinetic tests suggest that, as a result of strong water adsorption, the reactive surface of a relatively acidic zeolite (H-Mordenite-40) was not sufficiently accessible for MIB to effectively participate in dehydration reactions.
- At short contact times (< 2 hours), MIB removal from Lake Michigan water could not be effectively accomplished by mordenite and H-Y-810 zeolites. Geosmin removal by mordenite zeolites was markedly decreased by Lake Michigan water constituents, but Lake Michigan water constituents did not have a significant effect on geosmin removal by H-Y-810 zeolite. Apart from NOM, cations in the background water (e.g.,

Ca^{2+}, Na^{+}) strongly affected MIB and geosmin removal by mordenite zeolites. Cations can displace exchangeable hydrogen ions on the zeolite surface and thus reduced the reactivity of the zeolite surface towards MIB. In addition, the results of this study showed that the presence of cations such as Ca^{2+} and Na^{+} increased the intraparticle diffusion resistance.

For a summary assessment of the adsorption/reaction process, Figures 6.1 and 6.2 provide an overview of MIB removal data from UPW and LMW at adsorbent doses of 2 and 15.5 mg/L, respectively. Similar results are shown for geosmin in Figures 6.3 and 6.4. The UPW results show that (1) the mordenite and H-Y-810 zeolites exhibited MIB and geosmin removal efficiencies that were similar to those obtained with the activated carbon at the higher adsorbent dose (15.5 mg/L) and (2) at short contact times (15 minutes) and low adsorbent doses (2 mg/L), H-Mordenite-230 outperformed the activated carbon. The latter statement also applies to the geosmin removal performance of H-Y-810 zeolite. In LMW, MIB and geosmin removal was most effectively accomplished by the activated carbon and H-Y-810 zeolite. The H-Y-810 zeolite was especially effective for geosmin removal (Figures 6.3 and 6.4).

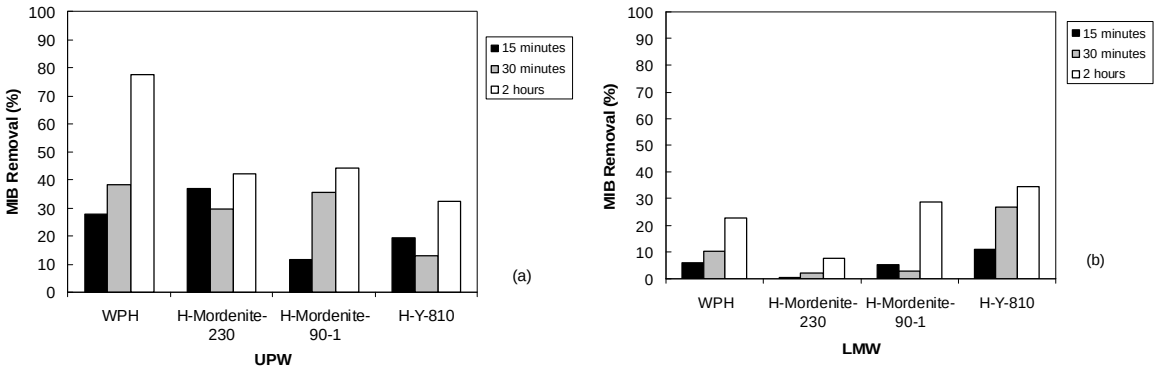

Figure 6.1 MIB removal comparison with an adsorbent dose of 2 mg/L in (a) UPW and (b) LMW

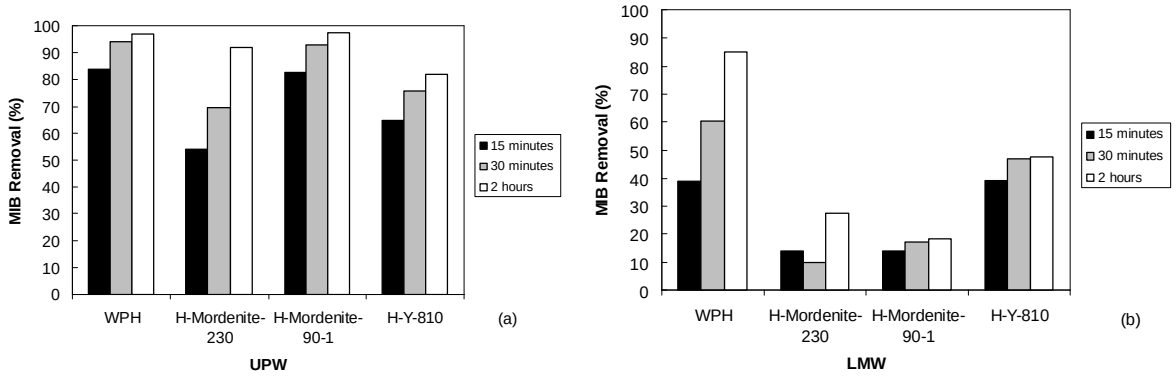

Figure 6.2 MIB removal comparison with an adsorbent dose of 15.5 mg/L in (a) UPW and (b) LMW

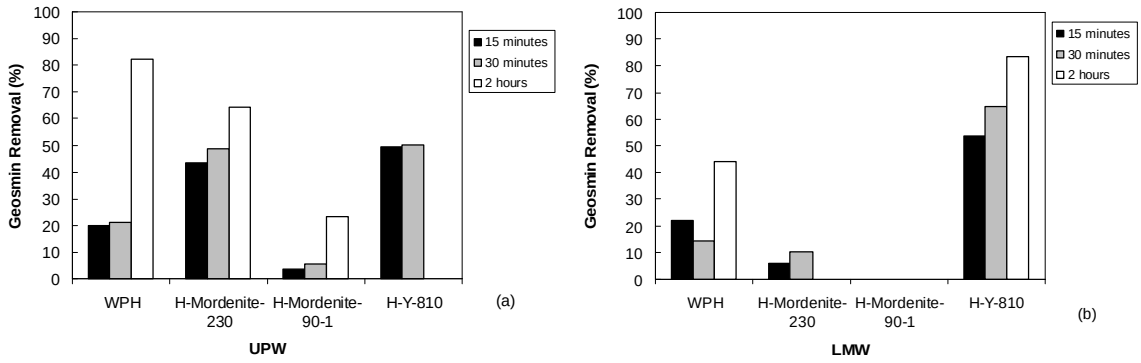

Figure 6.3 Geosmin removal comparison with an adsorbent dose of 2 mg/L in (a) UPW and (b) LMW. Note: Geosmin removal by H-Mordenite-90-1 in LMW was negligible and 2 hr data for H-Y-810 in LMW is missing.

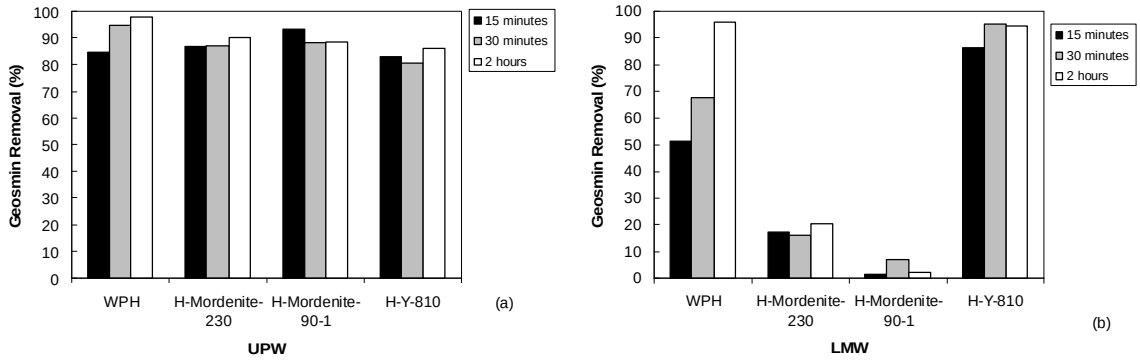

Figure 6.4 Geosmin removal comparison with an adsorbent dose of 15.5 mg/L in (a) UPW and (b) LMW.

Regarding the effectiveness of ozonation for MIB and geosmin removal in the presence of zeolites or powdered activated carbon, the results of this study showed that

- Mordenite and H-Y-810 zeolites are capable of adsorbing ozone such that the ozone concentration in zeolite pores can exceed the bulk water ozone concentration by approximately three orders of magnitude.
- The addition of mordenite or H-Y-810 zeolites did not measurably enhance the removal rate of MIB from LMW.
- Zeolite-enhanced ozonation with H-Y-810 produced slightly higher geosmin removals compared to ozonation alone, especially at shorter contact times.
- PAC/S-PAC addition did not measurably affect the effectiveness of ozonation for both MIB and geosmin removal when ozonation was the dominant removal process.

Similarly, the addition of ozone did not measurably affect the effectiveness of S-PAC for geosmin removal when adsorption by S-PAC was the dominant removal process.

- Additional process configurations (packed bed or fluidized bed) and zeolite framework types should be evaluated to test whether zeolites can enhance the performance of ozone oxidation processes when the removal of trace organic contaminants such as MIB and geosmin is required.

REFERENCES

American Water Works Association (AWWA). (2005). "Standard Methods for the Examination of Water and Wastewater." 21th Edition. American Public Health Association, American Water Works Association and Water Environment Federation.

Anderson, M.A. 2000. "Removal of MTBE and other organic contaminants from water by sorption to high silica zeolites." *Environ. Sci. Tech.* 34(4): 725-727.

AwwaRF and Lyonnaise des Eaux. 1995. *Advances in Taste-and-Odor Treatment and Control*. I.H. Suffet, J. Mallevialle, and E. Kawczynski, eds. American Water Works Association Research Foundation, Denver, CO.

AwwaRF and Lyonnaise des Eaux. 1987. *Identification and Treatment of Tastes and Odors in Drinking Water*. J. Mallevialle and I.H. Suffet, eds. American Water Works Association Research Foundation, Denver, CO.

Beltran, F.J., Rivas, J., Alvarez, P., and Montero-de-Espinosa, R. 2002a. "Kinetics of Heterogenous Catalytic Ozone Decomposition in Water on an Activated Carbon. *Ozone Sci. and Eng.* 24: 227-237.

Beltran, F.J., Rivas, F.J., Fernandez, L.A., Alvarez, P.M., and Montero-de-Espinosa, R. 2002b. "Kinetics of Catalytic Ozonation of Oxalic Acid in Water with Activated Carbon." *Ind. Eng. Chem. Res.* 41: 6510-6517.

Burlingame, G.A., Muldowney, J.J. and Maddrey, R.E. 1992. Cucumber flavor in Philadelphia's drinking water. *Journal AWWA* 84(8): 92-97.

Burlingame, G., Dann, R.M. and Brock, G.L. 1986. A case study of geosmin in Philadelphia's water. *Journal AWWA* 78(3): 56-61.

Carrott, P.J.M.; Kenny, M.B.; Roberts, R.A.; Sing, K.S.W.; and C.R. Theocharis. 1991. "The adsorption of water vapour by microporous solids." In *Characterization of Porous Solids II. Studies in Surface Science and Catalysis*, Vol. 62, F. Rodriguez-Reinoso et al., eds. Elsevier Sicence Publishers, Amsterdam, pp. 685-692.

Centi, G., Grande, A., and S. Perathoner. 2002. "Catalytic conversion of MTBE to biodegradable chemicals in contaminated water." Catalysis Today 75: 69-76.

Chen, G., Dussert, B.W., and Suffet, I.H. 1997. "Evaluation of granular activated carbons for removal of methylisoborneol to below odor threshold concentration in drinking water." *Wat. Res.* 31(5): 1155-1163.

Dodd, M.C., M. Buffle, and U. Von Gunten. 2006. "Oxidation of antibacterial molecules by aqueous ozone: Moiety-specific reaction kinetics and application to ozone-based wastewater treatment." *Environ. Sci. Tech.* 40, 1969-1977.

Ellis, J. and W. Korth. 1993. "Removal of geosmin and methylisoborneol from drinking water by adsorption on ultrastable zeolite-Y." *Wat. Res.* 27: 535-539.

Faria, P.C.C., Orfao, J.J.M., and Pereira, M.F.R. 2006. "Ozone Decomposition in Water Catalyzed by Activated Carbon: Influence of Chemical and Textural Properties." Ind. Eng. Chem. Res. 45: 2715-2721

Ferguson, D.W., M.J. McGuire, B. Koch, R.L. Wolfe, and E.M. Aieta. 1990. Comparing PEROXONE and Ozone for Controlling Taste and Odor Compounds, Disinfection By-products, and Microorganisms. *Journal AWWA* 82(4): 181-191.

Fravel, D.R., W.J. Connick, Jr., C.C. Grimm, and S.W. Lloyd. 2002. "Volatile compounds emitted by Sclerotia of *Sclerotina minor*, *Sclerotina sclerotiorum*, and *Sclerotinum rolfsii*. *J. Agric. Food Chem.* 50: 3761-3764.

Fujita, H., J. Izumi, M. Sagehashi, T. Fujii, and A. Sakoda. 2004a. "Adsorption and decomposition of water-dissolved ozone on high-silica zeolites." ***Wat. Res.*** 38: 159-165.

Fujita, H., J. Izumi, M. Sagehashi, T. Fujii, and A. Sakoda. 2004b. "Decomposition of trichloroethene on ozone-adsorbed high-silica zeolites." ***Water Research*** 38: 166-172.

Gillogly, T.E.T., V.L. Snoeyink, A. Holthouse, C.M. Wilson, and E.P. Royal. 1998a. "Effect of chlorine on PAC's ability to adsorb MIB." ***Journal AWWA*** 90(2): 107-114.

Gillogly, T.E.T., V.L. Snoeyink, J.R. Elarde, C.M. Wilson, and E.P. Royal. 1998b. "14-C MIB adsorption on PAC in natural water." ***Journal AWWA*** 90(1): 98-108.

Glaze, W.H., R. Schep, W. Chauncey, E.C. Ruth, J.J. Zarnoch, E.M. Aieta, C.H. Tate, and M.J. McGuire. 1990. "Evaluating oxidants for the removal of model taste and odor compounds from municipal water supply." ***Journal AWWA*** 82(5): 79-84.

Graham, M.R., R.S. Summers, M.R. Simpson, and B.W. Macleod. 2000. "Modeling equilibrium adsorption of 2-methylisobornoel and geosmin in natural waters." ***Wat. Res.*** 34(8): 2291-2300.

Hattori, K. 1988. Water treatment systems and technology for the removal of odor compounds. ***Wat. Sci. Tech.*** 20(8/9): 237-244.

Ho, L., J.P. Croué, and G. Newcombe. 2004. "The effect of water quality and NOM character on the ozonation of MIB and geosmin." ***Wat. Sci. Tech.*** 49(9): 249-255.

Ho, L., D. Hoefel, F. Bock, C.P. Saint and G. Newcombe. 2007. "Biodegradtion rates of 2-methylisoborneol (MIB) and geosmin through sand filters and in bioreactors." ***Chemosphere,*** 66:2210-2218

Izaguirre, G. Taylor, W. D. 2004. “A guide to geosmin- and MIB-producing cyanobacteria in the United States.” *Wat. Sci. Tech.* 49(9): 19-24.

Izaguirre, G., Hwang, C.J., Krasner, S.W. and McGuire, M.J. 1982. Geosmin and 2-methylisoborneol from Cyanobacteria in three water supply systems. *Appl. Environ. Microbiol.* 43: 708-714.

Jans, U., and Hoigne, J. 1998. “Activated Carbon and Carbon Black Catalyzed Transformation of Aqueous Ozone into OH-Radicals.” Ozone: Science and Engineering. 20: 67-90

Jüttner, F. 1983. Volatile odorous excretion products of algae and their occurrence in the natural aquatic environment. *Water Sci. Tech.* 15(6/7): 247-257.

Kawai, T., T. Yanagihara, and K. Tsutsumi. 1994. “Adsorption characteristics of chloroform on modified zeolites from gaseous phase as well as its aqueous solution”. *Colloid Polymer Sci*. 272: 1620-1626.

Kenny, M.B. and K.S.W. Sing. 1990. “The hydrophobicity of silicalite and ZSM-5.” *Chemistry & Industry* **2**: 39-40.

Knappe, D.R.U, A. Rossner, S.A. Snyder and C. Strickland. *Alternative Adsorbents for the Removal of Polar Organic Contaminants.* Awwa Research Foundation: Denver, Colorado, 2007.

Lalezary, S., M. Pirbazari, and M.J. McGuire. 1986. Oxidation of five earthy-musty taste and odor compounds. *Journal AWWA* 78(3): 62-69.

Li, S., Tuan, V.A., Noble, R.D.; and Falconer, J.L. 2003. “MTBE Adsorption on all-silica ß zeolite.” *Environ. Sci. Tech.* 37(17): 4007-4010.

Liang, C., D. Wang, X. GE, M. Yang, and W. Sun. 2006. "Comparative study on the removal technologies of 2-methylisoborneol (MIB) in drinking water." *Journal Environ. Sci.* 18(1):47-51

Lundgren, B.V., Grimvall, A. and Savanhed, R. 1988. Formation and removal of off-flavor compounds during ozonation and filtration through biologically active sand filters. *Wat. Sci. Tech.* 20 (8/9): 245-253.

Ma, J., Ming-Hao, S., Chen, Z., and Wang, L. 2004. "Degradation of Refractory Organic Pollutants by Catalytic Ozonation-Activated Carbon and Mn-Loaded Activated Carbon as Catalyst." Ozone: Science and Engineering. 26: 3-10.

Matsui, Y.; Murase, R.; Sanogawa, T.; Aoki, N.; Mima, S.; Inoue, T.; and Matsushita, T. 2005. "Rapid adsorption pretreatment with submicrometre powdered activated carbon particles before microfiltration." *Wat. Sci. Tech.* 51(6/7): 249-256.

Matsui, Y.; Aizawa, T.; Kanda, F..; Nigorikawa, N.; Mima, S., and Kawase, Y. 2007. "Adsorptive removal of geosmin by ceramic membrane filtration with super-powdered activated carbon." *J. Water Supply Res. Technol – AQUA* 56 (6/7): 411-418.

Matsui, Y.; Murai, K.; Sasaki, H.; Ohno, K.; and Matsushita, T. 2008. "Submicron-sized activated carbon particles for the rapid removal of chlorinous and earthy-musty compounds." *J. Water Supply Res. Technol* – AQUA 57(8): 577-583.

Matsui, Y.; Ando, N.; Sasaki, H.; Matsushita, T.; Mima, S.; and Ohno, K. 2009. "Branched pore kinetic model analysis of geosmin adsorption on super-powdered activated carbon" *Wat. Res.* 43 (12): 3095-3103.

McCusker, L.B. and C. Baerlocher. 2001. "Zeolite structures." *Introduction to Zeolite Science and Practice, 2nd Completely Revised and Expanded Edition*, van Bekkum, H., E.M. Flanigen, P.A. Jacobs, and J.C. Jansen, eds. Elsevier Science, Amsterdam, pp. 37-67.

McGuire, M.J. and Gaston, J.M. 1988. Overview of technology for controlling off-flavors in drinking water. ***Wat. Sci. Tech.*** 20(8/9): 215-228.

MWDSC. 2005. Standard operating procedure for the determination of 2-methylisoborneol and geosmin in drinking water using solid phase micro-extraction and GC/CI/MS/MS. La Verne, CA.

Nerenberg, R., B.E. Rittmann, and W.J. Soucie. 2000. Ozone/biofiltration for removing MIB and geosmin. ***Journal AWWA*** 92(12): 85-95.

Newcombe, G. 2005. Personal Communication.

Newcombe, G. and Cook, D. 2002. "Influences on the removal of tastes and odours by PAC." ***J. Wat. Supply Res. Tech. – AQUA*** 51(8): 463-474.

Newcombe, G., M. Drikas, and R. Hayes. 1997. "Influence of characterised natural organic material on activated carbon adsorption: II. Effect on pore volume distribution and adsorption of methylisoborneol." ***Wat. Res.*** 31(5): 1065-1073.,

Oh, B.S., Song, S.J., Lee, E.T., Oh, H.J., and Kang, J.W. 2004. "Catalyzed ozonation process with GAC and metal doped-GAC for removing organic pollutants." ***Water. Sci. Tech.*** 49 (4): 45-49

Peter, A. and von Gunten, U. 2007. "Oxidation Kinetics of Selected Taste and Odor Compounds During Ozonation of Drinking Water." ***Environ. Sci. Tech.*** 41, 626-631.

Pfenninger, A. 1998. "Manufacture and use of zeolites for adsorption processes." ***Molecular Sieves: Science and Technology***, Vol. 2, Karge, H.G. and J. Weitkamp, eds. Springer-Verlag, Berlin, pp. 163-198.

Rossner, A. and Knappe, D.R.U. 2008. "MTBE adsorption on alternative adsorbents and packed bed adsorber performance." ***Wat. Res.*** 42: 2287-2299.

Rouquerol, F.; Rouquerol, J.; and K. Sing. 1999. ***Adsorption by Powders and Porous Solids***. Academic Press, San Diego, CA.

Sagehashi, M., K. Shiraishi, H. Fujita, T. Fujii, and A. Sakoda, 2005a. "Ozone decomposition of 2-methylisoborneol (MIB) in adsorption phase on high silica zeolites preventing bromate formation." ***Wat. Res.*** 39: 2926-2934.

Sagehashi, M.; Shiraishi, K.; Fujita, H.; Fujii, T.; and Sakoda, A. 2005b. "Adsorptive ozonation of 2-methylisoborneol in natural water with preventing bromate formation." ***Wat. Res.*** 39: 3900-3908

Saito, A., T. Tokuyama, A. Tanaka, T. Oritani, and K. Fuchihgami. 1999. "Microbiological degradation of (-)-geosmin." ***Wat. Res.*** 33(13): 3033-3036.

Sanchez-Polo, M., and Rivera-Utrilla, J. 2003. "Effect of the Ozone-Carbon Raction on the Catalytic Activity of Activated Carbon During the Degradation of 1,3,6-naphthalenetrisulphonic acid with Ozone". ***Carbon.*** 41: 303-307

Sanchez-Polo, M., von Gunten, U., and Rivera-Utrilla, J. 2005. " Efficiency of Activated Carbon to Transform ozone into .OH radicals: Influence of operational parameters". ***Wat. Res.*** 39: 3189-3198

Schumann, R. and P. Pendleton. 1997. "Dehydration products of 2-methylisoborneol." ***Wat. Res.*** 31: 1243-1246.

Suffet, I. H., Corado, A., Chou, D., McGuire, M. Butterworth, S. 1996. "AWWA Taste and Odor Survey." ***Journal AWWA*** 88(4): 168-180.

Szostak, R. 1992. *Handbook of molecular sieves*. Van Nostrand Reinhold: New York, NY.

Szostak, R. 1998. *Molecular sieves: principles of synthesis and identification*. 2nd ed. Blackie Academic & Professional: New York, NY.

Tanaka, A., T. Oritani, F. Uehara, A. Saito, H. Kishita, Y. Niizeki, H. Yokota, and K. Fuchihgami. 1996. "Biodegradation of a musty odour component, 2-Methylisoborneol." *Wat. Res.* 30(3): 759-761.

Tarbuck, E.J., F.K. Lutgens, and D. Tasa. 2002. *Earth – An introduction to physical geology*. 7th ed. Prentice Hall: Upper Saddle River, NJ, p. 47.

Terashima, K. 1988. Reduction of musty odor substances in drinking water - a pilot plant study. *Wat. Sci. Tech.* 20(8/9): 275-281.

Volkov, A.G., S. Paula, and D.W. Deamer. 1997. "Two mechanisms of permeation of small neutral molecules and hydrated ions across phospholipid bilayers." *Bioelectrochem. Bioenergetics* 42: 153-160.

Westerhoff, P., B. Nalinakumari, and P. Pei. 2006. "Kinetics of MIB and geosmin oxidation during ozonation.'*Ozone:Science and Engineering* 28: 277-286

Young, W. F., Horth, H., Crane, R., Ogden, T. and Arnoot, M. 1996. "Taste and odor threshold concentrations of potential potable water contaminants." *Wat. Res.* 30(2): 331-340.

Zaitlin, B. and Watson, S.B. 2006. "Actinomycetes in relation to taste and odour in drinking water: Myths, tenets and truths." *Wat. Res.* 40: 1741-1753.

APPENDIX

THE DETERMINATION OF 2-METHYLISOBORNEOL AND GEOSMIN USING SOLID PHASE MICRO-EXTRACTION AND GC/CI/MS/MS

(ADAPTED FROM THE STANDARD OPERATING PROCEDURE DEVELOPED BY THE METROPOLITAN WATER DISTRICT OF SOUTHERN CALIFORNIA)

1. Scope and Application

This method is applicable to the determination of the taste and odor causing compounds geosmin and 2-methylisoborneol (MIB) in both raw and finished drinking waters.

2. Summary of Method

The semi-volatile organic compounds geosmin and MIB are extracted from the sample matrix by headspace solid-phase microextraction (SPME). The purged compounds are adsorbed to a SPME fiber that is exposed to the headspace of the heated and agitated sample vial. The fiber is then desorbed in the heated injector of a gas chromatotograph (GC) oven which is equipped with a capillary column. The column is temperature programmed to separate the method analytes that are then detected by an ion trap mass spectrometer (MS) in the chemical ionization MS/MS mode.

3. Definitions

3.1 Internal Standard (IS) – A pure analyte added to a sample in known amount and used to measure the relative responses of the other method analytes that are components of the same sample. The internal standard must be an analyte that is not a sample component.

3.2 Laboratory Duplicates (LD1 and LD2) - Two aliquots of the same sample taken in the laboratory and analyzed separately with identical procedures. Analyses of LD1 and LD2 indicate precision associated with laboratory procedures, but not with sample collection, preservation, or storage procedures.

3.3 Laboratory Reagent Blank (LRB) – An aliquot of reagent water of other blank matrix that is treated exactly as a sample including exposure to all glassware, equipment, solvents, reagents, internal standards, and surrogates that are used with other samples.

3.4 Laboratory Fortified Blank (LFB) - A LFB is an aliquot of reagent water or other blank matrix to which known quantities of the method analytes are added in the laboratory. The LFB is analyzed exactly like a sample, and its purpose is

to determine whether the methodology is in control, and whether the laboratory is capable of making accurate and precise measurements.

3.5 Calibration Standard (CAL) - A CAL is a solution prepared from the primary dilution standard solution or stock standard solutions and the internal standards and surrogate analytes. The CAL solutions are used to calibrate the instrument response with respect to analyte concentration.

4. Equipment and Supplies

4.1 Sample analysis vials – 20-mL Screw-cap glass vials (Varian 392620202, or equivalent).

4.2 Syringes – 10-uL, 25-uL microsyringes

4.3 Automated pipettor – capable of filling a 10-mL glass pipet

4.4 SPME Apparatus

4.4.1 SPME Autosampler. The CombiPal autosampler (CTC Analytics) is capable of processing up to 32 20-mL SPME vials per tray. The autosampler is equipped with a programmable heated agitator block. The SPME conditions are detailed in Table A.1.

4.4.2 SPME fiber. A 1-cm 50/30 μm DVB/Carboxen/PDMS StableFlex SPME fiber was used (Supelco 57329-U).

4.5 Gas chromatograph/Mass spectrometer (GC/MS)

4.5.1 The GC (Varian 3800) is equipped with a split/splitless injector, which can be heated to at least 250ºC. The GC oven is capable of multi-ramp temperature programming. GC program: 50ºC, 1 min; 10ºC/min **à** 200ºC, 2min; 10ºC /min **à** 240ºC; 5min

4.5.2 The capillary column is a Factor Four VF-5ms low bleed, 30m x 0.25mm ID, with film thickness 0.25 μm. Analyte retention times and quantitation masses are listed in Table A.2.

4.5.3 The MS (Varian Saturn 2200) is capable of running in electron impact (EI), chemical ionization (CI), and MS/MS modes. MS conditions are detailed in Table A.3.

Table A1. SPME Analysis Conditions

Incubation Temp.	65ºC
Agitator On Time	30 s
Agitator Off Time	2 s
Vial Penetration	22 mm
Extraction Time	30 min
Injection Penetration	54 mm
Desorption Time	4 min

Table A.2. Retention Time and Quantitation Ion

Analyte	**Retention Time (min)**	**Quantitation Ion**
Isoborneol (I.S.)	8.18	95
MIB	8.54	95
Geosmin	11.68	109

Table A3. Mass Spectrometer Parameters

Segment Parameter	**Isoborneol**	**MIB**	**Geosmin**
Emission Current	15	15	15
Multiplier Offset(V)	300	300	300
Scan Time (sec)	0.600	0.600	0.600
Low Mass	75	90	95
High Mass	155	155	185
Ionization Mode	CI Auto	CI Auto	CI Auto
Ion Prep Technique	MS/MS	MS/MS	MS/MS
Parent Mass	137	151	165
Waveform Type	Resonant	Resonant	Resonant

5. Reagents and Standards

- MIB and geosmin stock standards, 100 μg/mL in methanol (Supelco)
- Isoborneol (Aldrich)
- Methanol, LC-MS grade (Fluka)
- Acetone, GC grade (Fisher Scientific)
- Sodium chloride, granular (Fisher Scientific), baked at 450ºC for 4 hours

6. Stock Standard Dilutions

- MIB, geosmin and isoborneol. Prepare a stock solution of 5 μg/mL in acetone. Store the solution at -4ºC for up to two months.

7. Primary Dilution Standards

- MIB and geosmin. Dilute 2 μL of the stock standard dilution into 1 mL acetone to yield a 0.01 μg/mL solution. Prepare this solution daily.
- Isoborneol. Dilute 4 μL of the stock standard dilution into 1 mL acetone to yield a 0.02 μg/mL solution. Prepare this solution daily.

8. Sample Collection and Storage

- Collect samples in duplicate, headspace-free
- The samples must be chilled to 4ºC when collected and maintained at that temperature until analysis.
- The samples must be analyzed within 3 days of collection.

9. Quality Control

- Quality control measures include the regular analysis of laboratory reagent blanks (LRBs), and laboratory fortified blanks (LFBs).
- A LRB is analyzed at the beginning of each analytical batch to demonstrate low system background.
- A LFB is analyzed in the middle and at the end of each analytical batch to verify system calibration. Typically, an LFB of 5 ng/L was analyzed in the middle of the batch, and an LFB of 25 ng/L was analyzed at the end of each batch.

10. Calibration

- Calibration should be conducted for each fiber. A new fiber should be installed and conditioned prior to calibration.
- Six calibration standards that bracket the expected concentration range of the environmental samples are required. Analyze calibration concentrations of 1, 2.5, 5, 10, 17 and 25 ng/L. Samples exceeding a concentration of 25 ng/L were diluted with ultrapure laboratory water.
- Calibration standards are prepared by spiking reagent water with an appropriate amount of the MIB and geosmin primary dilution standard and by proceeding as outlined in Sect. 11.
- A continuing calibration check standard is analyzed in the middle and at the end of each analytical batch. Analyte recoveries must be within +/- 30% of the actual spiked amount.

11. Procedure

- Add 2.50 g NaCl to each 20-mL autosampler vial
- Pipet 10 mL of sample from the sample vial into the 20-mL autosampler vial and cap the vial.

- Add 10 μL of the isoborneol primary dilution standard to yield 20 ng/L isoborneol and recap the vial.
- Gently shake for 30 seconds to dissolve the salt.
- Load the sample onto the autosampler rack and start the analysis.